

**EXTRACELLULAR SUPEROXIDE DISMUTASE, OXIDATIVE STRESS AND
EXTRACELLULAR MATRIX SYNDECANS IN PULMONARY AND CARDIAC
FIBROSIS.**

by

Corrine RaShelle Kliment

BS, University of Nebraska – Lincoln, 2004

Submitted to the Graduate Faculty of
School of Medicine in partial fulfillment
of the requirements for the degree of
Doctor of Philosophy

UNIVERSITY OF PITTSBURGH
SCHOOL OF MEDICINE

This dissertation was presented

by

Corrine RaShelle Kliment

It was defended on

April 6, 2009

and approved by

Dr. Charleen T. Chu, MD, PhD, Department of Pathology

Dr. Wendy M. Mars, PhD, Department of Pathology

Dr. Cary Wu, PhD, Department of Pathology

Dr. Bruce A. Freeman, PhD, Chair, Department of Pharmacology

Dr. Steven D. Shapiro, MD, Chair, Department of Internal Medicine

Cellular and Molecular Pathology faculty

Thesis Advisor: Dr. Tim D. Oury, MD, PhD, Department of Pathology

Copyright © permission and non-profit use was granted for the use of parts of the following publications:

1. **Kliment, CR**, Englert, JM. Gochuico, BR., Yu, G., Kaminski, N., Rosas, IO., Oury, TD. “Oxidative Stress Alters Syndecan-1 Distribution in the Lung During Pulmonary Fibrosis.” J Biol Chem, 2009 Feb 6; 284(6):3537-45. PMID: 19073610

2. **Kliment, CR**, Tobolewski, J, Manni, M, Tan, R, Enghild, J, Oury, T. “Extracellular Superoxide Dismutase protects against matrix degradation of heparan sulfate in the lung.” Antioxid Redox Signal. 2008 Feb;10(2):261-8. PMID: 17961072

**EXTRACELLULAR SUPEROXIDE DISMUTASE, OXIDATIVE STRESS AND
EXTRACELLULAR MATRIX SYNDECANS
IN PULMONARY AND CARDIAC FIBROSIS.**

Corrine RaShelle Kliment

University of Pittsburgh, 2009

ABSTRACT

Oxidative stress and tissue remodeling are involved in the development of fibrosis of the lung and heart. Extracellular superoxide dismutase (EC-SOD) is an important antioxidant enzyme that has been shown to limit inflammation and fibrosis. Idiopathic pulmonary fibrosis is a lung disease characterized by severe, progressive interstitial fibrosis. Cardiac fibrosis has various causes but is a fatal side effect of treatment with the chemotherapeutic doxorubicin. Both of these diseases involve oxidant/antioxidant imbalances and can be studied through animal models. *It was hypothesized that one mechanism through which EC-SOD protects the lungs and heart from inflammation and fibrosis is by preventing oxidative shedding of extracellular matrix components, specifically syndecans.*

In the lung, wild type and EC-SOD KO mice were treated with titanium dioxide, asbestos, or Bleomycin. Over the course of injury, EC-SOD KO mice have significantly higher levels of shed syndecan-1 and -4 in their bronchoalveolar lavage fluid and tissue. By IHC staining, the lung distribution of EC-SOD decreases in areas of fibrosis while syndecan-1 increases. Furthermore, *in vitro*, EC-SOD prevents syndecan-1 shedding from epithelial cells

through its antioxidant activity and by directly binding to syndecan-1. Shed syndecan-1 is chemotactic to neutrophils and inhibits wound healing. In the heart, the significance of EC-SOD on normal heart morphology, fibrosis, and cardiac function were evaluated in wild type and EC-SOD KO mice in a doxorubicin-induced LV fibrosis model. The lack of EC-SOD causes LV posterior wall thinning and ventricular dilation without an insult. After an oxidative insult induced by doxorubicin, EC-SOD KO mice lost significantly more cardiac function compared to wild-type mice, had enhanced inflammatory cell recruitment, increased shedding of syndecan-1 from the heart and increased caspase-3 activation or apoptosis.

In summary, this study shows that EC-SOD is important in the maintenance of normal cardiac morphology, the development of cardiac fibrosis, inflammation, apoptosis, and the loss of function associated with oxidative cardiac injury. In the lung, this investigation shows that the loss of pulmonary EC-SOD leaves syndecan-1 vulnerable to oxidative stress and that oxidant-induced loss of cell surface syndecan-1 impairs re-epithelialization, induces inflammation, and promotes a fibrotic microenvironment in the lung.

TABLE OF CONTENTS

PREFACE	XII
1.0 INTRODUCTION	1
1.1 IDIOPATHIC PULMONARY FIBROSIS	1
1.1.1 Pathophysiology	2
1.1.2 Diagnosis and Pathological Findings.....	2
1.1.3 Treatment	3
1.1.4 Asbestosis – A related fibrotic lung disease.	5
1.2 EXPERIMENTAL ANIMAL MODELS OF PULMONARY FIBROSIS	7
1.2.1 Bleomycin.....	8
1.2.2 Asbestos.....	9
1.2.3 Silicosis	9
1.3 THE PATHOGENESIS OF PULMONARY FIBROSIS	10
1.3.1 Re-epithelialization and Alveolar Wound Healing	10
1.3.2 Inflammation	12
1.3.3 Growth Factors and Cytokines.....	13
1.3.4 Fibroblasts, Matrix Deposition and Turnover.	14
1.3.5 Matrix Metalloproteinases	15
1.4 CARDIAC FIBROSIS AND CARDIOMYOPATHY	17
1.4.1 Causes and Pathophysiology	17
1.4.2 Diagnosis, Pathological Findings and Treatment Options	18
1.4.3 Doxorubicin Experimental Animal Model of Cardiac Fibrosis.....	18
1.5 OXIDATIVE STRESS AND REACTIVE OXYGEN SPECIES	19
1.5.1 Reactive Oxygen Species	20
1.5.2 Reactive Nitrogen Species.....	24
1.5.3 Antioxidant Defenses	25
1.5.4 Oxidative Stress in Fibrosis.....	26
1.6 EXTRACELLULAR SUPEROXIDE DISMUTASE	28
1.6.1 EC-SOD Structure and Function	28
1.6.2 Tissue Distribution and Turn-over of EC-SOD	31
1.6.3 EC-SOD in Pulmonary and Cardiovascular Disease.....	32
1.7 HEPARAN SULFATE PROTEOGLYCANS	33
1.7.1 Family Members – syndecans and glypicans.....	34
1.7.2 Syndecan Biochemistry.....	37
2.0 RATIONALE AND HYPOTHESIS	39
2.1 PULMONARY FIBROSIS STUDIES	39
2.2 CARDIAC FIBROSIS STUDIES	41

3.0	MATERIALS AND METHODS	42
3.1	REACTIVE OXYGEN SPECIES GENERATION	42
3.2	ANIMAL STUDIES	42
	3.2.1 Mice Utilized	42
	3.2.2 Intratracheal Instillation of Fibrotic Stimuli to the Lung	43
	3.2.3 Doxorubicin treatment for Cardiac Fibrosis	43
	3.2.4 Pulmonary and Cardiac Tissue Harvest and Sample Collection	43
3.3	HUMAN IPF STUDIES	45
3.4	CARDIAC FUNCTION ANALYSIS	46
	3.4.1 Echocardiography and Functional Calculations	46
3.5	BIOCHEMICAL ANALYSIS	48
	3.5.1 Bronchoalveolar lavage analysis	48
	3.5.2 Lung and Heart Homogenization	48
	3.5.3 Western Blot Analysis	49
	3.5.4 Hydroxyproline Assay	50
	3.5.5 RNA Isolation and Quantitative reverse transcriptase polymerase chain reaction	50
3.6	HISTOLOGICAL ANALYSIS	51
	3.6.1 Hematoxylin and Eosin histology staining	51
	3.6.2 Picro-Sirius Red Staining	52
	3.6.3 Masson’s Trichrome Staining	52
	3.6.4 TUNEL Straining	52
	3.6.5 Immuno-fluorescent histochemistry	53
	3.6.5.1 Lung IHC	53
	3.6.5.2 Heart IHC	54
3.7	PURIFICATION OF HUMAN EC-SOD	54
3.8	GENERATION OF EC-SOD ANTIBODIES	55
3.9	SYNDECAN SPECIES UTILIZED	55
3.10	HEPARIN AND HEPARAN SULFATE FRAGMENTATION ANALYSIS	56
3.11	CELLULAR CHEMOTAXIS ASSAY	56
3.12	CELL CULTURE	58
	3.12.1 Primary mouse epithelial cell culture and epithelial cell lines	58
	3.12.2 Fibroblasts studies	59
	3.12.3 siRNA Treatment	60
	3.12.4 Syndecan-1 Shedding Assays	60
3.13	EPITHELIAL WOUND HEALING ASSAY	61
4.0	STATISTICAL ANALYSIS	62
5.0	RESULTS – PULMONARY FIBROSIS	63
	5.1 ASBESTOS AND BLEOMYCIN INJURY INDUCE HEPARAN SULFATE AND SYNDECAN SHEDDING	63
	5.2 SYNDECAN SHEDDING IN HUMAN IDIOPATHIC PULMONARY FIBROSIS	70
	5.3 FIBROTIC LUNG INJURY MODULATES EC-SOD AND SYNDECAN-1 DISTRIBUTION IN THE LUNG	74
	5.4 HEPARAN SULFATES & SYNDECAN-1 ARE OXIDATIVELY FRAGMENTED BY REACTIVE OXYGEN SPECIES	81

5.5	OXIDATIVELY FRAGMENTED HS AND SYNDECAN-1 INDUCE NEUTROPHIL CHEMOTAXIS.	84
5.6	OXIDATIVELY FRAGMENTED SYNDECAN-1 INDUCES ABHERRENT EPITHELIAL WOUND HEALING.....	92
5.7	SYNDECAN-1 ECTODOMAIN INDUCES FIBROGENESIS.....	97
6.0	DISCUSSION - PULMONARY FIBROSIS.....	99
6.1	CLINICAL SIGNIFICANCE AND FUTURE DIRECTIONS	104
7.0	RESULTS – CARDIAC FIBROSIS.....	107
7.1	LACK OF EC-SOD MODULATES CARDIAC MORPHOLOGY.....	107
7.2	LACK OF EC-SOD EXACERBATES LOSS OF CARDIAC FUNCTION.....	109
7.3	LACK OF EC-SOD RESULTS IN INCREASED FIBROSIS AFTER DOXORUBICIN.....	113
7.4	LACK OF EC-SOD AND OXIDATIVE INJURY INCREASES SHEDDING OF SYNDECAN-1, MYOCARDIAL INFLAMMATION, AND APOPTOSIS.....	116
8.0	DISCUSSION – CARDIAC FIBROSIS.....	121
8.1	CLINICAL SIGNIFICANCE AND FUTURE DIRECTIONS	125
9.0	FINAL DISCUSSION.....	128
	REFERENCES.....	131
	APPENDIX A : CURRICULUM VITAE.....	151

LIST OF TABLES

Table 1: Syndecan Expression by Cell Type	36
Table 2: Anatomic and Functional Cardiac Data for Wild type and EC-SOD KO mice.	109

LIST OF FIGURES

Figure 1: Generation of Hydroxyl Radicals Through a Fenton-like Copper Sulfate System.....	22
Figure 2: Schematic of EC-SOD Structure and Heparin Affinity	30
Figure 3: Syndecan Structure: Syndecans are composed of a transmembrane protein with a cytoplasmic, transmembrane and extracellular domain.....	40
Figure 5: Images and measurements of the Left Ventricle of the Heart.....	47
Figure 6: Heparan sulfate proteoglycans (HSPG) are shed into the BALF during asbestos induced injury	64
Figure 7: Syndecan expression in Primary Alveolar Epithelial Cells (AECs)	65
Figure 8: Syndecan-1 ectodomain is shed into the BALF during pulmonary fibrosis	67
Figure 9: Syndecan-1 changes in lung homogenates after asbestos exposure.....	68
Figure 10: Syndecan-4 ectodomain is shed into the BALF during pulmonary fibrosis	69
Figure 11: Syndecan-4 <u>trends</u> toward increased expression in lung homogenates after asbestos.....	70
Figure 12: IPF and normal volunteer pulmonary function and BALF characteristics.	71
Figure 13: Increased syndecan-1 ectodomain in the BALF and lung of IPF patients	72
Figure 14: Increased syndecan-4 in BALF and lung in IPF patients.....	72
Figure 15: Levels of BALF Syndecan-1 increase with all stages of IPF disease severity.....	73
Figure 16: H&E staining of control and IPF lung.....	74
Figure 17: Myofibroblastic foci within an IPF lung	75
Figure 18: Localization of EC-SOD and syndecan-1 in human lung sections	78
Figure 20: Localization of EC-SOD and syndecan-1 in mouse lung sections.....	79
Figure 21: EC-SOD and syndecan-1 expression by Real time RT-PCR.....	80
Figure 22: Superoxide production and fragmentation of heparin and heparan sulfate (HS).....	82
Figure 23: EC-SOD protects against oxidative shedding of Syndecan-1.....	83
Figure 24: Neutrophil chemotaxis is induced by ROS-fragmented heparin.....	85
Figure 25: EC-SOD inhibits neutrophil chemotaxis induced by oxidative fragmentation of heparin and HS.....	86
Figure 26: Antioxidant activity and direct binding of EC-SOD to heparan sulfate proteoglycan (HSPG) mediate inhibition of chemotaxis.....	87
Figure 27: Syndecan-1 ectodomain induces neutrophil chemotaxis.....	88
Figure 28: Oxidatively shed syndecan-1 ectodomain induces neutrophil chemotaxis.	89
Figure 29: Intratracheal instillation of EC-SOD decreases inflammation and prevents asbestos-induced shedding of syndecan-1	90
Figure 30: Toll-like receptor 4 partially mediates neutrophil chemotaxis induced by fragmented heparin.....	91

Figure 31: Chemotaxis induced by oxidatively fragmented HS is mediated through Integrin- β 1.	92
Figure 32: Primary mouse alveolar epithelial cells - type I pneumocytes.	93
Figure 33: Human syndecan-1 ectodomain (hS1ED) inhibits re-epithelialization of primary mouse AECs.	93
Figure 34: Human syndecan-1 ectodomain (hS1ED) inhibits wound healing while cell surface syndecan-1 promotes re-epithelialization	95
Figure 35: Syndecan-1 ectodomain peptide with GAG binding sites inhibits wound healing.	96
Figure 36: Asbestos fibers impair re-epithelialization of primary AECs	96
Figure 37: Human and mouse syndecan-1 ectodomains increase human lung fibroblast proliferation.	97
Figure 38: Syndecan-1 ectodomain induces TGF- β 1 bioavailability in human lung fibroblasts.	98
Figure 39: Summary of Oxidative Stress in the Lung.	103
Figure 40: Changes in left ventricular morphology are present in control EC-SOD KO mice and after doxorubicin treatment.	108
Figure 41: Lack of EC-SOD results in a significant decrease in cardiac function after doxorubicin.	111
Figure 42: Lack of EC-SOD and doxorubicin treatment lead to increases in extracellular oxidative stress.	112
Figure 43: Sirius red staining for collagen fibers in LV tissue.	114
Figure 44: Trichrome staining for collagen deposition in LV cardiac tissue.	115
Figure 45: Hydroxyproline analysis of collagen content in LV tissue.	116
Figure 46: Doxorubicin treatment cause alterations in antioxidant EC-SOD and syndecan-1 of the ECM.	119
Figure 48: Lack of EC-SOD exacerbates apoptotic cell death in LV tissue.	120

PREFACE

ACKNOWLEDGEMENTS

I would like to first thank my mentor, Tim Oury, for all of his guidance and support during the course of my PhD training. Your mentorship has taught me so much throughout the course of my training, not only how to do great science but how to balance work and life. I was so excited when you were awarded the prestigious MSTP Mentor of the Year Award because you truly are an example of an outstanding mentor. With what I have learned from you, I hope to one day be just as great of a mentor to others.

I would also like to thank the members of my thesis committee. Through your insightful suggestions and dedication to my progression as a physician scientist, you have each helped to shape and nurture my skills that will be so valuable for my future success.

I would also like to send special thanks to the present and past members of the Oury laboratory: Judson Englert, Beth Ganis, Fei Gao, Michelle Manni, Lasse Ramsgard, Lauren Jacob Tobolewski, Tomai, and Laura Voehtly. You always made the lab a lively place, even at 7am! Thank you for your help, support, and friendship – it has meant so much to me.

I would also like to thank my collaborators who have helped to shape my work and have provided wonderful scientific discussions. I hope to work with you all again. To my Pitt Medical School Class of 2009 and my MSTP class – your friendships have meant so much to me. Best of luck in all that you do!

Last but not least, I would like to thank my amazing family and friends for all of their support along the way. To my parents, you have shaped who I am and taught me how to find my passion in life, how to love and laugh, and the importance of giving to others. You offered every possible opportunity to me, for which I am grateful. Without your love and guidance, I would not be where I am today. Jolene, I am so lucky to have such a great sister. To Judson, it has been an amazing journey thus far and I am so happy that I have gotten to share so many special moments with you. You have been one of my greatest supporters. You have made life outside of science and medicine so great and I can think of no other smile that brightens my day more than yours. We sure make a great Chef duo in the kitchen and you truly are a “master of the grill” – always a potential second career choice! Thank you for bringing so much happiness to my life!

ABBREVIATIONS

ASB	Asbestosis	IPF	Idiopathic Pulmonary Fibrosis
α SMA	alpha Smooth Muscle Actin	KO	Knockout mice
BALF	Bronchoalveolar lavage fluid	mS1ED	Mouse Syndecan-1 ectodomain
Bleo	Bleomycin	MBD	Matrix binding domain
CuZnSOD	Copper Zinc Superoxide Dismutase	MnSOD	Manganese superoxide dismutase
DMEM	Dulbecco's Modified Eagle Medium	PMN	Polymorphonuclear leucocyte
DOX	Doxorubicin	ROS	Reactive Oxygen Species
ECM	Extracellular Matrix	RNS	Reactive Nitrogen Species
EC-SOD	Extracellular Superoxide Dismutase	SDS-PAGE	Sodium dodecyl sulfate – polyacrylamide gel electrophoresis
EF	Ejection Fraction (Cardiac)	siRNA	Small interfering riboneucleic acids
FGF	Fibroblast Growth Factor	TGF- β	Transforming growth factor β
FS	Fractional Shortening	TiO ₂	Titanium Dioxide
GST	Glutathione-S-Transferase	UIP	Usual interstitial pneumonia
HS	Heparan sulfate	WT	Wild type
HSPG	Heparan Sulfate Proteoglycan		
hS1ED	Human Syndecan-1 Ectodomain		

1.0 INTRODUCTION

Tissue remodeling and the development of fibrosis are reparative responses to injury and destruction of the pre-existing tissue structure. The body attempts to replace damaged cells and extracellular matrix, most commonly via the deposition of matrix components such as collagen and fibrin. The reversibility of fibrosis is under constant debate and differs by organ. In the lung and heart, chronic inflammation or injury and abnormal healing of residential cells can lead to fibrosis development. In order to move toward therapeutic options for pulmonary and cardiac fibrosis, a better understanding of the processes and mechanisms involved in fibrogenesis is required. Recent studies support a role for oxidative stress and antioxidant imbalances in the pathogenesis of both of these conditions.

1.1 IDIOPATHIC PULMONARY FIBROSIS

Idiopathic Pulmonary Fibrosis (IPF) is a detrimental interstitial lung disease characterized by severe and progressive fibrosis of the alveolar interstitium. In the United States, the prevalence of IPF is estimated to be 42.7 per 100,000 and the disease incidence to be 16.3 per 100,000¹. Patients develop symptoms of dyspnea (shortness of breath) and non-productive cough with presentation between 50-70 years old. IPF is slightly more common in males than females² and has a dismal prognosis with a 5-year mortality rate between 50-70%^{3,4}.

1.1.1 Pathophysiology

Pulmonary fibrosis can occur in various situations: due to an unknown stimuli (idiopathic); environmental/occupational exposure i.e. asbestos, silica; induced by pharmacological agents i.e. Bleomycin; radiation exposure and associated with other primary diseases such as scleroderma or familial forms^{2, 3}. While the pathogenesis of IPF remains unclear, inflammation and oxidant/antioxidant imbalances within the lung are believed to be involved^{5, 6}. Evaluation of bronchoalveolar lavage fluid (BALF) samples reveals increases in neutrophils, mild increases in eosinophils, and overall increases in cell counts³. Increases in BALF neutrophils and eosinophils suggest an increase likelihood of disease progression and lack of response to immunosuppressive agents^{4, 7, 8}. In IPF, these inflammatory cells may release exaggerated amounts of reactive oxygen species⁹. Studies show increased reactive oxygen species production in leukocytes from the serum and evidence of enhanced oxidative stress in plasma and BALF of IPF patients^{10, 11}. Levels of oxidative stress have been shown to negatively correlate with aspects of pulmonary function in IPF patients and may provide information about disease severity⁵.

1.1.2 Diagnosis and Pathological Findings

From the time of IPF diagnosis, there is a mean survival of 3-5 years^{3, 4}. A diagnosis of IPF is made from a thorough history and physical, chest radiography, pulmonary function tests, high resolution computed tomography (CT), and lung biopsy. In the presence of a surgical biopsy showing a histological pattern of Usual Interstitial Pneumonia (UIP), three major requirements must be met for diagnosis based on the American Thoracic Society/European Respiratory

Society consensus: 1) Exclusion of other causes of pulmonary fibrosis such as environmental exposures, drug toxicity or connective tissue disease 2) Associated abnormalities on high resolution CT or chest radiography 3) Impairment on pulmonary function tests^{3, 4}. Patients typically present with a history of greater than 3 months of dyspnea and a non-productive cough. On physical exam, bilateral dry inspiratory crackles may be appreciated at the lung bases. Chest radiography shows ground glass opacities and CT analysis shows irregular thickening of the alveolar septa. As fibrosis of the lung progresses, the normal lung architecture becomes distorted under the tension of the fibrosis. This change is often described as a “honeycomb” appearance of the lung¹². Histologically, IPF has a pattern of Usual Interstitial Pneumonia (UIP), which is characterized by areas of immature and mature fibrosis (temporal heterogeneity) and alveolar inflammation with intervening areas of normal tissue architecture¹². On H&E staining, myofibroblastic foci are present, which are light-staining areas of spindle-shaped mesenchymal cell expansion among collagen and matrix deposition. These foci are randomly dispersed throughout the lung and are a marker of active disease¹². Inflammation is also present and is assessed through bronchoalveolar lavage and interstitial microscopy which shows the presence of macrophages, neutrophils, eosinophils, mast cells and limited lymphocytes^{2, 12}.

1.1.3 Treatment

The primary cause of clinical deterioration and mortality in IPF patients is respiratory failure (38.7%), followed by heart failure (14.4%), bronchogenic carcinoma (10.4%), ischemic heart disease (9.5%), infection (6.5%), and pulmonary emboli (3.4%)^{2, 13}. Despite recent studies and advances in the understanding of the pathogenesis and clinical course, there are currently no effective therapies for IPF, aside from lung transplantation. Several options are available, such as

anti-inflammatories, however there are very few to no clinical studies that show significant improvements (some partial and transient) in progression-free survival, functional improvement or an increase in quality of life¹⁴. Over the last 50 years, corticosteroids have been commonly utilized to control inflammation. In retrospective studies, Flaherty et al. report that fewer than 20% of patients had improvement with corticosteroid therapy and that the severe side-effects of steroids were encountered including weight gain, osteoporosis, and hyperglycemia^{15, 16}. Chronic, low dose prednisone may be a maintenance therapy in responsive patients but is not recommended for all IPF cases^{3, 14}.

Immunosuppressive/cytotoxic agents, such as azathioprine and cyclophosphamide, are used in patients who are non-responsive to or cannot take corticosteroids. These agents have shown favorable results in 15-20% of IPF cases⁴. Azathioprine is a purine analog that inhibits adenine deaminase to impair leukocyte proliferation¹⁴. Raghu et al. completed a small comparative 1-year study of high dose prednisone therapy versus high dose prednisone plus azathioprine in IPF patients. While there was slightly less mortality in the azathioprine group when adjusted for age, they found no significant differences in clinical measures, such as forced vital capacity (FVC) and diffusion capacity of carbon monoxide (DLCO), with any of the therapies¹⁷. Cyclophosphamide is a cytotoxic alkylating agent and has shown no survival benefit in studies^{18, 19}. The side-effect profile and toxicity are profound^{14, 18} and limits the utility of cyclophosphamide. Due to the minimal efficacy of these immunosuppressive agents, the role of inflammation as a major driving force in IPF continues to be highly debated. Additional combination studies with these agents may be necessary.

Finally, anti-fibrotic agents such as colchicine and interferon gamma, have been tried but unsuccessful in humans. Colchicine functions by decreasing collagen formation in fibroblasts

and suppressing growth factor release by alveolar macrophages¹⁴. While colchicine showed promise *in vitro* and in animal models of pulmonary fibrosis^{20, 21}, it has shown no survival or lung function benefit in clinical IPF^{22, 23}. In a combination therapy study, Fiorucci et al. report finding no clinical improvements with prednisone alone or prednisone with either colchicine or cyclophosphamide in patients with early stage IPF²⁴. While many of these drugs are used as monotherapies or in combination, there have been no prospective placebo-controlled randomized trials performed.

Amidst the grim outlook of current therapies, the IPF research community continues to find new molecular targets. Pirfenidone, although not available in the United States or Europe, was successful in abrogating bleomycin-induced fibrosis in animal models^{25, 26} and shows potential for improving or stabilizing lung function in IPF patients²⁷. Lung transplantation is the only current option that prolongs survival in IPF patients. Considerations for lung transplantations should be made early on in the disease course, as the wait list time is around 46 months, during which time many patients with advanced disease die prior to transplant^{3, 14}. The 5 year survival post-transplant is approximately 40%²⁸.

1.1.4 Asbestosis – A related fibrotic lung disease.

While the cause of 41-70% of cases of pulmonary fibrosis is unknown, some are due to environmental or occupational inhalation of asbestos²⁹. Asbestosis is a prototypical pneumoconiosis that causes significant morbidity and mortality in patients and increases the risk of lung cancer and mesothelioma³⁰. Between 1940 and 1970, an estimated 27 million industrial workers were exposed to asbestos³¹. The intensity and duration of asbestos exposure is directly related to asbestosis development³². The majority of asbestosis and related-disease cases are

occupational exposures to the fibers. Workers in the cement, milling, insulation, shipyard and mining industries are at the highest risk of developing disease³³. During the 1980's, the United States placed restrictions on the use of asbestos, which has drastically decreased exposure risk³⁴. However, the risk of asbestosis remains in developing countries, such as India, that lack regulations. The development of severe disease has a latency of 20-40 years; therefore, it still remains a significant health concern in the United States as exposed individuals may still develop disease. Currently, there is no treatment available for asbestosis.

Asbestos is extremely chemical and heat resistant and has high tensile strength; properties which account for its industrial use. Various types of asbestos fibers can cause asbestosis. Fibers are identified through two main groups: amphiboles (crocidolite, amosite, tremolite, anthophyllite, and actinolite – straight fibers) and serpentines (chrysotile - curly fibers)³⁵. All of the fiber types are fibrous silicates with variable mineral components including iron, magnesium, sodium and calcium. Chrysotile accounts for greater than 95% of the fiber type used in US industry in the past^{30, 35}. Amphiboles such as crocidolite were also used the U.S. and are more potent in causing disease, most likely due to their straight, non-pliable structure and the inability of the lung to clear them³⁰.

Histologically, asbestosis emulates the fibrosis pattern of idiopathic pulmonary fibrosis (IPF) with the additional presence of asbestos bodies in tissue sections. The fibrosis is primarily heterogeneous and patchy with a subpleural distribution in the bases of the lungs³⁶. After inhalation, asbestos fibers get embedded in the lung parenchyma and alveolar macrophages attempt to phagocytose them. If the fibers are too large for the macrophage to digest, the fibers become asbestos bodies³⁷, where they are coated in an ferrous-proteinous-mucopolysaccharide material making them appear as beaded rod-like structures. Asbestos bodies commonly form

during human disease but do not in mice³⁷. These structures are less fibrogenic and cytotoxic than uncoated asbestos fibers³⁷, which suggests that this is a compensatory host defense response. Another hallmark of asbestosis includes the presence of parietal pleural plaques with pleural thickening which suggest asbestos exposure³².

Asbestos can lead to increased oxidative stress directly and indirectly. Asbestos fibers contain transition metals on their surface which can redox cycle and participate in direct ROS generation^{38, 39}. This has led to the “amphibole hypothesis” that states that amphiboles participate in redox cycling through their high iron content and that this contributes to asbestos-induced inflammation, injury and fibrosis^{40, 41}. Studies also show increased superoxide production indirectly through oxidative bursts from recruited neutrophils and macrophages exposed to asbestos^{42, 43}. Asbestos also causes injury through altering epithelial barrier function⁴⁴, inducing apoptotic cell death^{45, 46} and activating inflammatory^{43, 47, 48} and fibrogenic pathways^{49, 50}. Reactive oxygen species produced by asbestos fibers have been shown to activate profibrotic TGF- β in the lung^{39, 50}, which is important in fibrosis development.

1.2 EXPERIMENTAL ANIMAL MODELS OF PULMONARY FIBROSIS

Pulmonary fibrosis is modeled *in vivo* using several injury models that involve a stimuli with subsequent alveolar injury, inflammation and fibrosis development. The stimuli commonly used are Bleomycin (intratracheal, subcutaneous, or intraperitoneal administration), asbestos and silica, which are administered intratracheally or via an inhalation chamber. Each animal model has advantages and disadvantages that should be considered when choosing a model to use in experiments.

1.2.1 Bleomycin

Bleomycin is an antineoplastic antibiotic used in the treatment of lymphomas, testicular carcinomas and squamous cell carcinomas of the cervix, head and neck^{51, 52}. One detrimental side effect is lung fibrosis, which has provided utility in the animal model. It is thought that lung toxicity occurs due to the low levels of bleomycin hydrolase, an enzyme active in Bleomycin inactivation and metabolism^{51, 52}. Bleomycin forms a complex with redox-active iron, molecular oxygen and DNA, resulting in DNA strand breaks⁵¹. Bleomycin also produces superoxide and hydroxyl radicals that can damage cell membranes, lipids, and proteins⁵³. Studies support the involvement of oxidative species as antioxidants can prevent the injury, such as N-acetylcysteine and desferoxamine administration⁵⁴ and extracellular superoxide dismutase overexpression⁵⁵, a lack of ROS decreases fibrosis development⁵⁶, and a lack of superoxide dismutase exacerbates the injury⁵⁷.

Pathologically, Bleomycin causes an acute neutrophilic inflammatory response in the lung between 1-3 days. The alveolar spaces become hypercellular and the inflammation switches to a chronic lymphocyte-predominant response⁵⁸. The loss of epithelial cells results in subsequent fibrosis that begins around day 7 with the accumulation of fibroblasts and matrix deposition^{55, 57-59} and peaks between day 14 and 21. The fibrosis may resolve after day 21 which should be considered in experimental design. Regardless, Bleomycin is the most commonly used model.

1.2.2 Asbestos

The mouse model of asbestosis⁶⁰ produces a progressive, peribronchial and alveolar septal fibrosis with similar pathology to that seen in humans⁶¹ (temporal heterogeneity) and therefore provides an ideal way to study the mechanisms of asbestosis, IPF, and particle injury. Fiber size can range from 1-5 μ m in diameter and up to 200 μ m in length⁶². The disease course begins with an initial acute inflammatory response. Activated macrophages, neutrophils and eosinophils are present in the alveolar spaces within 24 hours of exposure⁶³. The activated alveolar macrophages attempt to clear the fibers and some fail to engulf medium and large asbestos fibers. The leukocytes respond to the asbestos insult by releasing cytokines and reactive oxygen species^{43, 64}, which can shift the oxidant/antioxidant balance. The fibers can remain for long periods of time in the lung interstitium and cause hyperplasia of Type II pneumocytes, fibroblasts, and smooth muscle cells^{62, 65}. By day 7, peri-bronchial fibrosis and alveolar septal thickening in a temporally heterogeneous pattern begins to form through deposition of collagen, elastin and matrix components^{66, 67}. The fibrosis is progressive and is unresolved out to 1-year post-asbestos exposure (unpublished observation from the laboratory of Dr. Tim Oury). Several benefits of the asbestos model over the Bleomycin model include: 1) the presence of fibers in BALF and histological sections of lung which confirms that the animal was treated; 2) the fibrosis is progressive and does not resolve, unlike Bleomycin.

1.2.3 Silicosis

Silicosis is another type of pneumoconiosis in humans, which has been utilized as an animal model of lung injury. Silica (SiO₂) is a crystalline tetrahedral particulate that can enter the distal

respiratory tract and cause fibrosis in humans and animals⁶⁸. Similar to the asbestos model, intratracheal instillation of silica results in an acute accumulation of inflammatory cells (neutrophils, macrophages, lymphocytes, and occasional eosinophils) in the alveolar spaces and interstitium⁶⁹⁻⁷¹, damage to epithelial cells^{72, 73}, and subsequent collagen deposition⁷⁴⁻⁷⁶ and fibrosis development^{76, 77}. The fibrosis is characterized by silicotic nodules with a core of hyalinized collagen and fibroblasts⁶⁸. Activated leukocytes play a large role in the production of cytokines and growth factors, such as TNF- α and TGF- β , that are believed to be involved with the injury and repair⁷⁸⁻⁸⁰.

1.3 THE PATHOGENESIS OF PULMONARY FIBROSIS

The underlying processes of pulmonary fibrosis are currently thought to involve the presence of a persistent stimuli or injury and dysregulated repair of the lung that results in fibrosis². The role of inflammation remains unclear. In idiopathic pulmonary fibrosis, the lack of an identifiable cause creates a challenge for studying pathogenesis. The asbestos and bleomycin animal models discussed previously offer insight to the pathogenesis.

1.3.1 Re-epithelialization and Alveolar Wound Healing

Type I epithelial cells comprise 95% of the alveolar surface in the lung^{81, 82}. They create the tight junctions of the lung and are critical for gas exchange. Type II cells are cuboidal pneumocytes that are progenitor cells for type I cells and function to produce proteins for the lung such as surfactant⁸². Epithelial injury is thought to be one of the initial steps in the pathogenesis of

pulmonary fibrosis. Furthermore, analysis of UIP lung biopsies revealed a significant loss in type I epithelial cells in fibroblastic foci and areas of lung deterioration, along with increases in epithelial apoptosis markers⁸³. The loss of alveolar epithelial cells has several effects⁸¹. When Type I cells are lost, the gas exchange and permeability barrier becomes disrupted and allows fluid leak in and out of the lung. This also allows for the entry of migrating leukocytes and interstitial fibroblasts. The loss of type II cells results in a decreased progenitor cell population for replacing epithelial cells and a decrease in active transport abilities of the cell surface⁸¹. After epithelial cell death, the basement membrane of the alveolar surface is left denuded and exposed. Apoptosis is thought to occur in IPF alveolar epithelial cells through pro-apoptotic signaling of Bid and Fas-ligand^{84, 85}.

Epithelial wound healing or re-epithelialization is a concerted effort by various cells types to restore the lung after an injury or cell death. Mesenchymal cell, such as myofibroblasts, undertake matrix synthesis to form a suitable scaffold upon which epithelial cells can repopulate lost cells. Integrins are membrane bound receptor proteins that aid cells in cell-cell and cell-matrix interactions and are critical in coordinating the healing process through the migration, proliferation and differentiation of cells^{81, 86}. Integrins are heterodimeric proteins composed of α and β subunits. There are approximately 18 different α subunits and 8 β , that are expressed by a variety of cells types and have variable ligand affinities⁸⁶. For example, $\alpha v \beta 6$ is restricted to epithelial cells and $\alpha 1 \beta 1$ is more ubiquitously expressed with a high binding affinity for collagen⁸⁶.

The role of integrins in pulmonary fibrosis is suggested in both human IPF⁸⁶⁻⁸⁸ and animal models⁸⁹⁻⁹¹. Abnormal integrin signaling has been seen in fibroblasts from IPF patients⁸⁸. In the Bleomycin model, neutralizing antibodies against integrins are capable of reducing

fibrosis and lung injury^{91, 92}. Integrins may also modulate the biological activity of growth factors. Sheppard et al. show that integrin $\alpha v\beta 6$ is involved in the binding and activation of latent TGF- β during pulmonary fibrosis and that mice lacking this integrin have exaggerated inflammation but diminished fibrosis development^{90, 93}. Additional research is required to explore the potential roles of integrins in pulmonary fibrosis.

1.3.2 Inflammation

The role of inflammatory cells in pulmonary fibrosis is a controversial issue. Therapeutic studies that target inflammation, such as corticosteroids, have failed to show clinical benefits^{15, 19, 23}. However, several studies have highlighted associations between the presence of inflammatory cells and disease prognosis. Neutrophilia and eosinophilia are seen in the bronchoalveolar lavage fluid (BALF) of 70-90% and 40-60% of IPF patients, respectively³. This increase in inflammatory cells has been associated with a worse prognosis and mortality in some clinical studies^{7, 94, 95}. Immune activation and inflammation have been shown to play an important role in fibrosis models^{48, 79}.

When the lung is challenged with a stimuli such as asbestos, additional leukocytes are recruited acutely to aid in re-establishing lung homeostasis. Inflammatory cells can damage the lung through the release of oxidative species, proteases (i.e. matrix metalloproteinases, elastase), peroxidases (i.e. myeloperoxidase), cytokines and growth factors^{96, 97}. This suggests that inflammation can contribute to a pro-fibrotic environment, affecting the wound repair process and the extent of remodeling. An acute inflammatory phase is a characteristic part of asbestos and Bleomycin-induced models^{43, 57, 58, 63}. Studies suggest that chemotactic factors and neutrophils, which are characteristic of this acute phase, are present in IPF^{98, 99}. The role of

inflammation has not been delineated in human disease, which likely explains why pulmonary fibrosis is still considered to be a disease of abnormal wound repair.

1.3.3 Growth Factors and Cytokines

Growth factor and cytokines/chemokines produced by the epithelium have been implicated in pulmonary fibrosis. The alveolar epithelium produces mediators such as TGF- β ¹⁰⁰⁻¹⁰³, platelet-derived growth factor (PDGF)^{104, 105} and TNF- α ^{96, 104, 106}, that alter the microenvironment of the lung. Unregulated local production of these mediators can mediate fibrogenesis and inflammation in the lung. Transforming growth factor- β (TGF- β) is a profibrotic protein released primarily by alveolar epithelial cells and macrophages within the lung. TGF- β has multiple functions including inducing the expression of collagens, proteoglycans and matrix components by fibroblast/myofibroblasts^{59, 102, 107}, is chemotactic to macrophages and fibroblasts, and can stimulate further cytokine production. Studies show that increased expression of this protein in alveolar epithelial cells leads to the development of fibrotic lesions¹⁰². TGF- β has also been shown to regulate inflammatory responses. It can drive Tcells toward a T_H-helper 17 phenotype by increasing the cellular response to cytokines, such as IL-23, which promote the resolution of inflammation¹⁰⁸. It also decreases superoxide production by macrophages¹⁰⁹, which have a key role in inflammatory responses. Kahlil et al. suggest that TGF- β 1 expression occurs in epithelial cells and macrophages in IPF lung and epithelial expression occurs only after chronic lung injury¹⁰⁰. TGF- β signals through intracellular Smad intermediates. Profibrotic Smads (Smads 2, 3, and 4) are increased in bleomycin-induced lung fibrosis, while anti-fibrotic Smad7 is

decreased¹¹⁰. Smad3 null mice are also resistant to TGF- β -induced pulmonary fibrosis¹¹¹, supporting the role for TGF- β signaling in fibrosis development.

Platelet derived growth factor (PDGF) is secreted by alveolar epithelial cells and induces the migration, growth and ECM synthesis of fibroblasts and smooth muscle cells¹⁰⁵. PDGF is a polypeptide formed by two chains (PDGF-1, A and PDGF-2, B). Studies have reported significant increases in PDGF-2 mRNA expression in alveolar epithelium from IPF lungs¹⁰⁵. Tumor necrosis factor (TNF- α) is a pro-inflammatory cytokine that has been implicated in pulmonary fibrosis^{112, 113}. TNF- α transgene expression in alveolar epithelial cells leads to fibrosis development¹¹⁴. It has also been linked to NF- κ B activation in asbestos-induced fibrosis¹¹⁵ and has a suggested role in eosinophil recruitment and activation¹⁰⁶.

1.3.4 Fibroblasts, Matrix Deposition and Turnover.

The mesenchymal cell population is an active participant in remodeling of the lung in IPF. Fibroblast expansion and excessive productivity of matrix components are features of pulmonary fibrosis^{116, 117}. Spindle-shaped myofibroblasts are characterized by the expression α -smooth muscle actin, increased collagen production and cytokine gene expression, and increased contractile properties¹¹⁸. Myofibroblasts appear during the active phases of fibrosis and the presence of these specialized cells has been documented both in human pulmonary fibrosis and animal models^{107, 116, 117, 119}. Myofibroblasts are potentially derived from 3 origins, the last two options being controversial: 1) fibroblasts directly differentiating into myofibroblasts by gaining additional characteristics of smooth muscle cells 2) epithelial-mesenchymal transition (epithelial

cell transdifferentiation to myofibroblasts)^{89, 120, 121} 3) from circulating fibrocytes or bone marrow progenitor cells¹²².

The extracellular matrix (ECM) is critical for maintaining a strong structure that can withstand mechanical stretch and recoil of the lung. Matrix deposition occurs primarily through fibroblasts and myofibroblasts but can involve endothelial and epithelial cells. The ECM is composed of various molecules including collagen, elastin, fibronectin, proteoglycans (discussed in section 1.7), hyaluronan, and laminin⁸¹. Pulmonary fibrosis is characterized by often drastic changes in the extracellular matrix, which can be the result of excessive deposition (an increase in collagen deposition^{2, 116, 117}), an impairment in ECM degradation and resolution or a combination of these two. Thus, ECM changes become very complex over the pathogenic course of IPF.

1.3.5 Matrix Metalloproteinases

ECM degradation and turnover is regulated by the activity of matrix metalloproteinase enzymes (MMPs) and their tissue inhibitor counterparts (TIMPS). MMPs are matrix degrading proteinases (currently a total of 22) that have been shown to be upregulated in models of pulmonary fibrosis^{123, 124}. The substrates of MMPs are extracellular matrix components and soluble factors and include, but are not limited to, the following: 1) MMP 1, 8 and 13 are collagenases targeting collagens I, II, III, VII, X, gelatin and pro-TNF- α ; 2) MMP 2 and 9 are gelatinases targeting type IV and V collagen, gelatin, elastin, fibronectin, pro-TGF- β , and pro-TNF- α ; 3) MMP3, 10 and 11 are stomelysins that target proteoglycans, laminin, fibronectin, gelatin and pro-TNF- α ; and 4) MMP 7 (matrilysin) targets proteoglycans, collagens, laminin,

decorin, gelatin, and fibronectin¹²⁵. The majority of MMPs are synthesized as proenzymes and activated by proteolysis of a cysteine-zinc pro-domain, called a “cysteine switch”^{125, 126}. Reactive oxygen species are also capable of activating MMPs, increasing their transcription, and deactivating proteases¹²⁶⁻¹²⁸. Thus, oxidants may play a significant role in unregulated activity of MMPs in pulmonary fibrosis. Tissue inhibitors of metalloproteinases (TIMPs 1-4) are extracellular or membrane bound enzymes that bind tightly to MMPs to inhibit their degradative activity¹²⁵.

In IPF patients, MMP 2 and 9 and TIMPs 1 and 2 are elevated in areas of alveolar damage and at disrupted basement membranes¹²⁹. McKeown et al. report increases in MMP 3, 7, 8 and 9 in BALF from IPF patients with levels higher in patients with earlier mortality¹³⁰. Rosas et al. report increases in MMP1 and 7 in serum, BALF and lung tissue in IPF patients, suggesting they may be blood biomarkers for IPF¹³¹. Increases in MMP7 expression have also been reported¹³². Animal studies show similar results with increases in MMP2 and 9 in the fibrotic phase of bleomycin-induced fibrosis¹²³. Cabrera et al. report that an over-expression of MMP9 diminishes bleomycin-induced fibrosis¹³³. While there are differences in findings related to the role of MMPs in pathogenesis, the balance of MMPs and TIMPs is likely complex along the course of fibrogenesis in the lung.

1.4 CARDIAC FIBROSIS AND CARDIOMYOPATHY

1.4.1 Causes and Pathophysiology

The most common cause of myocardial dysfunction is a primary or secondary dilated cardiomyopathy (DCM)¹³⁴. The WHO characterizes dilated cardiomyopathy as the dilation and impaired contraction of the left ventricle or both and causes of DCM include idiopathic, viral and/or immune, alcoholic/toxic, or associated with another cardiovascular disease¹³⁵. DCM typically presents with progressive heart failure. One agent that leads to chronic remodeling and DCM is doxorubicin, an anthracycline chemotherapeutic agent used to treat a wide variety of cancers^{136, 137}. The most common and dose-limiting side effect is the cardio-toxicity involving cardiac fibrosis that leads to non-ischemic dilated cardiomyopathy and congestive heart failure¹³⁶. Doxorubicin-induced cardiac injury and fibrotic remodeling in the heart are thought to involve reactive oxygen species (ROS) and oxidant/antioxidant imbalances. The cytotoxic activity of doxorubicin comes from its intercalation within DNA, which causes single and double strand breaks.

The primary mechanism of doxorubicin-induced myocardial damage involves the generation of oxidative stress through quinone-semiquinone reduction-oxidation reactions¹³⁸. Single electron reduction of a ring within the structure of doxorubicin results in a semiquinone radical that further reduces oxygen forming superoxide radicals¹³⁹. Intracellular radical generation has been shown with doxorubicin, however, the role of extracellular radicals remains unclear. Cellular ultra-structural pathology includes cytoplasmic vacuolization and loss of myofibrils¹⁴⁰.

1.4.2 Diagnosis, Pathological Findings and Treatment Options

Doxorubicin-induced cardiac fibrosis and dilated cardiomyopathy can occur at any point during the doxorubicin treatment process, from soon after initial treatment to months or years after the discontinuation of the drug. A total dosage of doxorubicin as low as 250mg/m² can cause toxicity and more than 30% of doxorubicin-recipients develop cardiac dilation and ventricular failure^{139, 140}. **There are currently no therapies for the prevention or treatment of this cardio-toxicity.** Patients are followed through baseline and follow-up cardiac functional testing via echocardiography¹⁴⁰. If decreases in ejection fraction and associated symptoms develop, treatment must be discontinued, however this does not preclude further progression of fibrosis. Patients who develop severe heart failure require heart transplantation¹³⁶. Studies suggest that adding antioxidants, such as flavonoids or Vitamin C and E, to dox administration may help to prevent the cardiac injury^{141, 142}. Despite this detrimental side-effect of doxorubicin treatment, it is still used in combination chemotherapy regimens because of its anti-tumor efficacy¹⁴³. Additional studies are required to understand the roles of key antioxidants so that better strategies can be developed to limit dox cardiac toxicity.

1.4.3 Doxorubicin Experimental Animal Model of Cardiac Fibrosis.

Doxorubicin cardiac injury progresses to fibrosis of the left ventricle. Typical dosing in animals ranges from 15-25 mg/kg per animal via intraperitoneal injection. The literature describes an important role for free radicals in the development of cardiac damage induced by doxorubicin¹⁴³. Doxorubicin also decreases glutathione peroxidase antioxidant activity and protein levels in animal models¹⁴⁴. Apoptosis has been proposed as a mechanism of doxorubicin-induced cell loss

and dysfunction and is oxidant dependent (H_2O_2 -mediated)^{138, 145, 146} and independent¹⁴⁷. The doxorubicin model provides a model of oxidant mediated cardiac fibrosis to study pathogenesis.

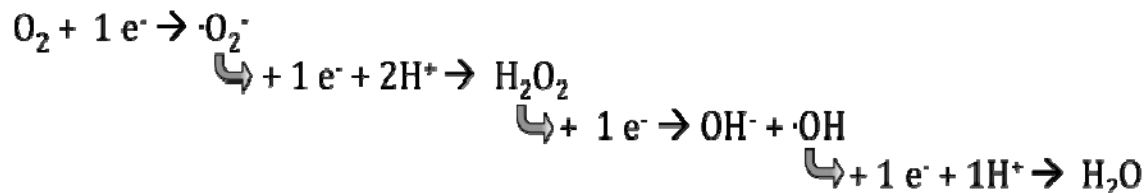
1.5 OXIDATIVE STRESS AND REACTIVE OXYGEN SPECIES

Oxidative stress is defined as the imbalance of oxidant species and antioxidant mechanisms, where oxidants dominate and can lead to tissue damage and cellular dysfunction. Free radicals are species that contain one or more unpaired electron allowing them to react with other molecules. Reactive oxygen species (ROS) are reduction-oxidation reaction and free radical products of oxygen and can be produced through electron leak from mitochondrial metabolism, enzymatic reactions (xanthine oxidase) and released from activated leukocytes^{134, 148}. ROS have the ability to react with local lipids, proteins, DNA, etc, to alter their structure and function. Reactive nitrogen species (RNS) are products of nitrogen reactions and are briefly discussed.

When considering oxidative stress, the lung is unique due to its exposure to higher oxygen tensions than other tissues. The oxygen pressure of inhaled air is 20kPa (150 mm Hg). Pressures in venous blood flow are around 6kPa (45 mm Hg) and may be as low as 0.13kPa in some tissues, while the oxygen at the alveoli of the lung is ~13.3 kPa (100 mm Hg)¹⁴⁹. Thus, the lung is constantly facing high oxygen tensions and oxidative insults. Unregulated production of ROS and RNS in the lung and other tissues can lead to an imbalance in oxidants to antioxidant species resulting in oxidative stress and nitrosative stress respectively.

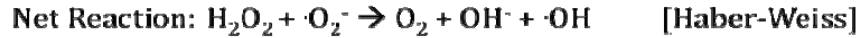
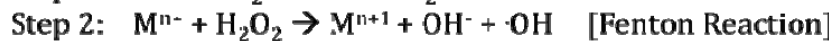
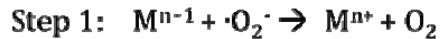
1.5.1 Reactive Oxygen Species

Diatomic oxygen O_2 is considered to be a free radical species because it has 2 unpaired electrons (di-radical). While not very reactive itself, oxygen can undergo a sequence of one-electron reductions to achieve more reactive oxygen by-products:



Free radical superoxide ($\cdot O_2^-$) is formed from one-electron reduction of oxygen and can undergo a subsequent one-electron reduction, as depicted above, or dismutation either spontaneously or through enzyme catalysis (superoxide dismutases) to form hydrogen peroxide (H_2O_2)^{134, 148}. Superoxide is not as damaging as other radical species but is important in their production such as H_2O_2 and hydroxyl radicals. While H_2O_2 is not a free radical, it is still a common reactive oxygen species albeit less reactive than hydroxyl radicals. A unique feature of H_2O_2 is that it can traverse cell membranes freely. Therefore, gaining it access to signal within the cell and damage intracellular organelles, proteins, and DNA. Additional single electron reductions of H_2O_2 form hydroxyl radical ($\cdot OH$), which is the most reactive species, and finally H_2O . Hydroxyl radical can be formed from the reaction of H_2O_2 with metal ions or breakdown of peroxyxynitrite (see section 1.5.2). It is one of the most reactive radicals and acts on local substrates at reaction rate between 10^7 – $10^{11} M^{-1}s^{-1}$ ¹³⁴. The half-life of hydroxyl radical is in the milliseconds range. The Fenton and Haber-Weiss reactions are the two most important mechanisms for the generation of hydroxyl radicals from transition metals. The Haber-Weiss reaction generates hydroxyl radicals from hydrogen peroxide and superoxide^{134, 148}.

FENTON-CATALYZED HABER-WEISS REACTION



M^{n+} = Transition metals such as Fe^{2+} or Cu^+

The Fenton reaction involves transition metal catalysis. Metals such as iron are typically bound to proteins and not readily free within the body to participate in these types of reactions. Therefore, this step may not occur as frequently. Asbestos fibers offer a unique reduction-oxidation potential because they contain varying amounts of free iron that can catalyze ROS production. Crocidolite and amosite asbestos fibers can contain up to 27% iron, where as chrysotile is between 1-6%¹⁵⁰. Indeed, free radical production has been observed with asbestos in cell and cell-free systems^{38,42}.

Within the laboratory, hydroxyl radicals can be generated through a Fenton-like system utilizing copper(II) sulfate and hydrogen peroxide¹⁵¹. Step 1, in figure 1 below, involves production of superoxide from oxidation of H_2O_2 and reduction of copper(II) to copper(I). In step 2, superoxide can further reduce additional Cu(II) to replenish Cu(I) within the system. In step 3, the reduction of hydrogen peroxide forms hydroxyl radicals via a Fenton-like reaction. Free radical production can be controlled by the presence of extracellular superoxide dismutase (EC-SOD), which scavenges superoxide. In the asbestos model of pulmonary fibrosis, free radicals are produced within the lung. We utilize the copper(II) sulfate and hydrogen peroxide system to model this free radical generation *in vitro*.

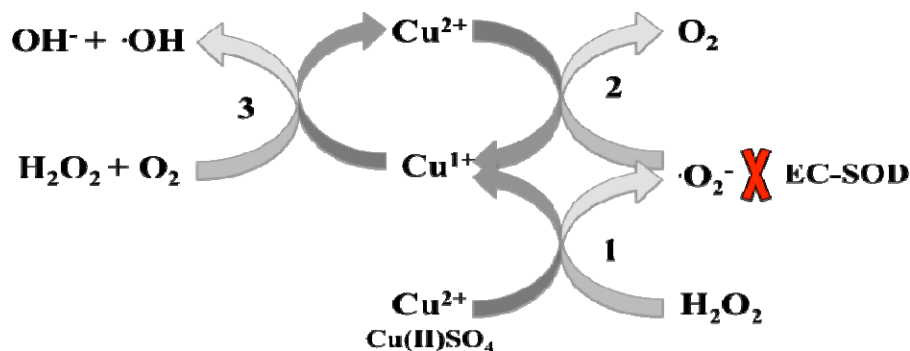


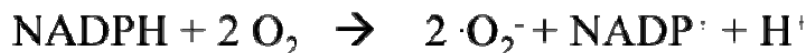
Figure 1: Generation of Hydroxyl Radicals Through a Fenton-like Copper Sulfate System: CuSO_4 and H_2O_2 are utilized to generate superoxide and hydroxyl radicals *in vitro*. Step 1: the production of superoxide from oxidation of H_2O_2 and reduction of copper(II) to copper(I); step 2, superoxide can further reduce additional Cu(II) to replenish Cu(I) ; step 3, the reduction of hydrogen peroxide forms hydroxyl radicals via a Fenton-like reaction.

In vivo, other mechanisms for free radicals and ROS generation include electron leak from mitochondrial metabolism, enzymatic reactions (xanthine oxidase) and released from activated leukocytes through oxidative bursts¹⁴⁸. The mitochondrial respiration chain culminates with the transfer of electrons to oxygen. Electrons can leak from this system and reduce oxygen to generate superoxide, which can undergo further reduction to form additional ROS. Intracellular scavenging enzymes help to balance this oxidative stress on the cell. Enzymatic production of ROS is highlighted through xanthine oxidase reaction with hypoxanthine in the presence of O_2 , producing superoxide, xanthine, urate and H_2O_2 . The importance of xanthine oxidase has been shown in both cardiovascular ischemia/reperfusion¹⁵²⁻¹⁵⁴ and pulmonary injury¹⁵⁵⁻¹⁵⁷.

Another primary source of large amounts of ROS are activated leukocytes (neutrophils, macrophages, eosinophils). The innate function of the leukocyte is to remove microorganisms through phagocytosis to protect the body from infection. Once a foreign body is ingested, the leukocyte produces an “oxidative burst” of ROS through an NADPH oxidase complex at the cell

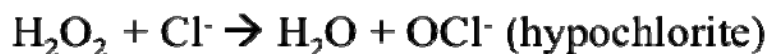
membrane. The oxidase catalyzes one or two electron reductions to form superoxide and H₂O₂, respectively, see below, that can kill a microbe or damage host tissues if released from the cell^{148, 158, 159}. Not only can the ROS damage tissues but they are involved in intracellular and extracellular signaling that can alter cell functions^{158, 160}.

NADPH Oxidase



Myeloperoxidase (MPO) is a second enzyme found in neutrophil azurophilic granules that aids in bacterial killing and can participate in redox reactions. MPO utilizes H₂O₂ and chloride ions to produce toxic hypochlorous acid (HOCl) or bleach.

MPO

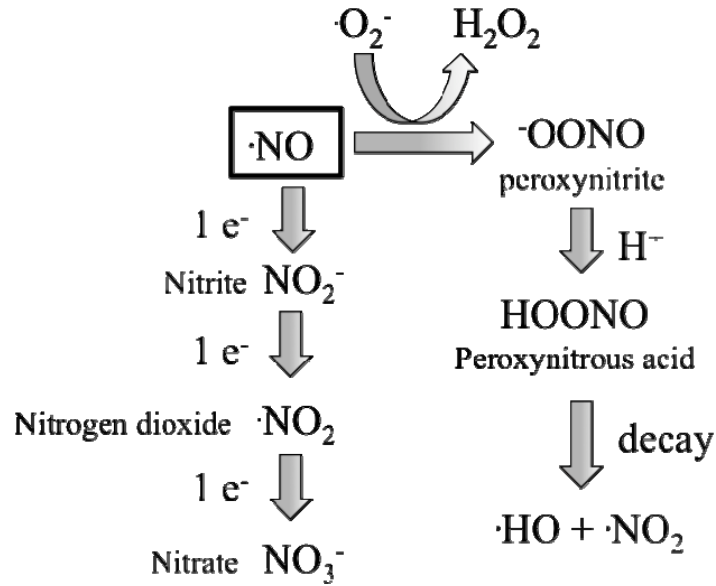


MPO has been implicated in cardiovascular damage, oxidative modifications to proteins in vessel walls and in atherosclerosis^{161, 162}. MPO is a highly cationic enzyme allowing it to localize to cell surfaces, especially endothelial surfaces, through interactions with glycosaminoglycan chains. HOCl can participate with hydroxyl radical in the fragmentation of extracellular matrix components such as hyaluronan and glycosaminoglycan side chains like heparan sulfate¹⁶³⁻¹⁶⁵. MPO has also been shown to catalyze the metabolism of nitric oxide (NO) to nitrite (NO₂⁻) through radical intermediates¹⁶⁶. Eosinophil peroxidase is the eosinophil equivalent of MPO and has similar biological activity.

1.5.2 Reactive Nitrogen Species

The excess of reactive nitrogen species within a system leads to nitrosative stress. Nitric oxide ($\cdot\text{NO}$) is an important nitrogen species produced by nitric oxide synthase enzymes through metabolism of L-arginine. There are three NOS enzymes, two of which are constitutively expressed: endothelial eNOS, neuronal nNOS (both constitutive) and inducible iNOS. Twenty times more $\cdot\text{NO}$ is produced by iNOS than the other enzymes¹⁴⁸. iNOS activity is induced by external stimuli such as bacterial lipopolysaccharide¹⁶⁷. Nitric oxide and iNOS are important in both pulmonary fibrosis^{168, 169} and doxorubicin-induced cardiac toxicity^{170, 171}.

The radicals produced by reduction of oxygen can react with freely diffusible nitric oxide to form additional radical species (see the following diagram), in effect inactivating nitric oxide, which is a potent signaling molecule (i.e. the inactivation of NF- κ B¹⁷²) and vaso-relaxant¹⁶⁷. Peroxynitrite anion (ONOO^-) can be formed through the reaction of superoxide with nitric oxide ($\cdot\text{NO}$) or by reactions between hydrogen peroxide and nitrite. Peroxynitrite is a powerful oxidant that can modify tyrosine residues producing nitro-tyrosine and oxidize thiols. At a physiologic pH, the protonated form of peroxynitrite (peroxynitrous acid) will decompose into hydroxyl radical and nitrogen dioxide. One electron reduction reactions of $\cdot\text{NO}$ will form nitrite, nitrogen dioxide, and nitrate.



1.5.3 Antioxidant Defenses

The lung and heart are continuously exposed to oxidative stress. A high oxygen tension in the lungs makes it particularly vulnerable to altered oxidant levels. The body uses several mechanisms to protect cells by counter-balancing oxidants¹³⁴. There are three superoxide dismutase (SOD) enzyme isoforms including intracellular CuZn SOD (SOD1), mitochondrial manganese MnSOD (SOD2), and extracellular CuZn SOD (SOD3) that catalyze the dismutation reaction of superoxide to produce H_2O_2 . CuZnSOD or SOD1 is found in the cytosol, nucleus, peroxisomes and mitochondrial inner membrane and functions to reduce intracellular levels of ROS^{173, 174}. MnSOD is found within mitochondria to eliminate ROS produced by mitochondrial respiration¹⁷³. Extracellular SOD is covered in more detail in section 1.6. Catalase, another antioxidant enzyme, catalyzes the reduction of H_2O_2 to H_2O . Glutathione peroxidase catalyzes the oxidation of thiol-containing glutathione to GSSG by H_2O_2 . It is also capable of decomposing other organic peroxides¹⁷⁵. Additional molecules such as vitamins (i.e. Vitamin A,

ascorbate or Vitamin C, α -tocopherol or Vitamin E) and albumin can also regulate levels of reactive species directly or indirectly by interacting with intermediates, such as albumin binding MPO¹⁷⁵. Metal binding proteins or chelating agents (i.e. transferrin, lactoferrin, desferoxamine) can also effectively remove metals that would otherwise participate in reduction-oxidation reactions^{134, 148, 175} and the production of oxidative and nitrosative species.

1.5.4 Oxidative Stress in Fibrosis

Oxidative stress has been implicated in many diseases such as pulmonary fibrosis^{6, 9, 11, 176}, cardiac injury^{139, 142, 177}, neurodegeneration^{178, 179}, and aging¹⁸⁰⁻¹⁸². Several studies have found evidence of increased oxidative stress in idiopathic pulmonary fibrosis. Increased markers of oxidative stress in have been reported in bronchoalveolar lavage fluid (BALF) of IPF patients (8-isoprostane)¹⁸³, as well as, in exhaled breath condensate (hydrogen peroxide and 8-isoprostane)¹⁷⁶ and were negatively correlated with pulmonary function in both studies. Decreased antioxidant enzyme status in patients with IPF has also been reported, such as decreased glutathione levels in alveolar epithelial lining fluid^{6, 184}. Kunnula et al report significant decreases in extracellular SOD in fibrotic regions of UIP lungs⁶¹, which suggests that oxidative stress would be increased in these areas.

Animal models of pulmonary fibrosis have offered opportunities to further evaluate the role of oxidative stress. In both models of Bleomycin- and asbestos-induced pulmonary fibrosis, extracellular superoxide dismutase protects against inflammation and fibrosis development^{57, 63, 185}. The extracellular matrix, such as hyaluronan, of the lung is also sensitive to oxidative stress during pulmonary fibrosis¹⁸⁶.

Oxidative stress is central to the pathogenesis of cardiac fibrosis caused by ischemia reperfusion injury such as myocardial infarction and by doxorubicin-induced cardio-toxicity. Doxorubicin treatment in patients causes increases in free radical species^{138, 187, 188} and has been shown to decrease the expression of cardiac antioxidants^{139, 144}. Supplementation with vitamin E, C, and A have provided antioxidant protection against cardiomyocyte death and have improved survival in CHF models and doxorubicin-induced injury^{142, 189}. *In vitro* cardiomyocyte studies suggest that superoxide dismutase-like and glutathione peroxidase-like compounds can protect against free radical production and cellular apoptosis due to doxorubicin^{145, 190}.

Research has identified several potential mechanisms through which the presence of oxidative stress in the heart and lungs can lead to increased inflammation and fibrosis. Reactive oxygen species can alter inflammation through the activation of nuclear factor-kappa B (NF- κ B) and activator protein-1 (AP-1)^{41, 191}. These redox sensitive transcription factors can bind to promoter regions in DNA and control the gene expression of a host of genes including those controlling pro-inflammatory cytokines, growth factors and apoptotic signals¹⁹¹. NF- κ B activation occurs in alveolar epithelial cells after asbestos exposure^{47, 115}. Oxidative stress is also evident in the fibro-proliferative response. *In vitro*, H₂O₂ can stimulate the proliferation of cultured human fibroblasts¹⁹². Furthermore, fibroblasts isolated IPF lung are capable of inducing apoptosis in epithelial cells *in vitro*¹¹⁹, further promoting the cycle of alveolar damage and abnormal repair. Hydrogen peroxide, as a diffusible factor, can lead to increased epithelial cell death, as well⁹⁷. Finally, oxidative species can control the proteolytic degradation of ECM through the activity of matrix metalloproteinases and tissue inhibitors of MMPs^{123, 125}.

1.6 EXTRACELLULAR SUPEROXIDE DISMUTASE

Superoxide dismutases are antioxidant enzymes found throughout tissues of the body and function to scavenge superoxide radicals that can damage cellular and matrix components. Superoxide dismutase (SOD) was first described by and its reactions were further described by Fridovich and McCord in 1969^{193, 194}. There are three SOD enzyme isoforms including intracellular CuZn SOD (SOD1), mitochondrial manganese MnSOD (SOD2), and extracellular CuZn SOD (SOD3). Extracellular superoxide dismutase (EC-SOD) was identified by Marklund et. al. in 1982 in human plasma, lymph, ascites, and cerebrospinal fluid^{195, 196}.

1.6.1 EC-SOD Structure and Function

EC-SOD is an active scavenger of superoxide free radicals by catalyzing the dismutation of superoxide into hydrogen peroxide and oxygen. This occurs at a rate constant of $>10^9 \text{ M}^{-1}\text{s}^{-1}$ ¹⁹⁷. EC-SOD also functions to preserve nitric oxide (NO) bioavailability within the cardiovascular system¹⁹⁸ by removing superoxide that can deplete NO. EC-SOD is a homo-tetramer enzyme formed by disulfide bridges between two dimers¹⁹⁹⁻²⁰¹. Each monomer contains an enzymatic domain containing one Cu(II) and one Zn(II) ions²⁰², a matrix binding domain, a N-linked glycation site and multiple free cysteines that determine the proteins structure and activity (Figure 2A). In human EC-SOD, monomers can be in an active or inactive form depending on their protein folding and Cys-mediated disulfide bonds²⁰¹. Approximately 1% of EC-SOD in human aorta can be distinguished as an octamer and is very stable²⁰³. It is highly expressed in the lung and localizes to cell surfaces by binding to heparan sulfate species^{197, 204-207} and type I collagen^{151, 199} through its matrix binding domain (MBD). The MBD contains a sequence of

positively charged Arginine and Lysine residues near amino acid 210 that makes this site suitable for binding to highly negatively charged heparan sulfate side chains. Through this domain, tetrameric EC-SOD has variable affinity for the ECM.

An important covalent disulfide bond is found at Cys219 within the C-terminus of EC-SOD that allows dimerization of two subunits through the MBD²⁰⁰. Enzymatic cleavage of any of the four MBDs will decrease or abolish the affinity of EC-SOD for the matrix and cell surfaces (Figure 2B). EC-SOD has 3 heparin affinity types: no affinity (type A), low affinity (type B) and high affinity (type C). Trypsin or endoproteinase treatment of EC-SOD, which targets lysine residues, can abolish or weaken the matrix binding affinity of EC-SOD²⁰⁴. This supports the important role of the cluster of basic amino acids in the C-terminus of EC-SOD.

On western blot analysis, EC-SOD from lung tissue homogenates runs as 2 distinct bands of full length and proteolyzed EC-SOD at 35 and 32 kDa respectively, under reduced conditions¹⁹⁹. Under non-denaturing, non-reducing conditions, native EC-SOD migrates as a tetramer at approximately 125 kDa, while the disulfide-linked dimer migrates at 51kDa on a non-reduced gel^{199, 200}.

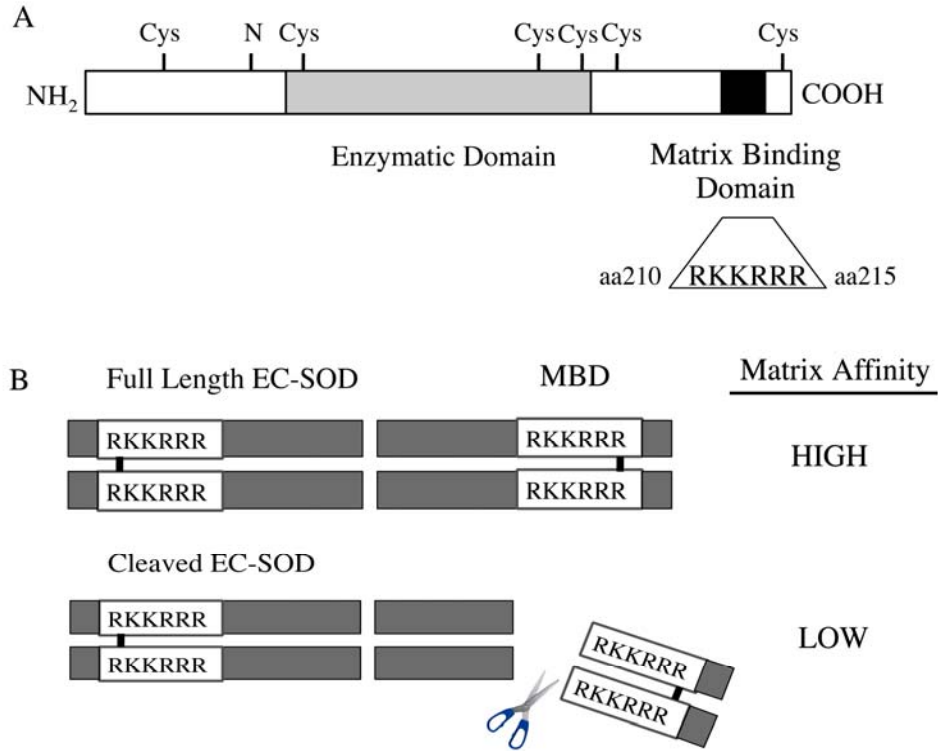


Figure 2: Schematic of EC-SOD Structure and Heparin Affinity. A) The EC-SOD monomer contains an enzymatic functional domain (grey), a unique matrix binding domain at the carboxyl terminus (black) which is composed of arginine (R) and lysine (K) residues, variable free Cysteine residues that can participate in disulfide bonding (Cys), and an N-linked glycosylation site. B) EC-SOD tetramer affinity for the matrix.

An EC-SOD gene variant has been implicated in increased risk for cardiovascular and ischemic heart disease. Studies report that an amino acid modification, EC-SOD^{R213G} arginine-213 to glycine substitution, in the MBD of EC-SOD results in decreased binding affinity of EC-SOD for the tissue matrix²⁰⁸⁻²¹⁰. Individuals with this mutation have increased levels of proteolyzed EC-SOD in their serum^{209, 211}. Population studies suggest that 2-6% of individuals may carry this altered sequence, thus it is considered to be a common gene variant^{211, 212}. A study from Denmark reports a 2.3 fold increase in the risk of ischemic heart disease in heterozygous individuals for EC-SOD^{R213G}²¹³.

The human EC-SOD gene has several regulatory regions including an antioxidant response element, a xenobiotic response element, an NF- κ B regulatory element, and a glucocorticoid response element^{174, 198}. The importance of these regions in expression regulation for EC-SOD is still unclear. Several stimuli are known to induce EC-SOD expression. In type II alveolar epithelial cells, TNF- α and IFN- γ are potent inducers of EC-SOD through NF- κ B activation²¹⁴. Vasoactive factors, such as nitric oxide from endothelial cells, endothelin-1, heparin, histamine and vasopressin can induce EC-SOD in smooth muscle cells²¹⁵. TGF- β can down-regulate EC-SOD expression in dermal fibroblasts and abolish stimulatory effects of cytokines such as IFN- γ on EC-SOD expression²¹⁶. TGF- β also decreases superoxide production by macrophages¹⁰⁹, thus altering oxidative stress. PDGF and fibroblast growth factor (FGF) can similarly down-regulate EC-SOD expression in vascular smooth muscle cells²¹⁵. Combinations of cytokines and growth factors may have variable effects on EC-SOD expression throughout acute and chronic phases of inflammation and fibrogenesis.

1.6.2 Tissue Distribution and Turn-over of EC-SOD

EC-SOD is found in most tissues and fluids with particularly high amounts in the lungs, heart, arteries, kidneys and placenta²¹⁷⁻²¹⁹. In tissues, EC-SOD is primarily secreted and maintained in the high affinity form with all MBDs intact²¹⁹. In plasma, variable EC-SOD species can be found including no matrix affinity, low affinity and high affinity EC-SOD^{220, 221}. Proteolytic modifications to the MBD²¹⁹ and glycation of lysine residues²²² can lead to the lower affinity species. The tissue half-lives of the three EC-SOD species have been reported as 85 hours for high affinity EC-SOD, 20 hrs for low affinity and 7 hrs for no affinity EC-SOD²²¹.

EC-SOD can be localized to the vasculature especially arteries^{215, 223, 224}, epithelium^{223, 224}, and on macrophages and neutrophils²²⁵. The human aorta is very abundant with EC-SOD, which makes up 70% of the SOD in this tissue²²⁴. Much of the vascular EC-SOD is produced by smooth muscle cells²¹⁵. Within the lung, EC-SOD localizes to the endothelial matrix of pulmonary vessels, the epithelium of the airway and alveoli, and the matrix of the alveolar septa^{199, 223}.

1.6.3 EC-SOD in Pulmonary and Cardiovascular Disease

EC-SOD has been implicated in the pathogenesis of pulmonary diseases involving oxidative stress^{185, 197, 199}. EC-SOD plays a role in several models of pulmonary fibrosis including Bleomycin-induced and asbestos-induced fibrosis, both of which produce reactive oxygen species in the tissue. Our lab has noted the protective effect of native EC-SOD in the lung by utilizing EC-SOD knockout mice. Knockout mice lacking EC-SOD throughout their tissues have significantly more lung fibrosis, acute lung injury, and inflammation dominated by a neutrophil influx due to Bleomycin and asbestos intratracheal administration^{57, 60, 63}. EC-SOD distribution in the lungs of wild-type mice also changes, as it is lost from the parenchyma where it normally resides and increases in air spaces in fibrosis models²²⁶, as well as, after hyperoxia⁴, and pulmonary bacterial infection²²⁶. Additional studies support a role for EC-SOD in the regulation of inflammation. EC-SOD null mice get significantly more neutrophilic inflammation in the lung following hemorrhage-induced lung injury²²⁷ and intratracheal lipopolysaccharide (LPS)²²⁸. In a bacterial pneumonia model of lung injury, EC-SOD may be brought in by activated inflammatory cells²²⁶.

EC-SOD has been shown to protect the heart from ischemic damage, hypertrophy, and inflammation^{177, 229-231}. As an antioxidant, EC-SOD is important throughout the cardiovascular system. Studies show that a percentage of the population has a mutation in the matrix-binding domain that diminishes its affinity for the extracellular matrix²³²⁻²³⁴. These individuals have a higher risk for the development of cardiovascular and ischemic heart disease²³². This suggests that these individuals would also be more susceptible to other oxidant-mediated injuries due to the loss of matrix-associated EC-SOD. In the heart, studies have found that EC-SOD is important in the prevention oxidative injury that may contribute to cardiac remodeling in the heart in myocardial infarction models and that it alters *ex vivo* heart function^{229, 230, 232, 235}. EC-SOD also protects against LDL oxidation and the enzyme's activity is reduced in patients with coronary artery disease²³⁶. EC-SOD gene transfer in a hind limb ischemia model suggests that EC-SOD improves tissue function and has a signaling role in tissue repair after ischemic injury²³⁷. The specific mechanisms by which EC-SOD protects against fibrosis and tissue damage in various organs, including the lung and heart, has been investigated however remain unclear.

1.7 HEPARAN SULFATE PROTEOGLYCANS

The extracellular matrix (ECM) is composed of 3 major components: collagens, adhesive glycoproteins, and proteoglycans⁸². Heparan sulfate proteoglycans are comprised of a membrane-bound core protein with attached sulfated polysaccharide side-chains²³⁸. Polyanionic proteoglycans, like heparan sulfates, have the ability to bind highly cationic proteins and transition metals. The binding of transition metals makes them potential sites for Haber-Weiss and Fenton-like chemistry within the body. Furthermore, cationic proteins such as

myeloperoxidase and eosinophil peroxidase bind to the ECM and are sites of additional radical production such as hypochlorous acid from Cl^- and hydrogen peroxide^{164, 165}.

1.7.1 Family Members – syndecans and glypicans

Heparan sulfate proteoglycans are separated into 2 major families: the syndecans and the glypicans. Syndecans (Syn 1-4) are composed of a core protein ~30-45kDa with an extracellular domain, transmembrane domain and cytoplasmic tail (Figure 3). Glypican is composed of a core protein ~60 kDa with a glycosyl phosphatidyl inositol (GPI) linkage and an extracellular domain that forms a globular protein structure due to disulfide bonding between 14 conserved Cys residues²³⁹. Both of these groups bear variable HS side chains that link to Ser-Gly regions within the core protein, adding to their complexity and diversity. The HS side chains can range from 5-70kDa. These side chains are synthesized in a process that creates a linker region to attach the polysaccharide chain to the core protein, followed by enzymatic modifications that result in acetylation and sulfation²³⁹. The polysaccharide chain is comprised of alternating N-glucosamine (GlcNAc) and glucuronic acid (GlcA) residues; thus, are called glycosaminoglycans (GAGs). Heparin is a heparan sulfate-like glycosaminoglycan made by mast cells and is known for its anticoagulant activity. Structurally it contains N-glucosamine and iduronic acid as its most common disaccharides and is not typically bound to a core protein. HS is made by almost all cells and has anticoagulant activity however less than heparin²³⁸. Heparin is modified with more sulfate groups than HS is, which provides some resistance against degradation. The molecular weight of HS proteoglycans is increased by the presence of the core protein, however, the GAG or HS side chains can be fragmented into much lower molecular weight species. Heparin is smaller in size and is characterized as high or low molecular weight. HS side chains appear to be

important in leukocyte-endothelial interactions and the transmigration of leukocytes^{240, 241}. Syndecans will be the focus of the remainder of this section.

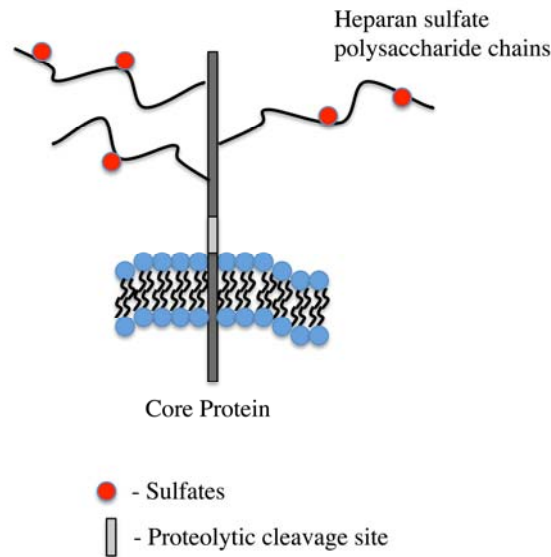


Figure 3: Syndecan Structure: Syndecans are composed of a transmembrane protein with a cytoplasmic, transmembrane and extracellular domain. Heparan sulfate side chains are linked to the core protein and contain variable amounts of sulfated residues. The extracellular portion of the core protein can be shed from the cell membrane by proteolytic cleavage.

Syndecans can function in various ways within the ECM: 1) bind and localize soluble and insoluble ligands, i.e. growth factors, TGF- β , FGF, cytokines, EC-SOD; 2) act as a soluble paracrine or autocrine factor when the ectodomain is shed; 3) maintain receptor abilities for internalization of ligands; 4) facilitate leukocyte migration and trafficking²³⁹. Syndecans are also linked to the actin cytoskeleton and have key roles in controlling cellular migration, proliferation and homeostasis. Known ligands for syndecans that are of importance with regard to inflammation and fibrosis include TGF- β 1 and 2, HGF, VEGF, PDGF-AA, FGF, cytokines and chemokines such as IL-8, MCP-1, TNF- α ^{239, 242-244}. Syndecans can also bind other ECM components such as fibronectin and laminin and can bind enzymes such as neutrophil elastase, tissue plasminogen activator and extracellular superoxide dismutase. Syndecan-1 and -4 can bind

elastase in dermal wound fluids protecting them from their inhibitors and modulating the proteolytic potential of the micro-environment²⁴⁵.

Table 1: Syndecan Expression by Cell Type

Syndecan Expression by Cell Type.	
Heparan Sulfate	Expression
Syndecan-1	Epithelia, plasma cells
Syndecan-2	Endothelia, fibroblasts, macrophages
Syndecan-3	CNS
Syndecan-4	Ubiquitous, Epithelia, macrophages

The syndecan family is comprised of 4 members that vary by their cellular expression patterns and functions (Table 1). Syndecan-2, on activated macrophages, binds macrophage-produced growth factors, such as PDGF and FGF, and promotes their activity/signaling²⁴³. Syndecan-3 is found predominantly within the central nervous system. Syndecan-4 is ubiquitously expressed and has characterized signaling abilities through binding to PIP-2 and activation of PKC- α . In skin fibroblasts from scleroderma patients, enhanced ERK activation was dependent on syndecan-4 and resulted in induction of profibrotic proteins and ECM contraction²⁴⁶. Syndecan-4 expression has also been described in macrophages²⁴⁷.

Syndecan-1 is expressed in epithelial cells. While the signaling potential of syndecan-1 is unclear, HGF binding to syndecan-1 appears to promote activation of PI3-kinase and MAP-Kinase pathways²⁴⁸. Syndecan-1 has an evident role in inflammation and wound healing²⁴⁹. Syndecan-1 expression can be upregulated in activated peritoneal macrophages and mediate their adhesion to cell surfaces²⁵⁰. Mice with global knock out of syndecan-1 are viable and have impaired wound healing and abnormal leukocyte-endothelial cell adhesion properties^{241, 245}.

Syndecan-1 null animals also display inhibition of keratinocyte proliferation and migration in dermal wound models^{251, 252}. Over expression of syndecan-1 led to a deficit in keratinocyte proliferation only²⁵¹. These studies suggest that syndecan-1 has an important role in organizing and remodeling newly laid cells and that there is an optimal expression level required for the regulation of cell proliferation. TGF- β can induce the expression of syndecan-1 in epithelial cells²⁵³. In cardiac remodeling, syndecan-1 expression changes in models of myocardial infarction²⁵⁴ and increased syndecan-1 expression protects the heart from dilation and remodeling²⁵⁵. Thus, syndecan-1 appears to be important during the repair process in the heart and potentially the lung epithelium.

1.7.2 Syndecan Biochemistry

Receptors that may be involved in syndecan interactions include Toll-like receptor 4 and integrins. TLR4 is a receptor that initiates innate and adaptive immune responses to microbes. Its signaling modulates neutrophil migration & cytokine production²⁵⁶ and it is suggested that soluble HS can activate TLR-4²⁵⁷. Integrin- β 1 mediates collagens interaction with syndecan-1²⁵⁸ and other integrins may mediate the interaction between neutrophils and syndecans²⁵⁹.

Proteolytic cleavage (MMPs, heparanase) or oxidative cleavage of the HS side chains or core proteins are two ways that syndecans can transform into soluble effector molecules. Heparanase is an endoglycosidic enzyme that cleaves HS side chains²⁶⁰ and is capable of cleaving syndecan-1²⁶¹. Syndecan core protein ectodomains can be shed from the cell surface through proteolytic cleavage of the juxtamembrane region (Figure 3). Matrilysin or MMP7 is a protease that binds to heparan sulfate²⁶² and induces shedding of the syndecan-1 ectodomain in a model of acute lung injury induced by bleomycin²⁶³. Consistent with this, MMP-2 and MMP-9

can also shed syndecan ectodomains *in vitro*²⁶⁴. This shedding can be regulated by tissue inhibitors of matrix metalloproteinases, such as TIMP-3²⁶⁵.

Studies also indicate that oxidative fragmentation of HS side chains can occur through hypochlorite species generated by MPO^{161, 163-165} and through hydroxyl radicals generated by xanthine oxidase^{266, 267}. This is particularly important in sites of inflammation and neutrophil influx. Potential oxidative reactions can occur to the core protein itself or the polysaccharide side chains. Protein backbone oxidation is more complex and significant cleavage occurs only with very reactive oxygen species such as hydroxyl radicals¹⁷⁵. Oxidation and cleavage of the core protein can occur through hydrogen abstraction from a central α -carbon and subsequent reaction with oxygen to form a peroxy radical²⁶⁸. This radical can undergo conversion to an α -C alcohol and the peptide bond can be cleaved by hydrolysis or to an alkoxy species resulting in cleavage of the peptide bond. Polysaccharide side chain fragmentation can occur through hydrogen abstraction from any of the C-H bonds on the sugar residue creating a C-centered radical, called an α -hydroxyalkyl radical ($\cdot\text{C}(\text{OH})\text{RR}'$)¹⁷⁵. This radical can then be converted to a peroxy radical in the presence of oxygen and undergo chain hydrolysis or can undergo β -scission of the glycosidic bond which would fragment the chain^{175, 268}.

2.0 RATIONALE AND HYPOTHESIS

2.1 PULMONARY FIBROSIS STUDIES

Idiopathic pulmonary fibrosis (IPF) is a detrimental lung disease characterized by progressive fibrosis of the alveolar interstitium^{2, 3}. Reactive oxygen species (ROS) and markers of oxidative stress are evident in human IPF^{10, 11} and levels of ROS negatively correlate with pulmonary function in IPF and may predict disease severity⁵.

Extracellular superoxide dismutase (EC-SOD) binds heparan sulfates in the extracellular matrix through a matrix binding domain^{204, 269}. EC-SOD protects against the development of bleomycin and asbestos-induced pulmonary fibrosis^{57, 63}. Further more, with these injuries EC-SOD is lost from the alveolar interstitium and collects in the airspaces⁶⁰.

In vitro studies, show that heparan sulfate (HS) is susceptible to reactive species such as hydroxyl radicals²⁶⁶ and HOCl leading to chain and protein modifications^{164, 165}. Proteolytic shedding of syndecan-1, a HS, is involved in bleomycin-induced lung fibrosis²⁶³.

Because matrix proteoglycans are known to be sensitive to oxidative fragmentation and EC-SOD is known to bind HS, *it is hypothesized that one mechanism through which EC-SOD protects the lung from oxidant-induced damage, inflammation, and fibrosis is by preventing oxidative fragmentation of heparan sulfate (HS), specifically syndecan-1, in the extracellular matrix (ECM).*

To investigate the relationship of EC-SOD and HS/syndecan-1 in pulmonary fibrosis, a human IPF population and two mouse models of pulmonary fibrosis (intratracheal asbestos and bleomycin) were utilized in wild type and EC-SOD null (EC-SOD KO) mice. In addition, I investigated the effects of shed syndecan-1 ectodomains on neutrophil chemotaxis and alveolar epithelial wound healing – both of which are important in the inflammatory and remodeling phases of pulmonary fibrosis pathogenesis.

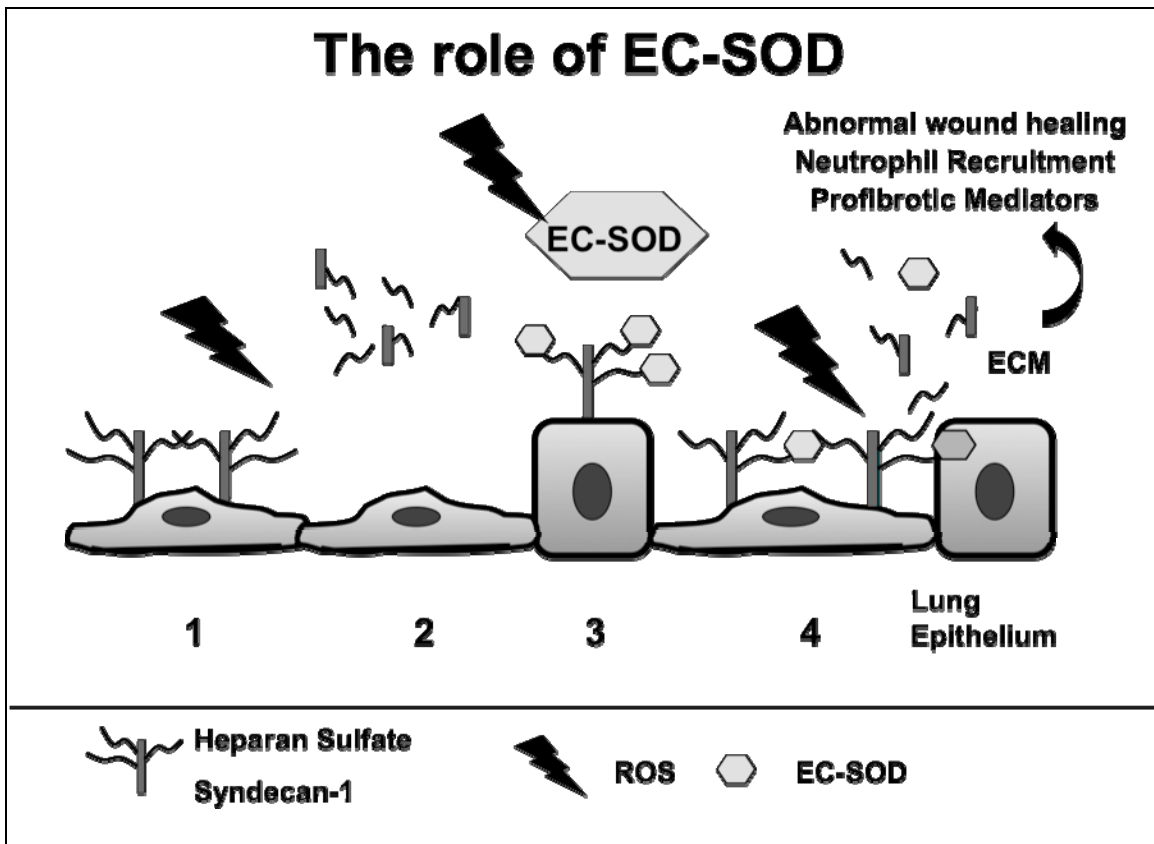


Figure 4: Proposed Interactions of EC-SOD, ROS and Matrix Components. (1) Reactive oxygen species (ROS) are generated near the lung epithelium by asbestos fibers or a stimuli; (2) Heparan sulfate side chains or core proteins of syndecan-1 are fragmented and released into the extracellular airspace; (3) EC-SOD is localized to the cell surface through its matrix binding domain and may prevent fragmentation of matrix components by scavenging ROS; (4) If EC-SOD is insufficient, HS or syndecan will be shed by attacking ROS. This may release bound factors such as cytokines and EC-SOD from the epithelium. Loss of HS, syndecan and EC-SOD could increase tissue susceptibility to oxidative injury and mediate inflammation, wound healing and fibrosis.

2.2 CARDIAC FIBROSIS STUDIES

As an important cardiovascular antioxidant enzyme, EC-SOD has been shown to protect the heart from ischemic damage and inflammation^{177, 229-231}. Studies have found that EC-SOD is important in the prevention of oxidative injury to the heart that may contribute to cardiac remodeling after myocardial infarction and that EC-SOD alters *ex vivo* heart function^{229, 230, 232, 235}. Our laboratory has previously found that EC-SOD can protect against pulmonary fibrosis and inflammation in mouse models of asbestos and bleomycin-induced lung injury^{57, 60, 63}. In the heart, cardiac fibrosis can be modeled utilizing the chemotherapeutic agent, doxorubicin. The primary mechanism of doxorubicin-induced myocardial damage involves the generation of oxidative stress through quinone-semiquinone reduction-oxidation reactions that produces superoxide radicals¹³⁸. Doxorubicin causes cardiac fibrosis that results in a non-ischemic dilated cardiomyopathy and heart failure^{137, 139, 140}. *In vitro* studies have found that doxorubicin also induces myocardial apoptosis^{138, 270}.

While the role of oxidative stress has been shown in doxorubicin-induced injury to the heart, the specific role of EC-SOD in normal cardiac morphology and injury-mediated fibrosis is unclear. Thus, *we hypothesize that EC-SOD protects the heart from oxidant-induced fibrosis and loss of function by mediating inflammation and preventing oxidative ECM shedding.*

To investigate the direct role and functional significance of cardiac EC-SOD in oxidant-induced inflammation and fibrosis of the heart, a mouse model of doxorubicin-induced cardiac injury in wild type and EC-SOD null mice (EC-SOD KO) was utilized. The role of EC-SOD was evaluated through functional echocardiography, biochemical and histological assessment of left ventricle fibrosis, inflammatory cell infiltration, syndecan-1 fragmentation and apoptosis induction.

3.0 MATERIALS AND METHODS

3.1 REACTIVE OXYGEN SPECIES GENERATION

Reactive oxygen species (ROS) were generated *in vitro* using a Fenton-like system utilizing copper sulfate and hydrogen peroxide (see Figure 1). Variable amounts of 0.1M H₂O₂ (1.1 – 2.0mM) and CuSO₄ solution, 0.1M NaH₂PO₄/ 5mM CuSO₄ at pH7.4, (working concentrations 0.8 – 2.0μM CuSO₄) were combined to produce superoxide radicals. The amount of superoxide produced by the CuSO₄/H₂O₂ system was determined to be 0.068 nmol/min/ml of superoxide at 1.25 μM CuSO₄ using the acetylated cytochrome-c method for detecting superoxide as previously described^{60, 271}. For comparison, approximately 0.3 units of xanthine oxidase in a xanthine/XO system generated 3 times more superoxide (0.2 nmol/min/ml).

3.2 ANIMAL STUDIES

3.2.1 Mice Utilized

The University of Pittsburgh IACUC approved all animal protocols. Wild-type C57BL/6 (Taconic) and EC-SOD-null mice (EC-SOD KO)²⁷² were utilized in studies. For pulmonary models, male mice were used at 8-10 weeks old. For cardiac models, female mice were used at

8-10 weeks old. Female mice were used because of extreme sensitivity and mortality in the male mice due to cardio-toxic agents. This gender sensitivity is commonly seen in cardiac experiments.

3.2.2 Intratracheal Instillation of Fibrotic Stimuli to the Lung

Mice were weighed daily or every other day throughout the experiments. C57BL/6 wild type and EC-SOD KO mice were treated intratracheally with 0.14 mg sterile crocidolite asbestos (NIEHS, Bethesda, MD) or 0.14 mg titanium dioxide (inert control particle, Sigma), as previously described^{63, 273}. After 1 day, 14 days, and 28 days, mice were euthanized and tissues were harvested for analysis, as described below. In select experiments, wild type and EC-SOD KO mice were treated with 0.05 Units of bleomycin intratracheally and mice were processed after 7 days in the same manner as the asbestos experiments.

3.2.3 Doxorubicin treatment for Cardiac Fibrosis

Mice were treated with a single intraperitoneal injection of 15 mg/kg doxorubicin (Adriamycin[®], Bedford Laboratories, Bedford, OH) or saline on day 0. The experimental end-point was cardiac fibrosis that developed by day 15. Mice were weighed daily.

3.2.4 Pulmonary and Cardiac Tissue Harvest and Sample Collection

For pulmonary experiments, mice were euthanized with 150 mg/kg nembutol intraperitoneally and blood samples for serum were collected by cardiac puncture. Blood was placed into serum

separator tubes (BD Microtainer[®]) to incubate at room temperature for 30 minutes and subsequently centrifuged at 12,500 rpm for 6 minutes. The resulting serums were collected, assayed for protein concentrations at a 1:40 dilution using a Bradford Assay (Pierce) and stored at -80°C until analysis.

Bronchoalveolar lavage fluid (BALF) was also collected. Briefly, the trachea was surgically exposed, encircled with suture, and a 24-gauge lavage needle was placed into a horizontal cut in the trachea. The needle was tied down and 800µl of saline was instilled into the lungs and recovered. The lungs were then perfused by cutting the abdominal aorta, and instilling 8mL sterile saline into the right ventricle of the heart at a 90° angle to the body. After the lungs are perfused to white, they are either removed for hydroxyproline analysis, flash frozen in liquid nitrogen for homogenization or RNA isolation, or fixed for histology. Fixation was completed by instilling 1.2 mL of 10% buffered formalin into the lavage needle and incubating for 8 minutes. Lungs were removed and embedded in cassettes with paraffin.

For cardiac experiments, mice were first anesthetized with 2.5% Avertin for echocardiography, as described below in more detail. After echo testing, mice were euthanized with 150mg/kg nembutol i.p. and blood samples for serum were collected by cardiac puncture to the right ventricle and processed as previously described. The left ventricle of the heart and interventricular septum were dissected out, sectioned into separate pieces for protein homogenization and RNA isolation, and flash frozen in liquid nitrogen. Weights were collected for the LV tissue prior to and after sample sectioning. For histology, whole hearts were weighed, perfused/fixed with 10% buffered formalin and paraffin embedded in cassettes.

3.3 HUMAN IPF STUDIES

Human samples from idiopathic pulmonary fibrosis (IPF) and normal lungs were obtained (bronchoalveolar lavage fluid (BALF) and paraffin-embedded lung) at the University of Pittsburgh or the Clinical Center, National Institutes of Health (NIH), in Bethesda, MD. Written informed consent was obtained from subjects seen at the NIH, who were enrolled in protocols 99-H-0068, 04-H-0211, and/or 04-HG-0211, which were approved by the National Heart, Lung, and Blood Institute and the National Human Genome Research Institute Institutional Review Boards. Tissue samples for lung homogenates were obtained through the University of Pittsburgh Health Sciences Tissue Bank, as previously described²⁷⁴. Nine samples were obtained from surgical remnants of biopsies or lungs explanted from patients with IPF who underwent pulmonary transplant and control normal lung tissues obtained from the disease free margins with normal histology of lung cancer resection specimens. The morphologic diagnosis of IPF was based on typical microscopic findings consistent with usual interstitial pneumonia. All patients fulfilled the diagnostic criteria for IPF outlined by the American Thoracic Society and European Respiratory Society^{3, 4}. The use of all samples was approved by the Institutional Review Board at the University of Pittsburgh. The homogenization process was the same as used for mouse lung samples described in 3.5.2. For immunohistochemistry, see the section 3.6.

3.4 CARDIAC FUNCTION ANALYSIS

3.4.1 Echocardiography and Functional Calculations

Echocardiography was completed using a Visual Sonics machine with a 25-MHz transducer, as previously described^{275, 276}. Mice were anesthetized with 2.5% wt/vol Avertin at 8.5 $\mu\text{L/g}$ body weight by intraperitoneal injection. Parasternal short axis B-mode and M-mode images and heart rate were collected (Figure 5). Measurements were performed on 5 complete beats and averaged. Left ventricular end diastolic dimension (LVEDD; mm) and posterior wall thickness (LVPWT, mm) were determined at maximal ventricular relaxation and LV end systolic dimension (LVESD; mm) was determined at maximal posterior-wall motion.

The relative posterior wall thickness is a ratio of LVEDD / LVPWT, as previously described²⁷⁷. Heart rate (bpm, beats per minute) was determined from 5 consecutive full wave intervals. The percentage of fractional shortening and ejection fraction were calculated using the following equations from measurements taken on M-mode images:

$$\text{Fractional Shortening \%} = ((\text{LVEDD} - \text{LVESD}) / \text{LVEDD}) \times 100$$

Left ventricular volume LV volume, μl :

$$\text{LV Vol}_{\text{diastolic}} = (7 / (2.4 + \text{LVEDD})) \times \text{LVEDD}^3 \times 1000$$

$$\text{LV Vol}_{\text{systolic}} = (7 / (2.4 + \text{LVESD})) \times \text{LVESD}^3 \times 1000$$

$$\text{Ejection Fraction \%} = ((\text{LV Vol}_{\text{diastolic}} - \text{LV Vol}_{\text{systolic}}) / \text{LV Vol}_{\text{diastolic}}) \times 100$$

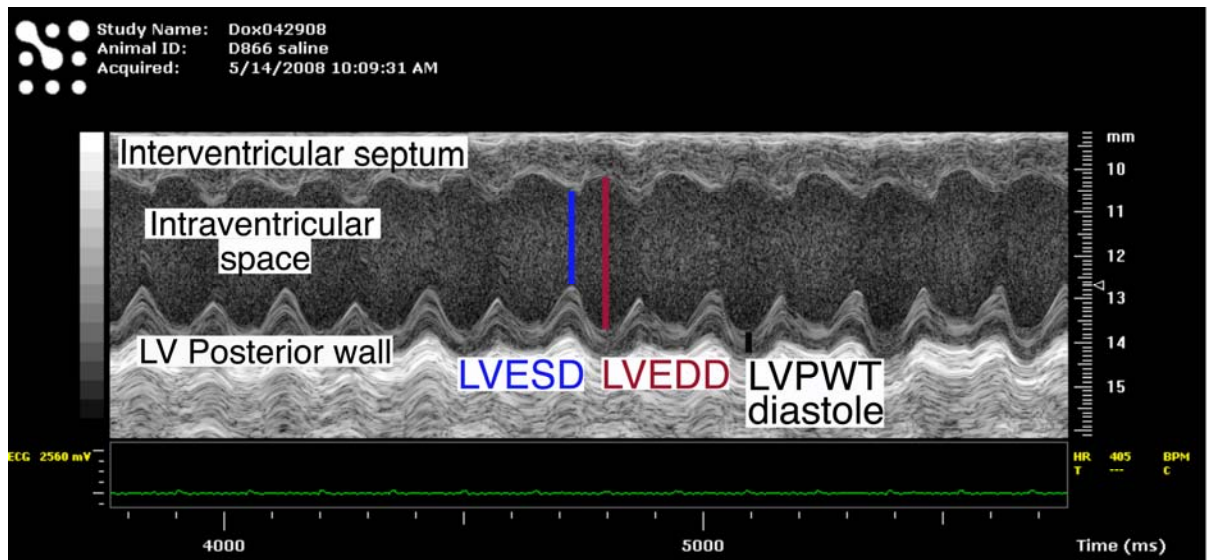


Figure 5: Images and measurements of the Left Ventricle of the Heart. A) B-mode image with LV within the highlighted area. Images were collected in the middle of the left ventricle just below the papillary muscles. B) M-mode image (LV cross-section) containing 3 measurements: left ventricular end diastolic dimension (LVEDD; mm) and posterior wall thickness (LVPWT, mm) were determined at maximal ventricular relaxation and LV end systolic dimension (LVESD; mm) was determined at maximal posterior-wall motion.

3.5 BIOCHEMICAL ANALYSIS

3.5.1 Bronchoalveolar lavage analysis

Bronchoalveolar lavage fluid (BALF) total cell counts were determined using a Bechman Coulter Counter. Cytospins slides were created using 50 μ l of BALF (Cytospin machine) and 50 μ l 50mM Tris-HCl. Slides were dried for 24 hours, stained with Diff Quick Cellular Stain (Dade Behring, Newark, DE), and cover-slipped using Peramount mounting media (Sigma). Cell differentials were determined by counting 200 total cells/slide (including neutrophils, macrophages, eosinophils/basophils, and lymphocytes) at 40X magnification using bright field. The evaluator was blinded to all sample groups.

3.5.2 Lung and Heart Homogenization

Frozen excised lung and dissected left ventricular tissue were homogenized on ice in homogenization buffer (50 mmol/L potassium phosphate, pH 7.4, 0.3 mol/L potassium bromide) with protease inhibitors (10 μ mol/L Dichloro-isocoumarin and 100 μ mol/L E-64 (L-transeoxysuccinyl-leucylamido-[4-guanidino]butane), Sigma) and sonicated. The samples were centrifuged at 20,000 g for 20 minutes at 4°C. The supernatant was collected as the soluble LV fraction and stored at -80°C until use. Two volumes of CHAPS detergent (50 mmol/L Tris-HCl, pH 7.4, 150 mmol/L NaCl, 10 mmol/L CHAPS) with the same protease inhibitors, were used to re-suspend the pellet. The samples were rotated for 2 hours at 4°C followed by sonication and centrifuged. The supernatants were collected as the membrane protein fraction and stored at -80°C until use.

3.5.3 Western Blot Analysis

Serum, human and mouse BALF and lung homogenate samples, and mouse left ventricular (LV) homogenate protein concentrations were determined by a Bradford assay (Pierce). Samples were separated by SDS-PAGE and transferred to PVDF membranes¹²³ and probed for proteins of interest. Membranes were probed for EC-SOD (rabbit anti-mouse or rabbit anti-human EC-SOD antibody)²⁷⁸, heparan sulfate proteoglycan HSPG (MAB2040), syndecan-1 ectodomain (rat anti-mouse syndecan-1 antibody 1µg/ml, clone 281.2 BD Biosciences), syndecan-4 (1µg/ml, clone KY8.2, BD Biosciences), mouse anti-human syndecan-1 (B-A38, Diaclone, Besancon, France) for human lung samples, or caspase-3 (anti-mouse caspase-3, recognizes 37kDa pro-form and 12-17kDa active form), then a Horseradish Peroxidase (HRP)-conjugated donkey anti-rabbit IgG or goat anti-rat IgG secondary antibodies (Jackson ImmunoResearch, West Grove, PA). ECL detection reagents were used for visualization (ECL-plus, GE Healthcare). Ponceau red was used to normalize BALF samples and coomassie blue membrane staining or β-actin densitometry was used to normalize homogenates and serum for protein loading. Images were captured with a Gel Logic 2200 system (Kodak) for densitometry (mean normalized net intensities ± SEM).

To confirm extracellular oxidative stress in the doxorubicin heart experiment, LV homogenates were assayed using an Oxyblot Kit (Chemicon). Briefly, this kit detects carbonyl groups which are a marker of oxidative modification of proteins. Equal amounts of protein were derivatized to 2,4-dinitrophenylhydrazone by reacting each with dinitrophenylhydrazine (DNPH). Non-derivatized samples were used as assay controls. Samples were separated by SDS-PAGE and transferred to a PVDF membrane. The membrane was probed with an antibody against DNP, according to the manufacturers instructions.

3.5.4 Hydroxyproline Assay

Whole lungs (right and left sides) or cardiac left ventricle tissue were dried in glass vacuoles in a 110°C oven for 48 hours and then dry weights were collected. Acid hydrolysis of each sample was completed by adding 2 ml of 6M HCl and oxygen from each vial was replaced by nitrogen gas under vacuum. Vials were sealed and incubated for 24 hours at 110°C, dried and assayed for hydroxyproline content using chloramine-T, as previously described²⁷⁹.

Briefly, the hydroxyproline standard curve (0-5µg/ml) was created using 10µg/ml trans-4-Hydroxy-L-proline in PBS. Standards and acid-hydrolyzed samples were incubated with chloramine-T solution for 20 minutes at room temperature and subsequently incubated with 3.15M perchloric acid for 5 minutes. To each sample, p-dimethylaminobenzaldehyde solution was added and incubated for 20 minutes at 60°C for color development and read in a 96-well plate at 557nm on a spectrophotometer (SpectraMax plus, Molecular Devices, Sunnyvale, CA) to obtain the hydroxyproline concentrations.

3.5.5 RNA Isolation and Quantitative reverse transcriptase polymerase chain reaction

RT PCR was used to determine mRNA expression (ddCt relative quantification) of EC-SOD from wild-type mice and syndecan-1, MMP2, MMP7, and MMP9 from wild type and EC-SOD KO mice. All reagents were purchased from Applied Biosystems (Foster City, CA) unless noted. RT reactions were performed as previously described^{278, 280}, using 1µg of RNA isolated from lung and left ventricular tissue using an RNeasy kit (Qiagen) and 5 mmol/L MgCl₂, PCR buffer II, 1 mmol/L nucleotide mix (Promega, Madison, WI), 1.0 U RNAsin (RNase Inhibitor), 2.5 U MuLV reverse transcriptase enzyme, and 3µg of random hexamers. Reactions were

performed on a Techne thermocycler (MIDSCI, St. Louis. MO) programmed for 42°C for 40 minutes, 99°C for 5 minutes, and 5°C for 5 minutes.

Quantitative PCR was performed by adding Universal PCR buffer and primer/probe assay reagents for EC-SOD, syndecan-1, MMP2, MMP7 and MMP9 (EC-SOD: Mm00448831_s1; syndecan-1: Mm00448918_m1 Sdc1, MMP2: Mm00439506_m1; MMP7: Mm01168420_m1; MMP9: Mm00442991_m1, Applied Biosystems) according to the manufacturer's protocol. GAPDH was used for sample normalization and loading control. An ABI Prism 7300 (Applied Biosystems, Foster City, CA) was used to run the default program (50°C for 2 minutes, 95°C for 10 minutes, and 40 cycles of 95°C for 15 seconds, and 60°C for 1 minute). Sequence Detection Software Version 1.4 (Applied Biosystems) was used to analyze the data based on the crossing threshold and to obtain mRNA expression relative quantities for each sample. The ddCt relative expressions for the treatment groups were averaged and the expression of the control group was set to 100%. Data are reported as relative percent ddCT expression versus control, n=5 samples per group, per gene (mean \pm SEM).

3.6 HISTOLOGICAL ANALYSIS

3.6.1 Hematoxylin and Eosin histology staining

Mouse lungs or hearts were fixed with 10% buffered formalin and paraffin embedded. 4 μ m thick sections of tissue were placed on to slides and heated at 60°C overnight, deparaffinized with xylene, rehydrated with an ethanol series, and stained with Hematoxylin and Eosin then cover-slipped with Permount mounting fluid. H&E sections of the heart were imaged at 2X

magnification on a macro-dissecting scope (Olympus America Inc., Center Valley, PA) and lung H&E sections were imaged using bright field at 40X magnification on an Olympus IX7 microscope (Olympus, Center Valley, PA).

3.6.2 Picro-Sirius Red Staining

Sirius red staining was completed similarly to that previously described^{281, 282}. Briefly, nuclei were stained for 1 minute with Weigert's hematoxylin, washed with distilled water for 5 minutes, then stained for 1 hours in 0.1% Sirius red stain (Direct Red 80, Sigma) in saturated picric acid. Slides were washed twice in acidified water (5% acetic acid), dehydrated with an ethanol series, and cleared with xylene. Sections were cover-slipped and mounted with Peramount (Sigma). This stain identifies collagen fibers by staining them orange/red. Fibers can also be seen using polarized light, which results in collagen fibers visualized as yellow/green.

3.6.3 Masson's Trichrome Staining

This stain is used to detect the presence of collagen within tissue. Collagen stains blue, nuclei stain dark brown and cytoplasm and backgrounds stain red. Staining was completed by Histological Services at the University of Pittsburgh.

3.6.4 TUNEL Straining

Using the TUNEL (terminal deoxynucleotidyl transferase (TdT)-mediated dUTP nick-end labeling) method, cardiac sections were stained for the detection of fragmented DNA, which is

indicative of apoptotic cells. Sections were incubated with TdT-reaction solution and nuclei were visualized with streptavidin-rodamine labeled fluorescence using a TUNEL kit (Promega, Madison, WI) and DAPI (4',6 diamidino-2-phenylindole, dihydrochloride) nuclear stain. Conventional fluorescence images were obtained by using a Nikon Microphot-FXA fluorescence microscope (Nikon Instruments, Inc, Melville, NY), as previously described²⁸³.

3.6.5 Immuno-fluorescent histochemistry

3.6.5.1 Lung IHC

Mouse lungs were inflation fixed with 10% buffered formalin for 4 hours and embedded in paraffin. Fixed and embedded human control and IPF lung samples were also used. Sections were cut at 5µm and were adhered to slides for 30 minutes to overnight at 60°C followed by deparaffinizing with xylene and rehydration in an ethanol series. The sections were treated with sodium citrate buffer at 95°C for antigen retrieval. Human and mouse lung sections were stained for colocalization with antibodies specific to syndecan-1 (human: .2µg/ml, B-A38, Abcam, Cambridge, MA; mouse: 1µg/ml, 281.2, BD Bioscience) and EC-SOD (1:500, generated as described below) and secondary antibodies labeled with Cy3 and Alexa 488 (1:500, Jackson immunoresearch, Westgrove, PA). Stained sections were imaged at 40X using an Olympus IX7 microscope (Olympus, Center Valley, PA). Control sections were stained with non-immune mouse IgG and pre-immune serum (AnaSpec). Areas of fibrosis were confirmed with H&E staining of serial lung sections by a board certified pathologist (T.D.O.).

3.6.5.2 Heart IHC

Mouse hearts were fixed with 10% buffered formalin overnight at 4°C and embedded in paraffin. Sections were cut at 4µm and were adhered to slides for 30 minutes to overnight at 60°C followed by deparaffinizing with xylene and rehydration in an ethanol series. The sections were treated with sodium citrate buffer at 95°C for antigen retrieval. Sections were stained with an anti-mouse CD45 antibody (1µg/ml, ab25386, Abcam, Cambridge, MA) and a secondary antibody labeled with Cy3 (1:5000, Jackson immunoresearch, Westgrove, PA). Hoecht stain was used for nuclear localization. Stained sections were imaged at 40X using an Olympus IX7 microscope (Olympus, Center Valley, PA). Control sections were stained with non-immune mouse IgG.

3.7 PURIFICATION OF HUMAN EC-SOD

EC-SOD was purified from human aorta (84g total), as previously described with minor modifications²⁰⁰, and homogenized in 800ml of homogenization buffer (50mM KPO₄, 0.3M KBr pH 7.4) with protease inhibitors (0.5mM PMSF, 0.01 m ME-64 and 0.1mM orthophenantholine). The homogenate was centrifuged and run over a Con-A column. Proteins bound to the column were eluted with elution buffer (50mM HEPES pH 7, 0.25M NaCl, 200mM methyl a-mannopyranoside). The eluted protein was dialyzed and loaded onto a heparin-sepharose column. Fast protein liquid chromatography was completed on the eluted EC-SOD fractions, as previously described. Pooled fractions were run on a mono-Q sepharose column and fractions analyzed by FPLC. Pooled fractions of purified EC-SOD were run over an AffinityPak DetoxiGel Column (Thermo-Fisher) to remove endotoxin. The final endotoxin level in the

purified EC-SOD was less than 0.2 EU/mg using a Limulus Amebocyte Lysate assay according to the manufacturers protocol (Cape Cod Inc., Falmouth, MA). The EC-SOD activity was 3,374 U/ml and was determined utilizing the acetylated cytochrome-c method, as previously described²⁷¹.

3.8 GENERATION OF EC-SOD ANTIBODIES

Mouse and human EC-SOD specific polyclonal antibodies were generated by immunizing rabbits with a Keyhole Limpet Hemocyanin (KLH) conjugated peptide containing either the first 19 amino acids in mouse EC-SOD and an additional cysteine residue at position 20 (SSFDLADRLDPVEKIDRLDC) or a peptide containing human EC-SOD amino acid residues 19-37 and an additional cysteine residue in position 20 (WTGEDSAEPNSDSA EWIRDC) by AnaSpec Corporation (San Jose, CA). Antiserums containing the EC-SOD antibodies were collected at the time of sacrifice 2 weeks after the second boost. Titers against the peptide were performed to confirm immunogenicity. Antibody specificity for EC-SOD was confirmed by the detection on Western Blot analysis of lung homogenate. Pre-immune serum was also collected to obtain control IgG.

3.9 SYNDECAN SPECIES UTILIZED

A Glutathione-S-Transferase (GST)-human syndecan-1 ectodomain fusion protein (hS1ED) was used in cell experiments at concentrations between 500ng/ml and 1 µg/ml (provided by Dr. Alan

Rapraeger and purified as previously described²⁸⁴). The present studies focus on the functions of the ectodomain protein itself, as there are no glycosaminoglycan chains present on the protein. In addition, a peptide was synthesized from 20 amino acids of the syndecan-1 ectodomain, syn peptide (95.2% purity, GenScript Corporation, Piscataway, NJ). Region aa11-30 include 2 of 4 glycosaminoglycan (GAG) side chain attachment sites and are composed of serine-glycine repeats. Figure 35A shows the peptide.

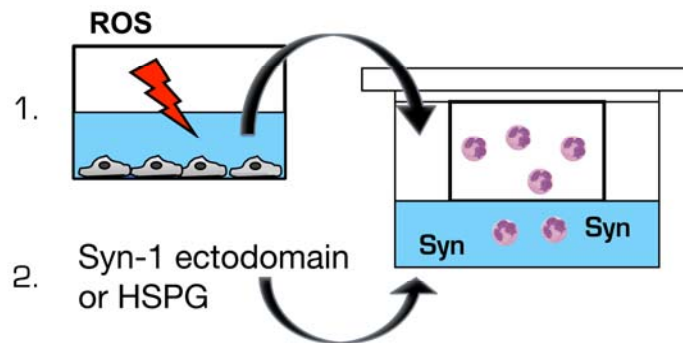
3.10 HEPARIN AND HEPARAN SULFATE FRAGMENTATION ANALYSIS

For evaluation of GAG chain oxidative fragmentation, heparin and heparan sulfate were incubated with reactive oxygen species as described in section 3.1. Reactions were immediately vortexed and incubated for 2 hours at room temperature on a rocker. Samples were separated by electrophoresis on 15% polyacrylamide gels. The gels were stained overnight in StainsAll (Sigma), which binds polyanionic carbohydrate species, and photo-destained.

3.11 CELLULAR CHEMOTAXIS ASSAY

A neutrophil chemotaxis assay, consisting of a modified Boyden chamber, as previously described²⁸⁵, as shown in the image below. The assay was used to evaluate the migration of primary human neutrophils (PMNs) in response to oxidatively shed syndecan-1 in A549 cell supernatants (step 1 of the following image) or to syndecan-1 peptide (50 ng/ml to 1 µg/ml, Abcam, Cambridge, MA) or heparan sulfate proteoglycan, (HSPG; 6 µg/mL, Sigma) treated with

reactive oxygen species (ROS) (step 2 of the following image). In select experiments the effect of EC-SOD was investigated. HSPG was treated with ROS in the absence or presence of 5-100 units of human EC-SOD, purified from human aorta, as previously described²⁰⁰, or CuZn SOD (Bovine liver, Alexis, San Diego, CA).



In brief, human neutrophils (PMNs) were isolated using dextran and Ficol gradient sedimentation, as previously described²⁵⁹. PMNs (2×10^6) were added to the upper chamber of transwell inserts (5 μm pore size, Corning Inc., Corning, NY) in a 24-well plate. The lower chambers contained Hanks Balanced Salt Solution (HBSS, Sigma) with the appropriate treatments indicated in the figures.

For select experiments, A549 cell monolayers were treated media, control siRNA or syndecan-1 siRNA for 24 hours then treated with HBSS or ROS for 2 hours at $37^\circ\text{C}/5\% \text{CO}_2$. Cell supernatants were collected and applied to the lower chamber of the chemotaxis assay with neutrophils added to the upper chamber as described above. ROS were generated in sterile HBSS using a $\text{CuSO}_4/\text{H}_2\text{O}_2$ system as previously described^{151, 186, 273}. The chemotaxis chambers were incubated for 2 hrs at $37^\circ\text{C}/5\% \text{CO}_2$. Cell counts were completed on lower chamber supernatants on a Beckmann Coulter Counter (Beckmann Coulter, Fullerton, CA). A neutrophil migration index was calculated²⁸⁶ as follows: (Migrated cells to treatment/ randomly migrated cells (HBSS)). An index greater than 1 represents chemotaxis (mean \pm SEM).

3.12 CELL CULTURE

3.12.1 Primary mouse epithelial cell culture and epithelial cell lines

Primary mouse epithelial cells were harvested and cultured from C57BL-6 mice, as previously described²⁸⁷ and grown on collagen IV coated 24-well plates for experiments. Briefly, cells were isolated from 6-week-old female C57BL/6 mice by a method of Rice et al. Mice were anesthetized with 200µl i.p. Nembutal. The chest and abdominal cavities were exposed and the trachea was exposed and cannulated with a 20-gauge luer-stub adapter. The anterior ribs were removed to expose the heart and lungs and the abdominal aorta was severed. The lungs were perfused with 10ml 0.9% saline by inserting a 21-gauge needle on a 10-ml syringe in to the right ventricle at a 90° angle. Dispase (3 ml) was instilled through the tracheal cannula followed immediately by 0.5 ml low melt agarose at 45°C. Lungs were immediately covered with ice for 2 min to gel the agarose. After this incubation, lungs were removed and incubated in 1 ml dispase for 45 min at 25°C. Lungs were subsequently transferred to a 60-mm culture dish containing 7 ml of HEPES-buffered DMEM and 100 U/ml DNase I. Lung tissue was gently teased apart and the cell suspension was filtered through progressively smaller cell strainers (100 and 40 µm) and nylon gauze (20 µm). Cells were collected by centrifugation at 130 g for 8 min (4°C) and placed on prewashed/antibody pre-coated 100-mm tissue culture plates (coated for 24-48 h at 4°C with 42 µg CD45 and 16 µg CD32 in PBS). After incubation for 1-2 h at 37°C, type II cells were gently panned from the plate and collected by centrifugation.

Type II cells were resuspended in culture media and cultured on collagen IV coated plates. The media was changed after the 1st day of culture. By day 7, the cells have differentiated from type II into type I alveolar epithelial cells. The approximate cell yield for this isolation

protocol is 4 to 6×10^6 cells/mouse. The purity of type II cell preparations was typically $>90\%$ and assessed by modified PAP stain^{287, 288} on cytopsin slides. PAP stain, a modified Papanicolaou stain, enables the visualization of cellular inclusions of type II alveolar cells (Figure 32). Briefly, 2×10^5 cells were cytopspun onto slides and dried. Slides were incubated in hematoxylin solution for 3 minutes, swished in distilled water, incubated in lithium carbonate (1:1000 of saturated solution) for 2 minutes. Slides were rinsed with water, incubated in 70% ethanol for 1.5 minutes, 80% ethanol for 15 seconds, 95% ethanol for 15 seconds, 100% ethanol for 30 seconds, and xylene for 1 minute.

A549, alveolar epithelial cells (ATCC), were grown on 24-well plates with DMEM plus 10% fetal bovine serum for experiments. Cells were serum starved for 18-24 hours prior to experiments.

3.12.2 Fibroblasts studies

A human lung fibroblast cell line, LL47 (ATCC), was grown on 6-well plates with F12K medium plus 10% fetal calf serum for experiments. LL47 fibroblasts were plated on 96 well plates (4,000 cells/well) and placed in serum free F12K media 24 hours prior to treatment. Cells were treated with media or 1 $\mu\text{g/ml}$ human syndecan-1 ectodomain (hS1ED) for 24 hours at 37°C/5% CO₂. Fibroblast proliferation was determined over 2 hours using CellTiter 96 AQ Non-Radioactive Assay at 333 $\mu\text{g/ml}$ MTS and 25 μM PMS (Promega, Madison, WI). Absorbance at 490 nm, which is proportional to the number of metabolically active cells, was recorded on a plate reader and reported as mean \pm SEM, n=8. LL47s were also cultured to confluency on 12 well polystyrene plates, placed in serum free media for 24 hours, and treated with 1 $\mu\text{g/ml}$ hS1ED for 48 hours. Supernatants were collected and assayed by ELISA for latent and active

TGF- β 1 (R&D Systems, Minneapolis, MN). For α -smooth muscle actin (α -SMA) detection, fibroblast cell lysates were collected in ice-cold cell lysis buffer with protease inhibitors and separated on SDS page. After transfer to a membrane, mouse anti- α -SMA primary antibody (Sigma) was used for detection and normalized to β -actin as described.

3.12.3 siRNA Treatment

For select experiments, A549 cell monolayers were treated with media, human syndecan-1 siRNA (sc-36587, Santa Cruz) or negative control siRNA (#AM4611, Ambion) 24 hours prior to ROS treatment in order to knockdown cell surface syndecan-1 expression. The syndecan-1 siRNA is a pool of 3 separate siRNA that individually specifically target syndecan-1 expression. The optimal siRNA concentration was determined at 30 and 60 μ M. A concentration of 30 μ M was used for all additional experiments along with Lipofectamine 2000 (Invitrogen) and Opti-mem I (Gibco) reagents according to the manufacturer's protocol. For neutrophil chemotaxis experiments, A549 cells were treated with siRNA and controls for 24 hours then treated with HBSS or ROS for 2 hours at 37°C/5% CO₂. Cell supernatants were collected and applied to the lower chamber of the chemotaxis assay. For wound healing experiments, A549s were treated with siRNAs and wounds were created 24 hours after siRNA treatment. hS1ED (1 μ g/ml) was added immediately after the wound was created and washed, as described in section 3.3.

3.12.4 Syndecan-1 Shedding Assays

For shedding assays, A549s were exposed to ROS and EC-SOD for 30 minutes at 37°C/5% CO₂. Cells were fluorescently labeled for syndecan-1, as previously described²⁶⁵, and supernatants

were analyzed for shed syndecan-1 ectodomain by dot blot. Samples were applied to PVDF membranes using a dot blot apparatus. The membrane and filter papers were pre-soaked in transfer buffer. Samples were applied and suctioned through onto the membrane, which was then incubated in 5% dry milk in PBS-tween overnight at 4°C. The membrane was probed for syndecan-1 ectodomain, as described in section 3.5.3.

3.13 EPITHELIAL WOUND HEALING ASSAY

For wound assays, primary mouse alveolar epithelial cells or A549 cells were grown to confluency in 24 well collagen IV-coated culture plates with growth media. (primary cells: DMEM with 10% fetal bovine serum and antibiotics; A549s: F12K media with 10% FBS; Invitrogen, Carlsbad, CA). Straight wounds were created with a p-200 pipet tip²⁸⁹. Wounds were washed and treated with syndecan-1 (hS1ED). Wound images were captured using a 4x objective with phase contrast at time 0 and 18 hours or 24 hours. Metamorph software (Molecular Devices, Downingtown, PA) was used to determine wound areas. The measurement tools were calibrated for the objective lens used. Percent wound healing was calculated with the following equation: $(\text{Wound Area (initial)} - \text{Wound Area (final)}) / \text{Wound area (initial)} \times 100$.

For select experiments, primary AECs were treated with 9.5µg/ml crocidolite asbestos immediately after monolayers were wounded and washed. Asbestos was suspended at 1mg/ml in sterile media, sonicated and run through a 22 gauge needle prior to treatment of cells. Wounds were assessed at 24 and 48 hours.

4.0 STATISTICAL ANALYSIS

Mean densitometry and all other quantitative data (mean \pm SEM) were assessed for significance using the Student's t-test or ANOVA (one or two-way determined by the experiment parameters) followed by Tukey's post-test using Graphpad Prism software (Graphpad, San Diego, CA). Significance was achieved by a p-value < 0.05 . Sample sizes (n) are indicated in the figure legends.

5.0 RESULTS – PULMONARY FIBROSIS

5.1 ASBESTOS AND BLEOMYCIN INJURY INDUCE HEPARAN SULFATE AND SYNDECAN SHEDDING

To investigate heparan sulfate (HS) shedding in pulmonary fibrosis and oxidative injury, we utilized wild type (WT) and EC-SOD KO mice that were treated with asbestos or bleomycin and bronchoalveolar lavage fluid (BALF) was collected at various timepoints. HS was evaluated by western blot analysis. EC-SOD KO mice are more susceptible to oxidative damage and lung fibrosis^{57, 63}. At 24 hours post-asbestos exposure, shed HS significantly increases in the BALF of WT mice (Figure 6A). Furthermore, EC-SOD KO mice have significantly more shed HS species in their BALF at 24 hours, 14 and 28 days post-asbestos exposure. By molecular mass, we predict that HS2 is syndecan-1 and that HS3 is syndecan-4.

To verify that the pulmonary epithelium expresses syndecan-1 and syndecan-4 species, primary mouse alveolar epithelial cells were isolated and stained for syndecan-1 or syndecan-4 *in vitro*. Figure 7 shows punctate clusters of syndecan-1 on the cell surface of the AECs and a more diffuse expression for syndecan-4 with some areas of clustering on the cell borders and sites of adhesion.

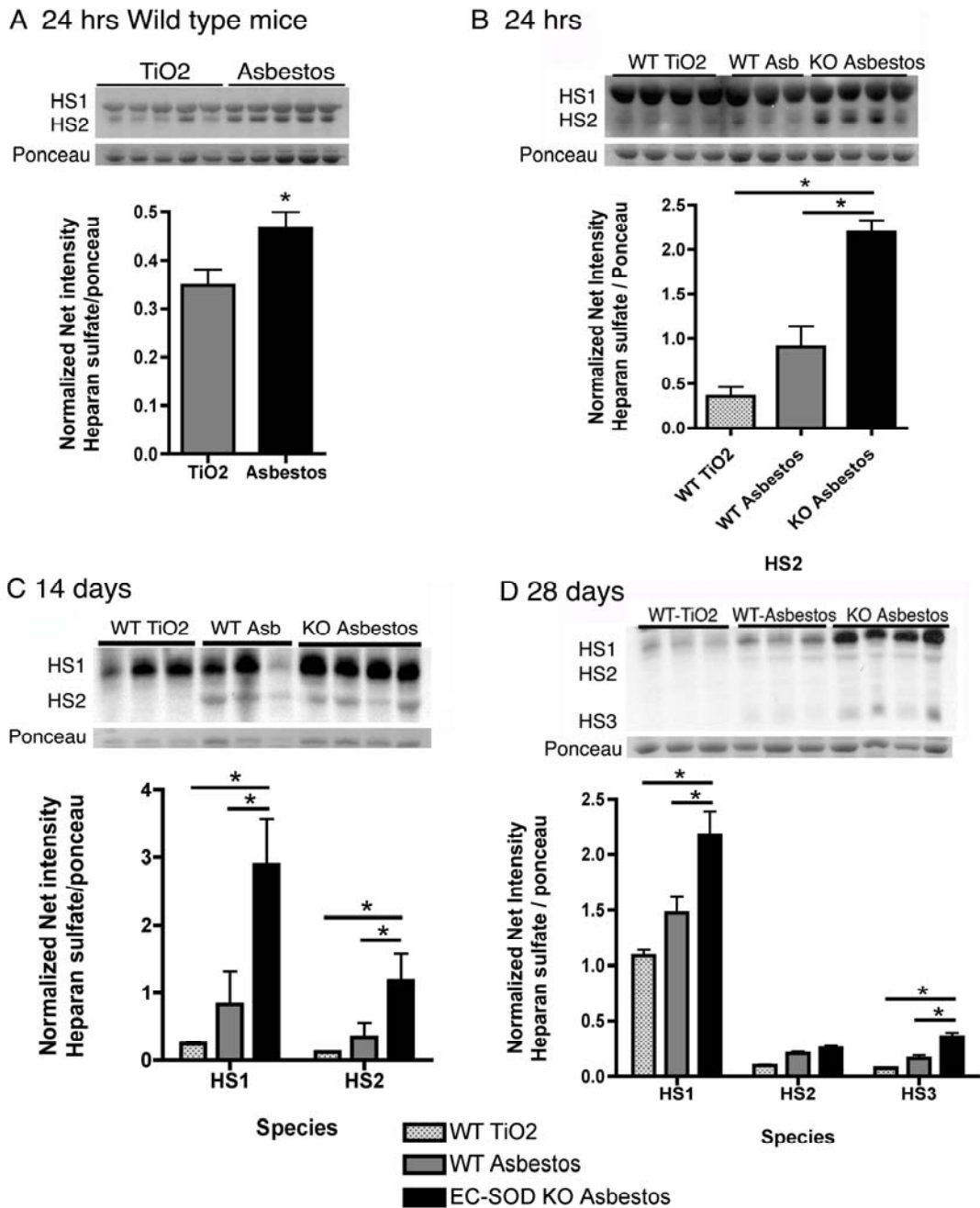


Figure 6: Heparan sulfate proteoglycans (HSPG) are shed into the BALF during asbestos induced injury. EC-SOD KO mice and wild type mice were exposed to asbestos and HSPG levels in the BALF were analyzed by western blot (antibody MAB2040) and were normalized to ponceau red and reported as mean \pm SEM. The various detected species are labeled HS1, HS2, HS3. *, $p < 0.05$ A) Wild type mice after 24 hours asbestos

exposure; B) 24 hours post-asbestos exposure; C) 14 days post-asbestos exposure; D) 28 days post-asbestos exposure.

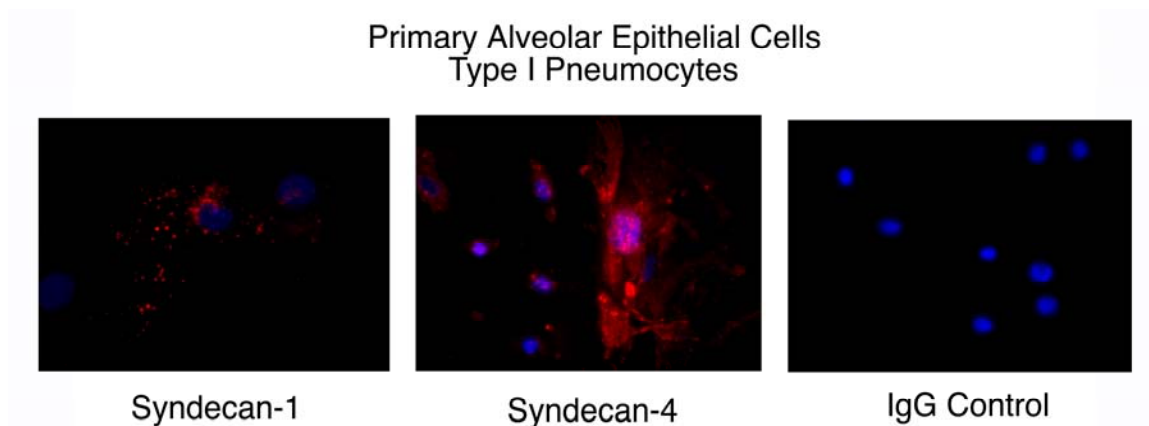


Figure 7: Syndecan expression in Primary Alveolar Epithelial Cells (AECs). Primary AECs were isolated from C57BL/6 mice and cultured. Cells were stained for cell surface syndecan-1 or syndecan-4. Images are representative of multiple wells of stained cells. A non-immune IgG antibody was used as the primary antibody for the control cells.

To confirm the identity of the shed HS species, BALF samples were analyzed for the shed ectodomains of the syndecan-1 and syndecan-4 core proteins. After asbestos injury, levels of shed syndecan-1 are significantly increased in the BALF of WT mice at 1 day, 14 and 28 days post-exposure (Figure 8A-C, n=5). Additional significant increases in shed syndecan-1 were seen in asbestos-treated EC-SOD KO mice at the 1 day and 28 day time points compared to WT asbestos mice (Figure 8A and C). Initial studies show that titanium dioxide (control particulate) does not induce heparan sulfate or syndecan shedding into the BALF in wild type nor EC-SOD KO mice. To keep animal numbers to a minimum, the titanium dioxide control was not included for the EC-SOD KO strain for every time point and experiment.

In a second model of pulmonary fibrosis, bleomycin injury caused a significant increase in shed syndecan-1 in the BALF of EC-SOD KO mice when compared to WT mice at day 7 after bleomycin treatment (Figure 8D). Syndecan-1 cell surface expression also increases by day 28 in

tissue homogenates of asbestos-exposed EC-SOD KO mice, with the trend beginning at 14 days post-exposure (Figure 9). These findings suggest that syndecan-1 is sensitive to oxidative shedding during the inflammatory (1 day time point) and fibrotic (7-28 day time points) phases of pulmonary fibrosis and that syndecan-1 cell surface expression increases with fibrosis development.

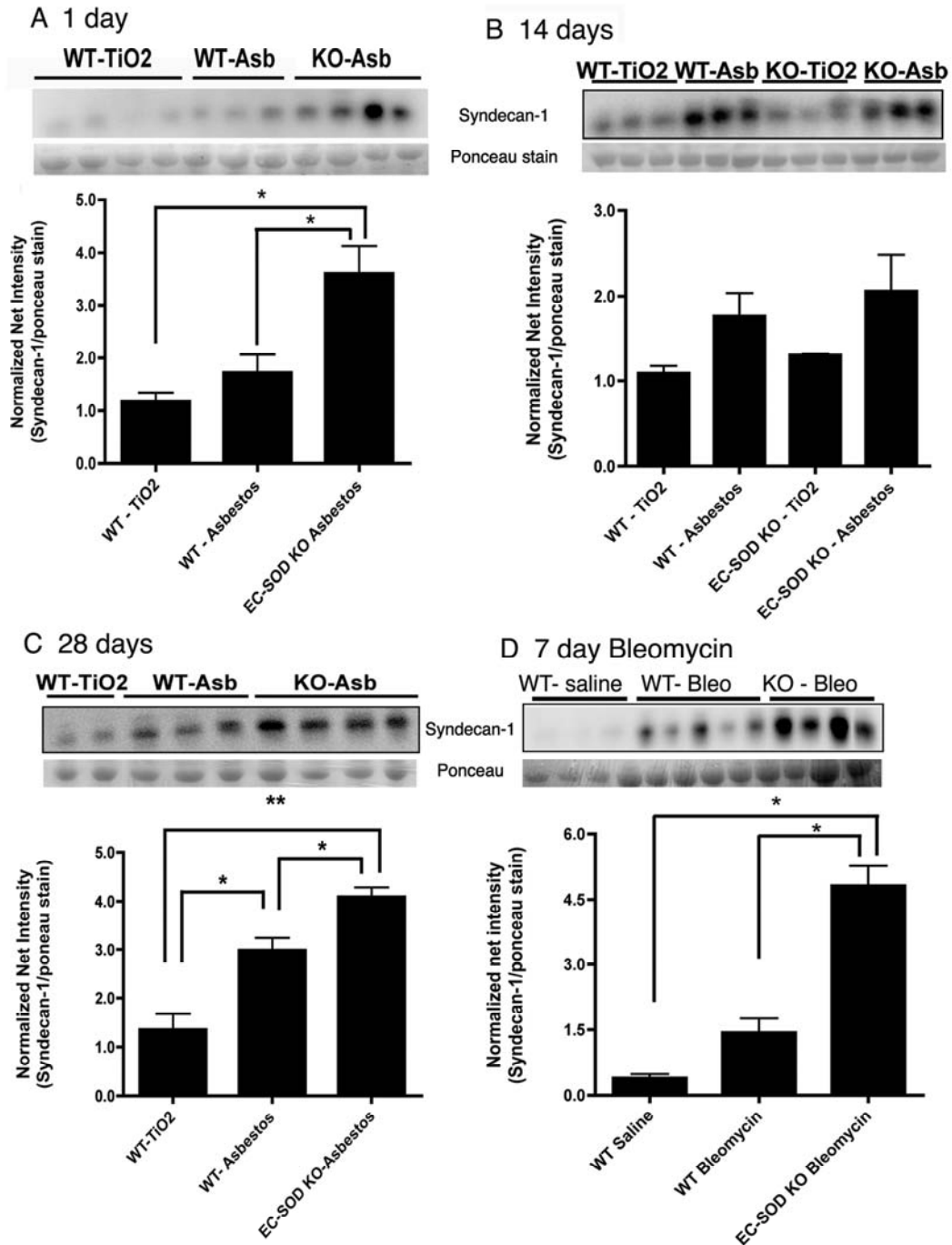


Figure 8: Syndecan-1 ectodomain is shed into the BALF during pulmonary fibrosis. The syndecan-1 ectodomain protein was detected in BALF samples using western blot analysis with normalization to ponceau red and reported as mean \pm SEM. A) 24 hours post-asbestos exposure; B) 14 days post-asbestos exposure; C) 28 days post-asbestos exposure; D) 7 days post-Bleomycin exposure. *, $p < 0.05$.

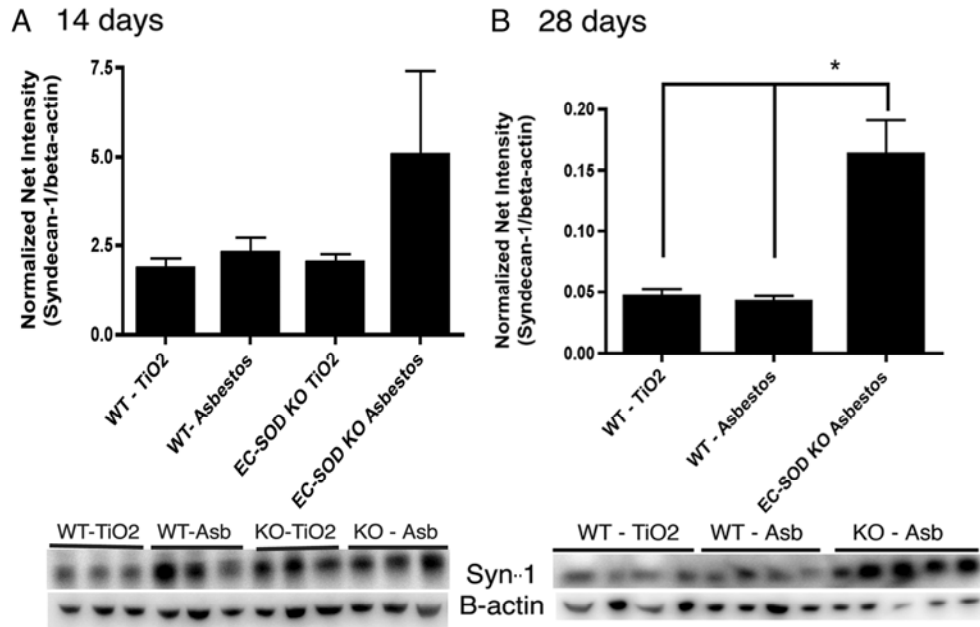


Figure 9: Syndecan-1 changes in lung homogenates after asbestos exposure. Syndecan-1 in lung homogenates was determined by western blot at A) 14 days post-asbestos exposure and B) 28 days post-asbestos, *, $p < 0.05$, $n = 3-5$; A significant increase in syndecan-1 protein expression is seen at 28 days in the EC-SOD KO mice compared to WT.

Syndecan-4 is also sensitive to oxidative shedding in the lung. BALF was analyzed by western blot analysis for the syndecan-4 ectodomain of the core protein. At day 1 and 28 post-asbestos exposure, shed syndecan-4 was significantly increased in the BALF of asbestos-treated EC-SOD KO mice compared to asbestos WT mice (Figure 10A, C). Syndecan-4 levels were significantly elevated in asbestos-treated WT mice only at the 14 day time point (Figure 10B). Similar to syndecan-1 in the bleomycin fibrosis model, syndecan-4 shedding is also increased in BALF of EC-SOD KO at day 7 after bleomycin (Figure 10D). There is a trend toward increased syndecan-4 cell surface expression in tissue homogenates by day 28 post-asbestos exposure (Figure 11).

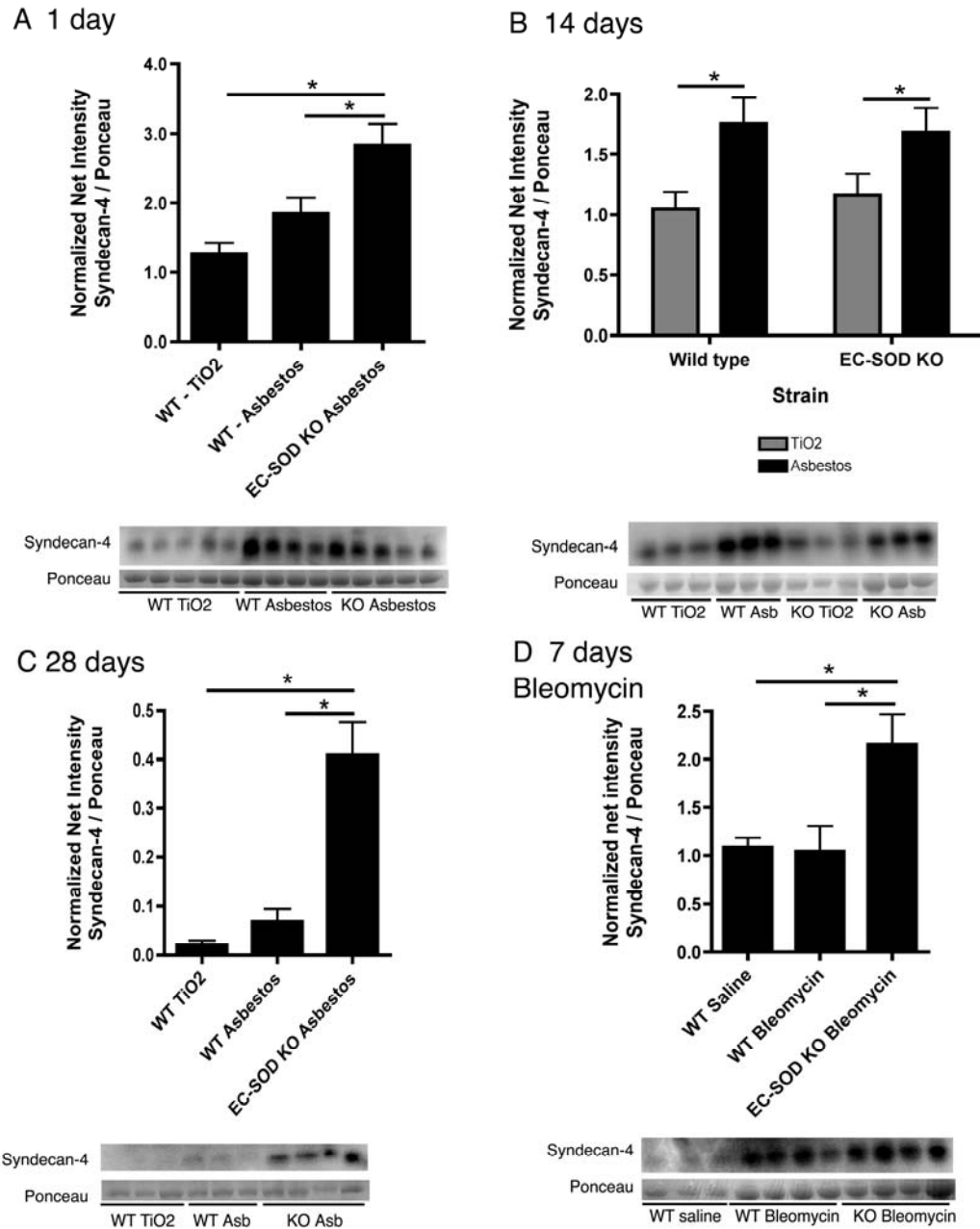


Figure 10: Syndecan-4 ectodomain is shed into the BALF during pulmonary fibrosis. The syndecan-4 ectodomain protein was detected in BALF samples using western blot analysis with normalization to ponceau red and reported as mean \pm SEM. A) 24 hours post-asbestos exposure; B) 14 days post-asbestos exposure; C) 28 days post-asbestos exposure; D) 7 days post-Bleomycin exposure. *, $p < 0.05$.

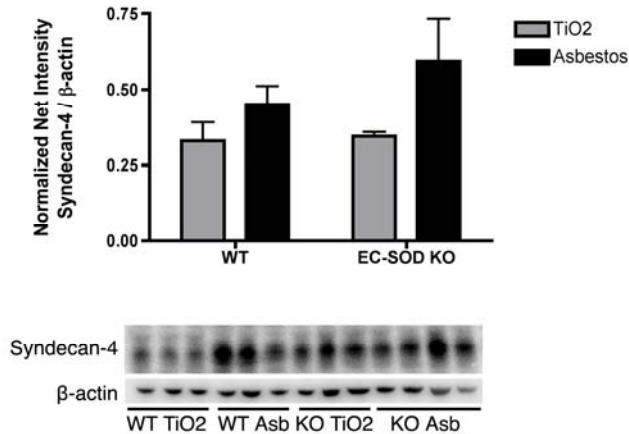


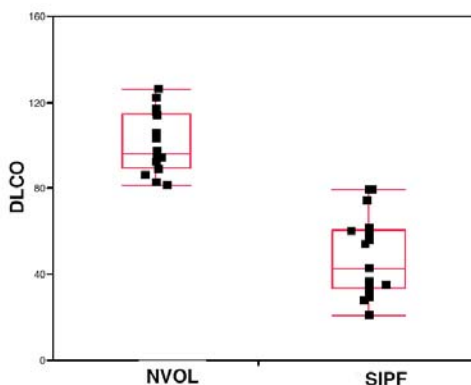
Figure 11: Syndecan-4 trends toward increased expression in lung homogenates after asbestos.

Syndecan-4 in lung homogenates was determined by western blot at 28 days post-asbestos, n=3-5.

5.2 SYNDECAN SHEDDING IN HUMAN IDIOPATHIC PULMONARY FIBROSIS

To investigate if syndecan shedding also occurs in subjects affected with Idiopathic pulmonary fibrosis (IPF), we measured syndecan-1 and syndecan-4 levels by western blot analysis in BALF and lung homogenates from patients who met ATS/ERS criteria for sporadic IPF⁴. The patient population studied includes normal control volunteers with an average age of 49 ± 15 , 60% male and >90% Caucasian. The average age of the IPF patient population was $66 \text{ yo} \pm 9$, 87% male and >90% Caucasian. Pulmonary function testing shows a restrictive pattern in the IPF patients, as well as, abnormal diffusion capacity of the lung for carbon monoxide (DLCO) (Figure 12A, Personal communication & permission from Ivan Rosas, M.D.). A decrease in percent predicted DLCO, as apparent in this IPF population, suggests thickening of the alveolar interstitium and decreased alveolar gas exchange. Cellular analysis of BALF samples show that the IPF patients have significant increases in total cell counts, neutrophils, and eosinophils (Figure 12B, *p<0.05).

Lung Function Measured by Diffusion Capacity



A

B

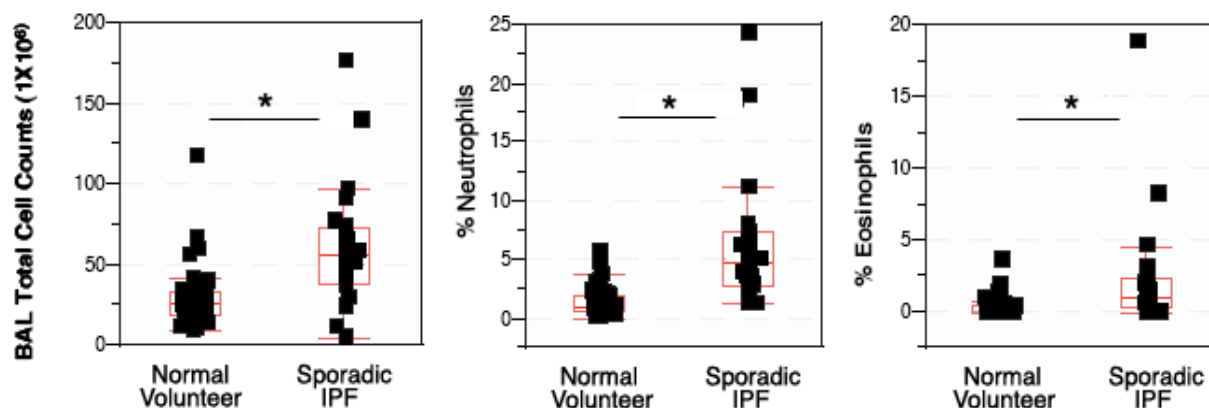


Figure 12: IPF and normal volunteer pulmonary function and BALF characteristics. The diffusion capacity of the lung for carbon monoxide (DLCO) was determined. A) DLCO percent of the predicted value; B) Total BALF cell counts, percent neutrophils, and percent eosinophils in BALF were determined from normal volunteers and IPF patients (personal communication & permission from Ivan Rosas, M.D.).

Shed syndecan-1 ectodomains in BALF samples from the normal volunteers and IPF patients were analyzed by western blot. Patients with sporadic IPF have significant increases in shed syndecan-1 in their BALF ($p < 0.01$, Figure 13A) and lung homogenates ($p < 0.05$, Figure 13B) compared to normal controls.

Syndecan-4 levels were also significantly increased in the BALF ($p < 0.05$, Figure 14A) and lung homogenates ($p < 0.05$, Figure 14B) of IPF patients compared to controls.

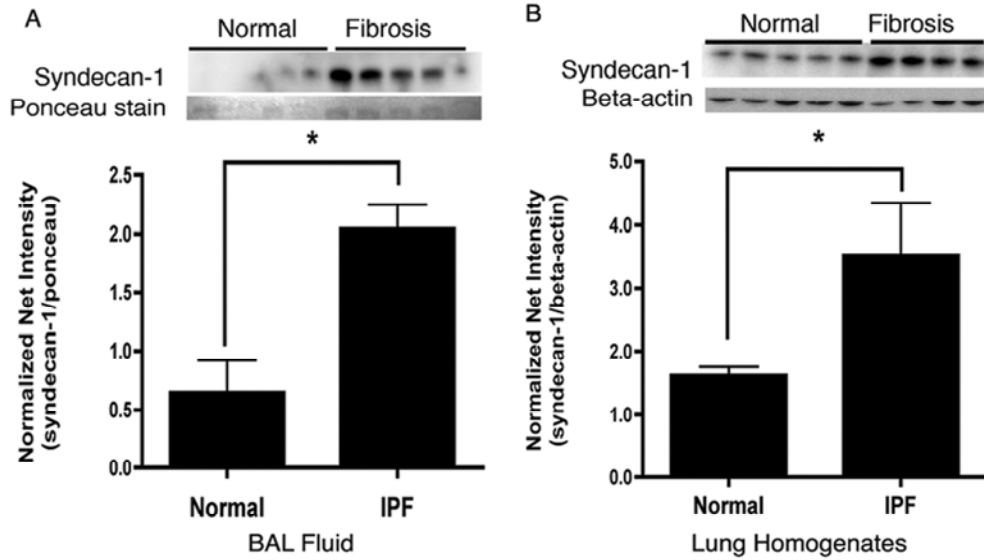


Figure 13: Increased syndecan-1 ectodomain in the BALF and lung of IPF patients. Syndecan-1 was detected by western blot analysis and presented as normalized net intensity. Protein loading was standardized by ponceau red stain for BALF samples and β -actin for lung homogenates (mean \pm SEM). Increased syndecan-1 in A) BALF samples, *, $p < 0.05$, $n = 5$ and B) lung homogenate samples, *, $p < 0.05$, $n = 4$ or 5.

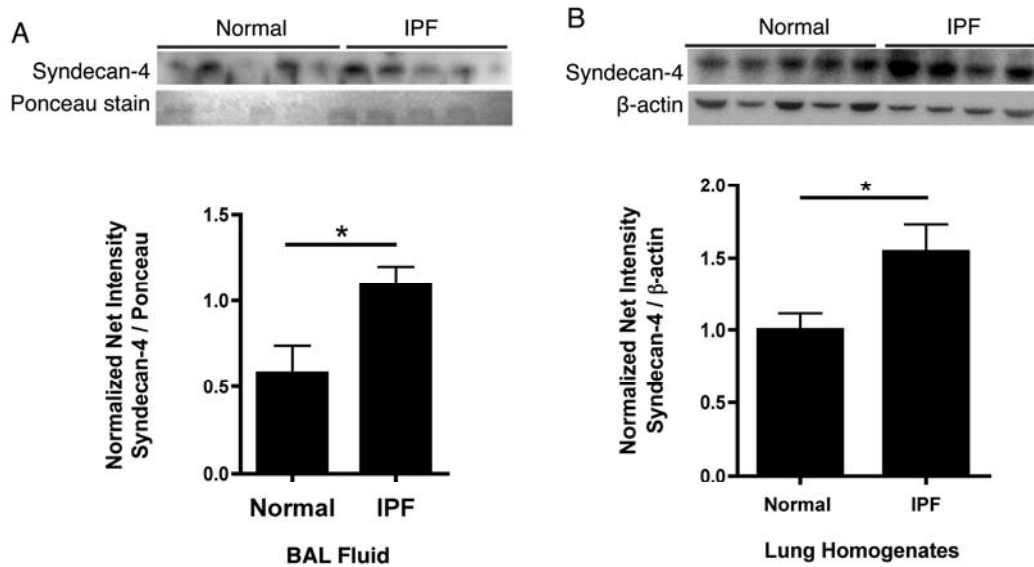


Figure 14: Increased syndecan-4 in BALF and lung in IPF patients. Syndecan-4 was detected by western blot analysis and presented as normalized net intensity. Protein loading was standardized by ponceau red stain for BALF samples and β -actin for lung homogenates (mean \pm SEM). Increased syndecan-4 in A) BALF samples, *, $p < 0.05$, $n = 5$ and B) lung homogenate samples, *, $p < 0.05$, $n = 4$ or 5.

IPF disease progression can be classified by disease severity stages based on pulmonary function testing: mild, moderate and severe IPF. Syndecan-1 levels in BALF samples were quantified by ELISA. IPF patients at all disease severity stages show increases in the levels of shed syndecan-1 in BALF samples (Figure 15). Syndecan-1 levels are lower in the cases of severe IPF, which may be due to lung burnout where the fibrosis and collagen deposition has encompassed much of the alveolar epithelium creating lower cell numbers and syndecan-1 levels.

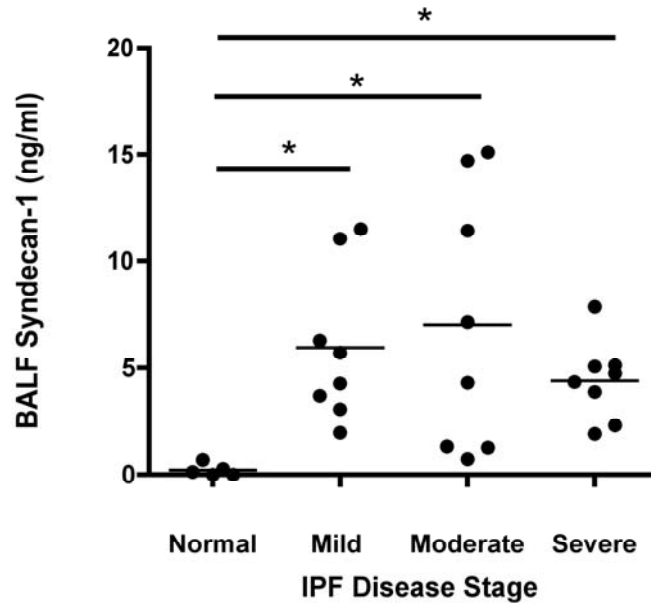


Figure 15: Levels of BALF Syndecan-1 increase with all stages of IPF disease severity. BALF samples from normal volunteers and IPF at mild, moderate and severe IPF stages were assayed for syndecan-1 using a CD138 (Syn-1) ELISA kit. Samples were assayed in triplicate and data are reported as mean \pm SEM for each sample, * $p < 0.05$, $n = 8$ per disease stage. Disease stages were clinically determined by lung function testing and DLCO.

5.3 FIBROTIC LUNG INJURY MODULATES EC-SOD AND SYNDECAN-1 DISTRIBUTION IN THE LUNG.

To further investigate syndecan-1 and EC-SOD expression in the lung in response to pulmonary fibrosis, H&E staining and immunofluorescent staining for syndecan-1 and EC-SOD were performed on human and mouse lungs with and without fibrosis. H&E staining confirmed the presence of fibrosis in human lungs with IPF (Figure 16). IPF lungs show heterogeneous fibrosis with areas of thickened alveolar septae and increased collagen deposition (Figure 16 B, D). Classic histological findings in IPF lungs were observed including myofibroblastic foci (Figure 17), which are considered to be active areas of inflammation and progressive fibrosis.

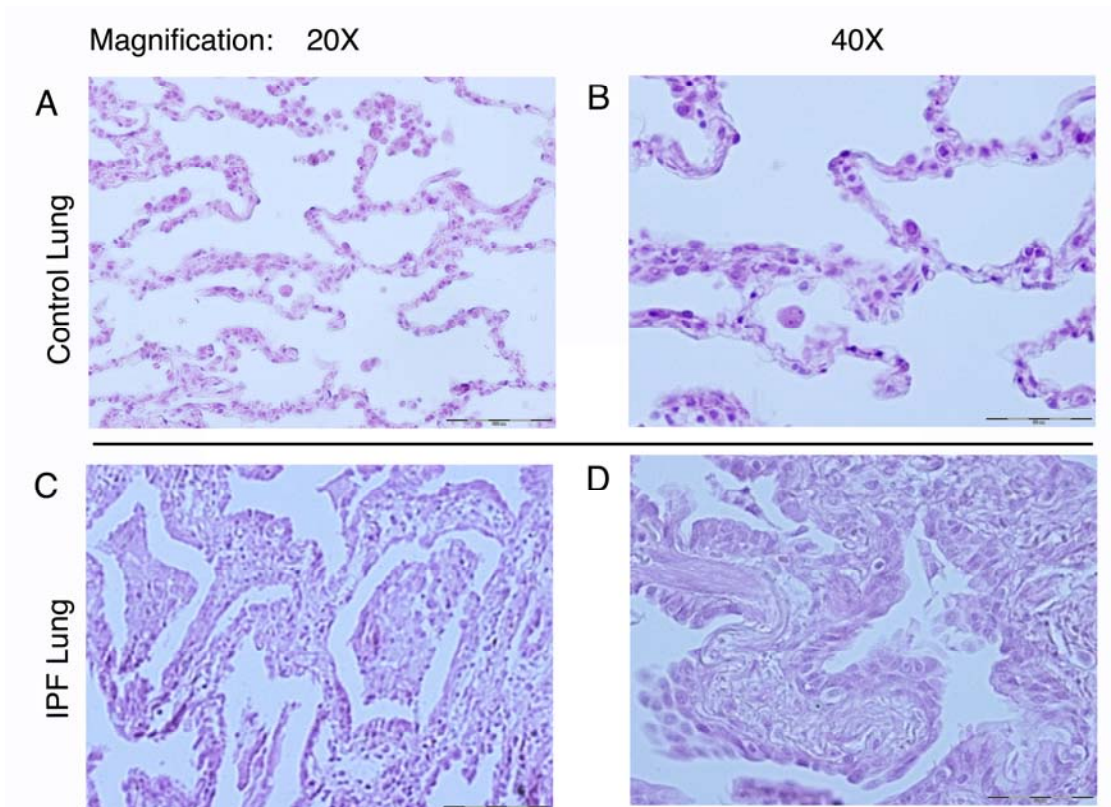


Figure 16: H&E staining of control and IPF lung. Control and IPF lung sections (4 μ m) were stained with H&E. A) Control human lung at 20X; B) Control lung at 40X depicting thin alveolar septae; C) IPF lung at 20X magnification showing thickening of the interstitium; D) IPF lung at 40X showing wispy collagen deposition.

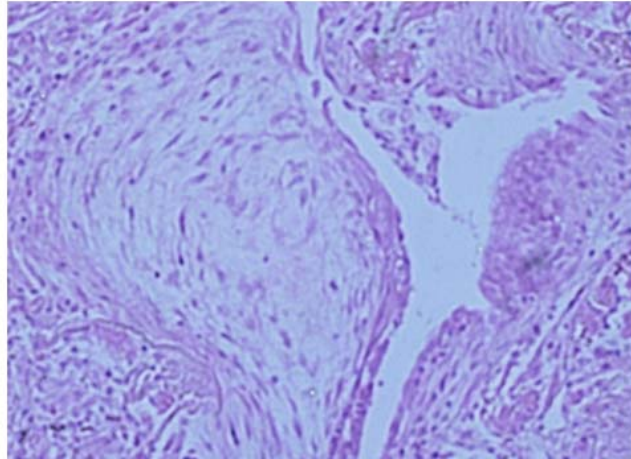


Figure 17: Myofibroblastic foci within an IPF lung. This H&E section cut from IPF paraffin-embedded lung shows a classical myofibroblastic foci. This area contains spindle-shaped myofibroblast cells with dispersed collagen deposition.

Syndecan-1 and EC-SOD localization was determined by immunofluorescent staining of lung sections from normal human lung and sporadic IPF (Figure 18). Normal human lung in figure 18-a shows ubiquitous staining for EC-SOD (*green*) with sparse staining for syndecan-1 (*red*) and colocalization of the two proteins (*yellow*, arrows). Similarly, in an area of normal lung architecture in an IPF lung section (Figure 18-c), EC-SOD staining is ubiquitous with sparse syndecan-1. In contrast, in areas of fibrosis in IPF lung, figure 18-b and d, syndecan-1 stains strongly on the abluminal surface of alveolar epithelial cells, terminal bronchiolar epithelial cells, and within areas of fibrosis (*double asterisks*) while EC-SOD staining decreases in fibrotic areas (*single asterisk*, Figure 18-b). Syndecan-1 and EC-SOD colocalize in some areas (Figure 18-d, *arrows*).

Human

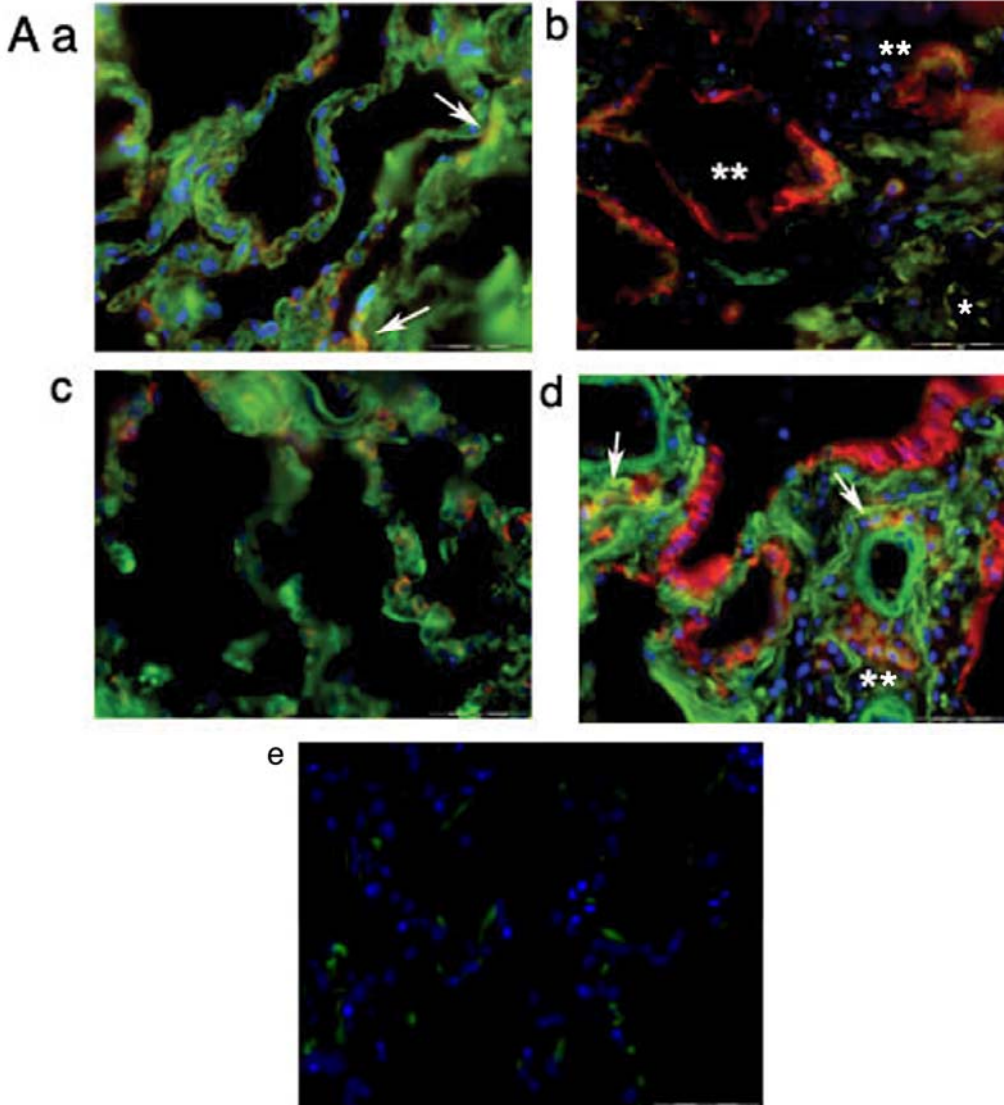


Figure 18: Localization of EC-SOD and syndecan-1 in human lung sections. *Green*, EC-SOD; *red*, syndecan-1; *blue*, nuclear stain; *yellow*, co-localization. a) Normal human lung shows diffuse staining for EC-SOD in the lung parenchyma with focal areas of syndecan-1 expression that co-localize with EC-SOD (*yellow*; arrows). c) Areas of IPF lung with normal lung architecture show similar staining for both syndecan-1 and EC-SOD. In contrast, areas of fibrosis in IPF lung (b and d) show increased staining for syndecan-1 (*red*, asterisks) and decreased EC-SOD (*green*, single asterisk). e) Non-immune IgG staining control on control human lung.

In the asbestos mouse model, the injury leads to peribronchial and alveolar fibrosis similar to that seen in IPF and was confirmed by H&E staining in our pulmonary fibrosis model (Figure 19). Asbestos fibers can pierce and become embedded in the interstitium or engulfed by alveolar macrophages, as depicted in figure 19-d. To confirm the localization findings in human IPF lung, mouse lungs were stained for syndecan-1 and EC-SOD at 28 days post-exposure to TiO₂ (control particulate) or asbestos. Normal lung from a wild type mouse treated with TiO₂ shows diffuse staining for EC-SOD (*green*) and sparse syndecan-1 (*red*) (Figure 20-a). In contrast, areas of fibrosis in figure 20-b show a decrease in interstitial EC-SOD (*single asterisk*), a diffuse increase in syndecan-1 (*double asterisks*), and co-localization of the two proteins in WT mice treated with asbestos (*yellow*, arrows). Likewise, EC-SOD KO mice show a significant increase in syndecan-1 in areas of fibrosis after asbestos exposure (Figure 20-d, *double asterisk*) compared to TiO₂-treated mice (Figure 20-c). In summary, both the human and mouse lung staining show that syndecan-1 staining increases in areas of fibrosis with a decrease in interstitial EC-SOD.

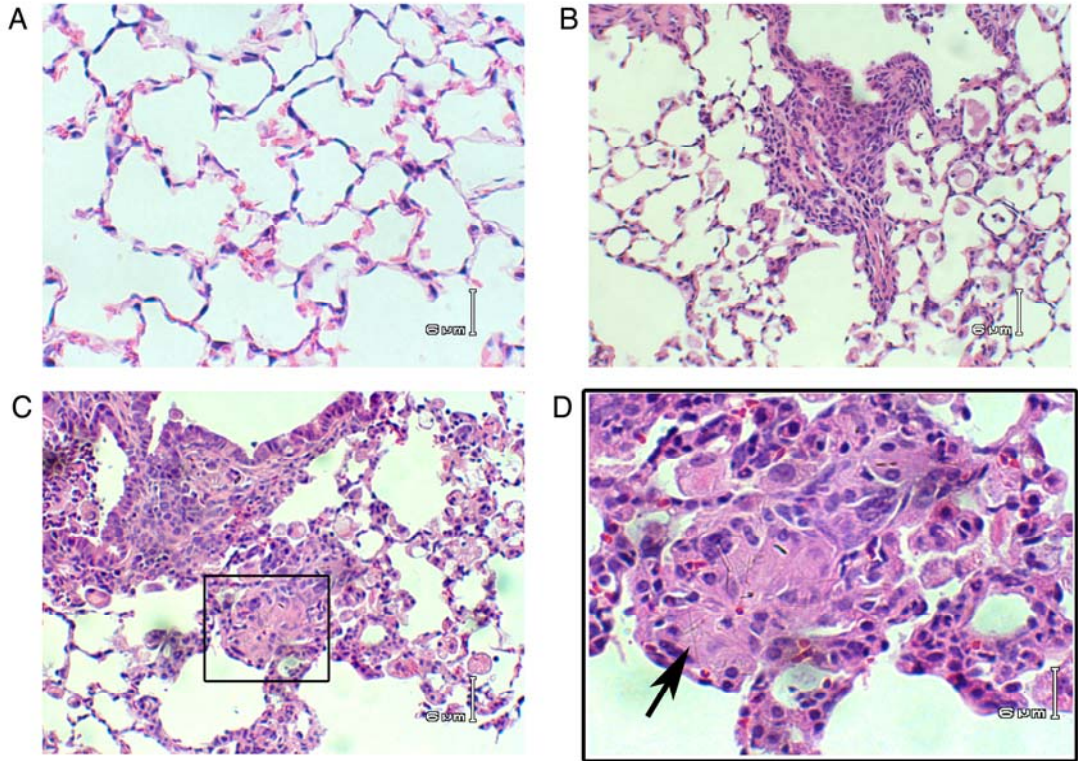


Figure 19: H&E staining of mouse lung after asbestos exposure. Paraffin blocks of WT mouse lung were sectioned (4µm) and stained with H&E. A) Normal mouse lung with thin alveoli and minimal inflammatory cells. B & C) Asbestos-treated mouse lung at 20X displaying interstitial fibrosis and inflammation. D) Higher magnification of the inset of C shows the presence of asbestos fibers surrounded by collagen and macrophages.

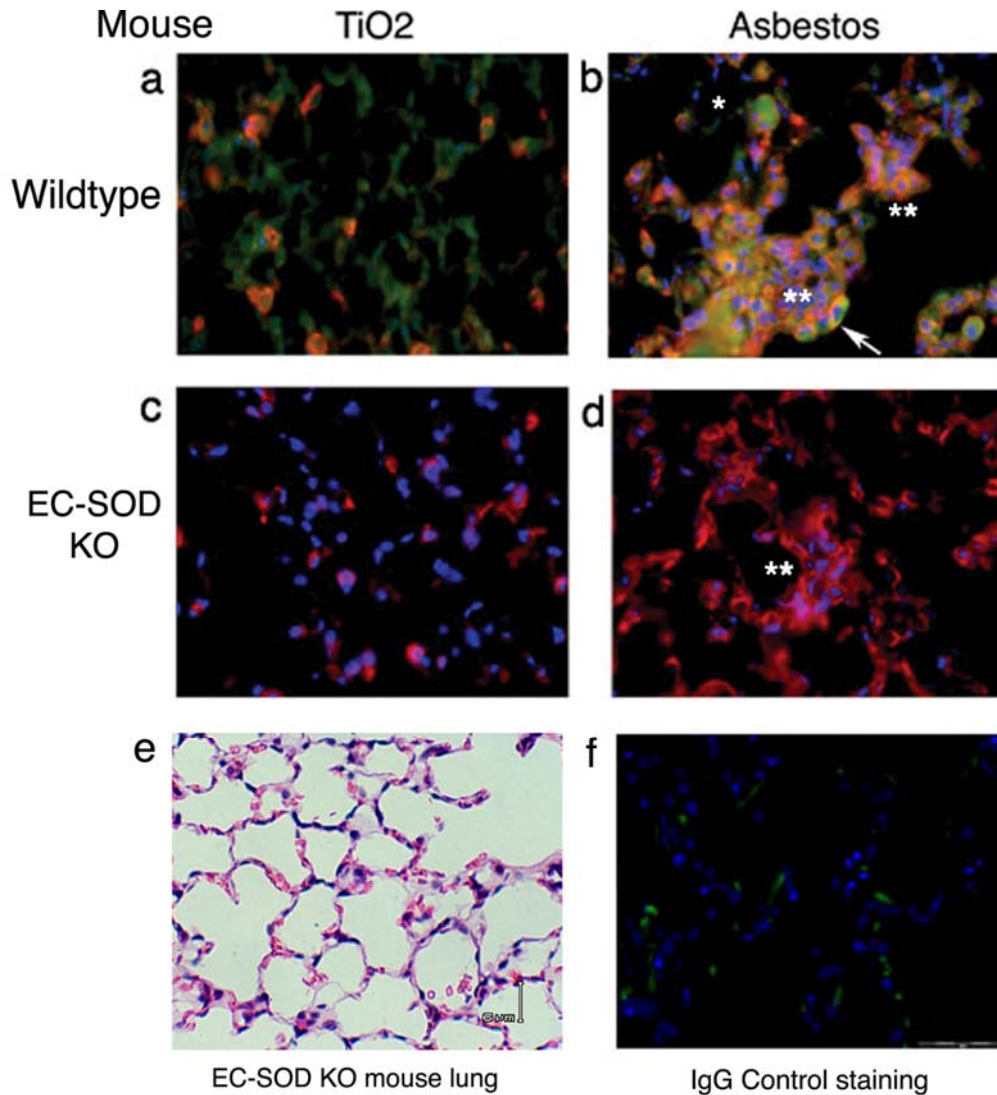


Figure 20: Localization of EC-SOD and syndecan-1 in mouse lung sections. *Green*, EC-SOD; *red*, syndecan-1; *blue*, nuclear stain; *yellow*, co-localization. Lung sections from WT and EC-SOD KO mice treated with asbestos or TiO₂ at 28 days post-exposure were stained for EC-SOD and syndecan-1. a) Normal lung architecture of TiO₂-treated WT mice shows diffuse EC-SOD staining and focal syndecan-1 staining that co-localizes with EC-SOD. b) Fibrotic areas of asbestos-treated WT mice show increased diffuse staining for syndecan-1 (double asterisks) that co-localize with EC-SOD (*yellow*, arrows). EC-SOD KO mouse lungs were stained for syndecan-1 depicting c) normal lung architecture with TiO₂ treatment and d) fibrosis with asbestos. There are significant increases in syndecan-1 staining in these fibrotic areas (double asterisk); e) H&E staining of normal lung architecture with TiO₂ treatment shown in section c; f) No staining was seen with non-immune IgG control staining.

Previous studies report that during fibrotic injury, EC-SOD decreases in the lung interstitium while increasing in the alveolar space, as determined by western blot analysis of lung homogenates and BALF, respectively^{60, 63}. Real time reverse transcriptase polymerase chain reaction (RT-PCR) was completed to confirm our IHC staining for EC-SOD in mouse lung. In wild type mice, asbestos exposure results in a significant decrease in EC-SOD gene expression (ddCT) at 14 days post-exposure (Figure 21A): percent relative EC-SOD gene expression from TiO₂-treated lungs: 100% ± 4.96 *versus* 76.32% ± 3.40 for asbestos-treated lungs; *, p<0.05. Syndecan-1 gene expression in the lung is not significantly different between TiO₂, control-treated WT mice (100% ± 4.51) and EC-SOD KO mice (99.46% ± 4.51); p = 0.95. **This led us to hypothesize that the absence of EC-SOD during pulmonary fibrosis, may leave syndecan-1 vulnerable to oxidative stress and lead to shedding of membrane syndecan-1.**

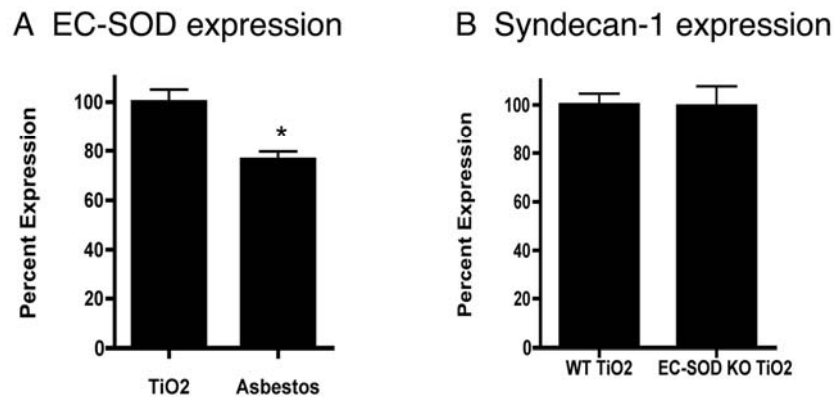


Figure 21: EC-SOD and syndecan-1 expression by Real time RT-PCR. Data are reported as percent relative ddCT gene expression for A) EC-SOD gene expression in WT mice treated with TiO₂ or asbestos and B) syndecan-1 expression in control-treated WT and EC-SOD KO mice. *, p<0.05.

5.4 HEPARAN SULFATES & SYNDECAN-1 ARE OXIDATIVELY FRAGMENTED BY REACTIVE OXYGEN SPECIES.

Asbestos injury to the lung results in increased production of reactive oxygen species (ROS) in the cell microenvironment of the lung. To mimic this production in an *in vitro* system, we utilized a $\text{CuSO}_4/\text{H}_2\text{O}_2$ system, which generates superoxide and highly reactive hydroxyl radicals. To confirm that reactive oxygen species are produced in our $\text{CuSO}_4/\text{H}_2\text{O}_2$ system, a colorimetric assay was used to confirm superoxide production. Superoxide was significantly higher in reactions that contained both CuSO_4 and H_2O_2 in the heparin system (Figure 22A). Similar ROS production was found in the heparan sulfate system (data not illustrated). Oxidative fragmentation of heparin and heparan sulfate in the ROS system was confirmed by gel electrophoresis followed by staining for polyanionic carbohydrate species with StainsAll. Both heparin and heparan sulfate were susceptible to oxidative fragmentation, as shown by a shift in the molecular weight bands of heparin or heparan sulfate to lower molecular weight species after ROS treatment (Figure 22B, blue boxes).

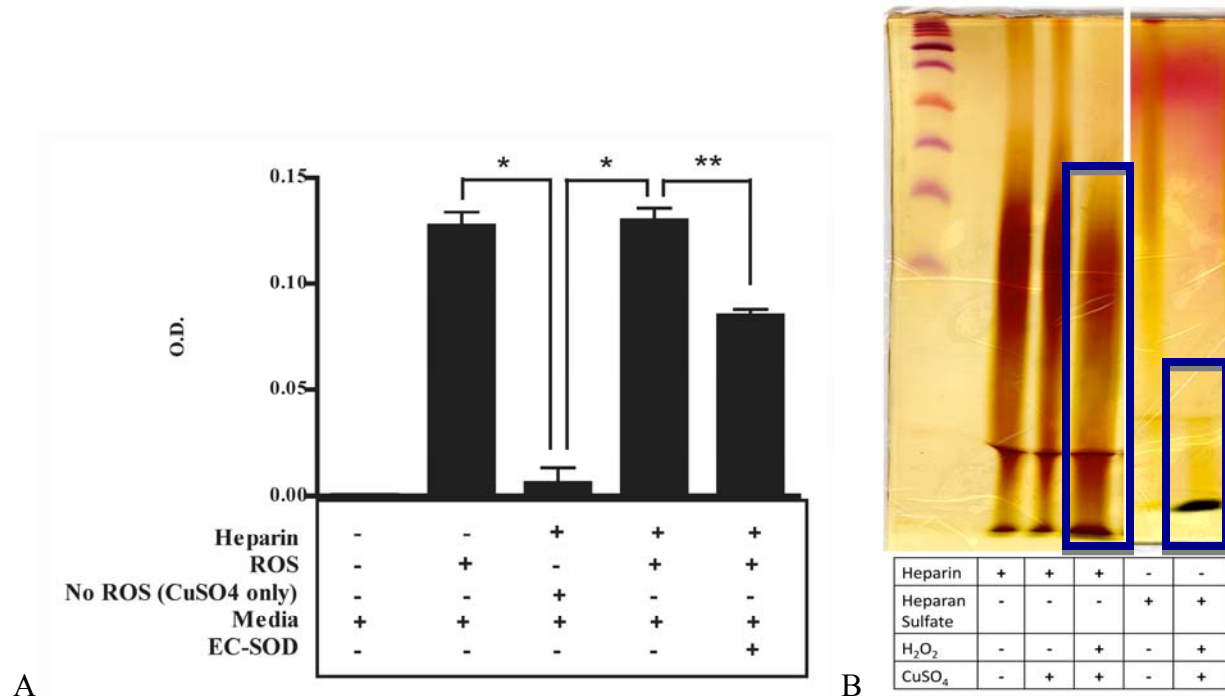


Figure 22: Superoxide production and fragmentation of heparin and heparan sulfate (HS). WST-1 reagent was utilized to determine the relative amount of superoxide produced in the CuSO₄/H₂O₂ reaction system. Optical density (O.D.) is proportional to superoxide production. A) Superoxide is produced in a Fenton-like reaction, which can be inhibited by EC-SOD. Similar superoxide levels were produced in the presence of HS as well. B) ROS production through the CuSO₄/H₂O₂ reaction can fragment heparin (left lanes) and heparan sulfate (right lanes). ROS causes a band shift to lower molecular weight species (blue boxed areas).

To determine if reactive oxygen species lead to shedding of syndecan-1 *in vitro*, A549 cells were exposed to ROS in the presence or absence of human EC-SOD. Syndecan-1 can be oxidatively shed from A549 cells, as shown by a significant increase in levels of shed syndecan-1 ectodomain in supernatants after ROS treatment (dot blot analysis, Figure 23 A and B). Syndecan-1 shedding was partially independent of protease activity because the shedding response was not completely abrogated by protease inhibitors for serine and cysteine proteases (DCI, Dichloro-isocoumarin and E-64, L-transepoxy succinyl-leucylamido-[4-guanidino]butane)

and broad matrix metalloproteinases (GM2001 inhibitor). Furthermore, the presence of EC-SOD can significantly protect these cells from ROS-induced shedding of syndecan-1 ectodomains.

Consistent with these findings, we fluorescently labeled syndecan-1 on cell monolayers and observed loss of cell surface syndecan-1 staining after ROS exposure and a recovery with the presence of EC-SOD. This confirms that shedding can occur oxidatively and can be inhibited by EC-SOD (Figure 23 C).

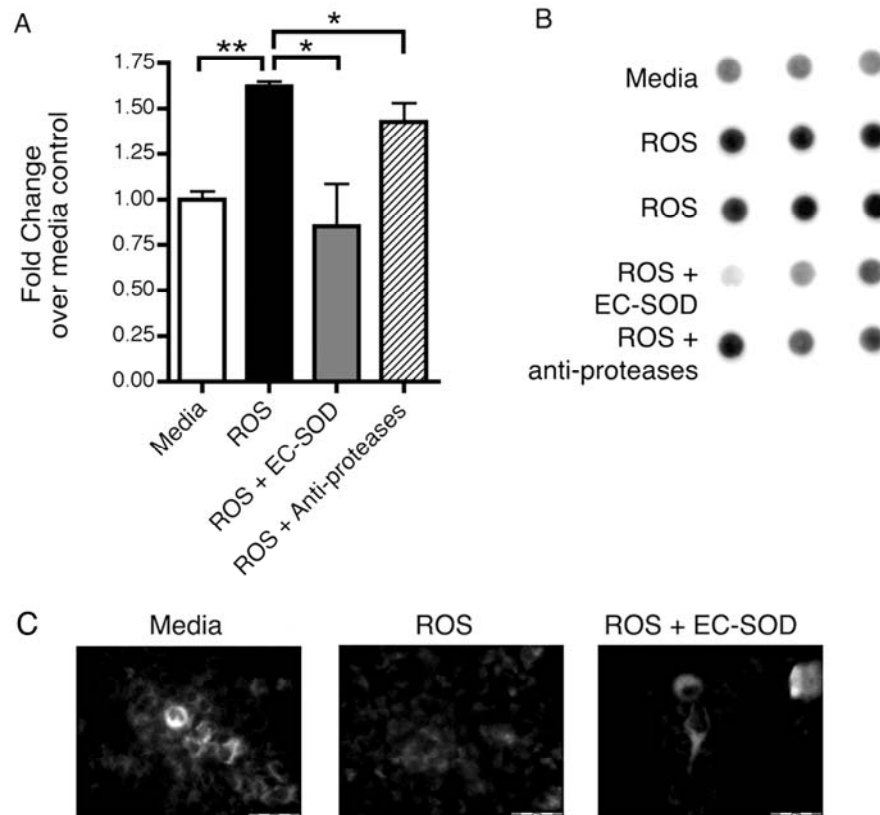


Figure 23: EC-SOD protects against oxidative shedding of Syndecan-1. A549 cells were treated with ROS in the presence or absence of purified human EC-SOD. A & B) Dot blots of the culture medium were probed for human syndecan-1 ectodomain. Results are presented as fold increase in dot intensity over medium-treated controls (mean \pm SEM). *, $p < 0.05$. **, $p < 0.01$. C) Representative images of fluorescent staining of syndecan-1 on A549 cells after ROS treatment in the presence or absence of EC-SOD (100 Units).

The concentration of syndecan-1 in A549 cell supernatant was quantified by ELISA for medium *versus* ROS treatment and were determined to be 9.2 ng/ml \pm 2.3 and 42.3 ng/ml \pm 1.9 (p<0.0001), respectively. ROS treatment does not induce apoptosis in the cells, as there are no changes in caspase-3 activity in cell lysates after ROS treatment (caspase-3 activity, RFUs: medium 657.1 \pm 73.1 *versus* ROS 405.3 \pm 75.1; p = 0.073, n=3).

5.5 OXIDATIVELY FRAGMENTED HS AND SYNDECAN-1 INDUCE NEUTROPHIL CHEMOTAXIS.

Inflammatory cell influx is a feature of the pathogenesis of pulmonary fibrosis, both in IPF^{7, 9, 290} and animal models^{57, 60, 62, 63, 226}. The IPF patient population studied in this investigation had neutrophilia and eosinophilia in their BALF (Figure 12), as well as, increased levels of shed syndecan-1 (Figure 13 and 14). Because heparan sulfate (HS) and syndecan-1 have been shown to be important in IPF and animal models of pulmonary fibrosis, we hypothesize that oxidatively shed heparan sulfate and syndecan-1 would promote neutrophil chemotaxis in the lung. A modified Boyden chamber was used to evaluate the effect of EC-SOD and oxidatively fragmented heparin/HS or the shed syndecan-1 ectodomain on human neutrophil chemotaxis. Various amounts of ROS produced from CuSO₄ and H₂O₂ could induce heparin/HS fragmentation and subsequent chemotaxis of neutrophils, specifically within the range of 0.8-2.0 μ M CuSO₄ and 1.1–2.0 mM H₂O₂ (Figure 24). Neutrophil chemotaxis demonstrated increasing chemotaxis with higher concentrations of ROS, followed by a decrease with the highest concentration of ROS. All subsequent data presented are for concentrations of ROS produced by 1.25 μ M CuSO₄ and 1.5 μ M H₂O₂.

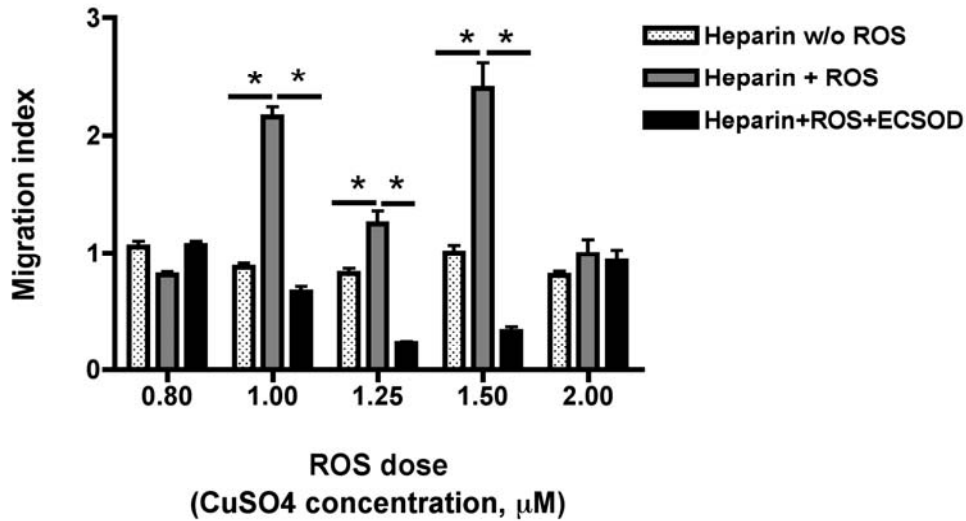


Figure 24: Neutrophil chemotaxis is induced by ROS-fragmented heparin. Heparin was treated with ROS in the presence or absence of EC-SOD for 2 hrs then applied to the lower chamber of the chemotaxis assay. Data reported as neutrophil migration index. An index >1 represents positive chemotaxis. ROS significantly induced neutrophil chemotaxis and EC-SOD was capable of preventing this. *, p<0.05.

ROS-treated heparin significantly (p<0.001) induces neutrophil chemotaxis compared to heparin without ROS (Figure 25A) and EC-SOD can inhibit this response (p<0.001). Unfragmented heparin does not induce chemotaxis. No significant differences were found between heparin without ROS and heparin with both ROS and EC-SOD. EC-SOD was able to inhibit chemotaxis at 50 Units (not illustrated) and 100 Units/lower well chamber by preventing superoxide from going to hydroxyl radicals and preventing heparin fragmentation and subsequent neutrophil chemotaxis. Similar results were found with ROS-fragmented heparan sulfate (HS) with inhibition of chemotaxis by EC-SOD (Figure 25 B). No chemotaxis was seen with ROS in the absence of heparin and heparan sulfate, nor with heparan sulfate proteoglycan (HSPG) alone. DMEM media, ROS and EC-SOD (100 Units) alone do not stimulate chemotaxis.

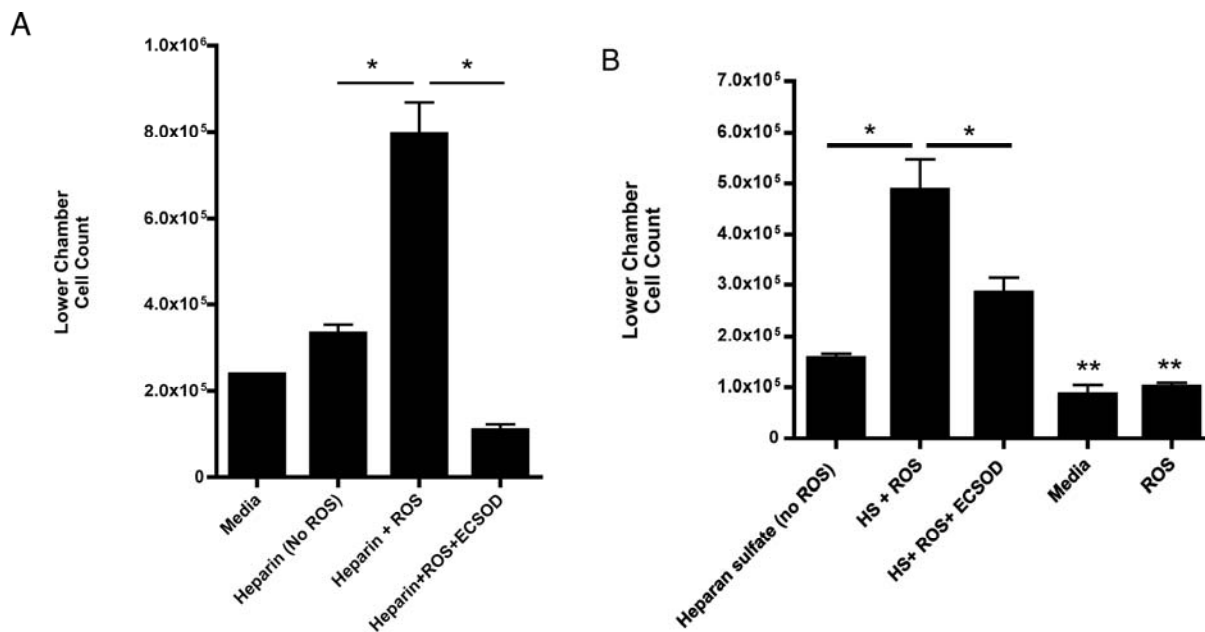


Figure 25: EC-SOD inhibits neutrophil chemotaxis induced by oxidative fragmentation of heparin and HS. Chemotaxis was assessed using a modified Boyden chamber and ROS were produced using 1.25 μ M CuSO₄ and 1.5mM H₂O₂. Purified EC-SOD significantly inhibits neutrophil chemotaxis induced by ROS-fragmented (A) heparin *, p<0.001 and (B) heparan sulfate *, p<0.05 **, p<0.05 versus HS+ROS and HS+ROS+EC-SOD. Data are reported as mean cells number in the lower chamber \pm SEM. 100 Units of EC-SOD was used and scavenges superoxide radicals to prevent further hydroxyl radical formation.

The protection offered by EC-SOD can occur in two ways – through the superoxide scavenging activity or through direct binding to HS through the matrix-binding domain of EC-SOD. To determine the mechanism through which EC-SOD inhibits HS oxidative fragmentation, EC-SOD and CuZnSOD were analyzed in the chemotaxis assay. CuZnSOD differs from EC-SOD primarily from its lack of a matrix-binding domain. In the chemotaxis assay, human EC-SOD (5-100 units) effectively prevents chemotaxis induced by HS and ROS. CuZnSOD is less effective in preventing chemotaxis at similar doses of SOD. CuZnSOD protection shows increases in protection at 5 and 100 units of SOD but less protection at 50 units. This phenomenon may be occurring due to molecular interactions in the cellular environment. ROS,

H₂O₂, EC-SOD and CuZnSOD alone do not induce chemotaxis (data not illustrated). This data suggests that EC-SOD prevents fragmentation of HSPG through both mechanisms: effective antioxidant activity and direct binding to HS through the matrix-binding domain.

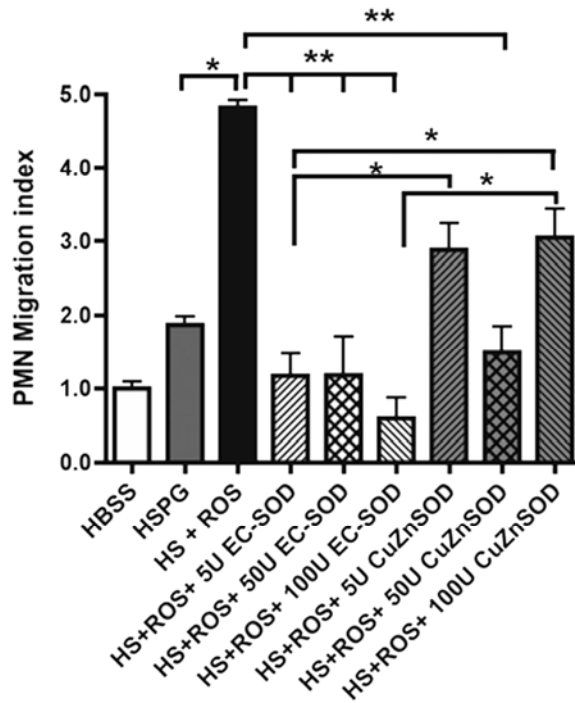


Figure 26: Antioxidant activity and direct binding of EC-SOD to heparan sulfate proteoglycan (HSPG) mediate inhibition of chemotaxis. The effect of EC-SOD binding with HSPG on the ability to fragment HS to cause neutrophil chemotaxis was assessed in a modified Boyden chamber. EC-SOD significantly inhibits chemotaxis induced by oxidatively fragmented HS at all concentrations used. CuZnSOD, which lacks the matrix-binding domain partially inhibits chemotaxis. Data are reported as mean migration index \pm SEM; * or **, $p < 0.05$.

Data from human IPF and *in vivo* mouse studies implicate shed syndecan-1 ectodomains in the pathogenesis of pulmonary fibrosis. To determine role of the syndecan-1 ectodomain in neutrophil chemotaxis, we applied a human syndecan-1 ectodomain (hS1ED) protein to the chemotaxis assay. The human S1ED is derived from a glutathione S-transferase fusion protein. The GST segment is proteolytically removed and the remainder is the syndecan-1 ectodomain of the core protein with no heparan sulfate side chains. hS1ED alone significantly ($p < 0.05$)

increases chemotaxis of human neutrophils (Figure 27, HBSS 1.0 ± 0.49 versus hS1ED 4.42 ± 0.83 , $p < 0.005$).

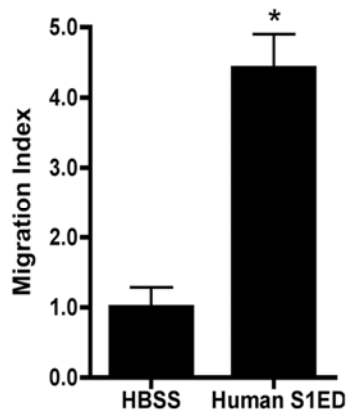


Figure 27: Syndecan-1 ectodomain induces neutrophil chemotaxis. Human syndecan-1 ectodomain (hS1ED) was analyzed in the chemotaxis assay at 1 $\mu\text{g/ml}$. Unmodified hS1ED promotes neutrophil chemotaxis ($n=6$, $*, p < 0.05$). Data are reported as mean neutrophil migration index \pm SEM. Data are representative of three separate experiments.

Furthermore, supernatants from A549 cells containing syndecan-1 ectodomains shed by ROS are chemotactic to neutrophils (Figure 28B; migration index of ROS alone 1.70 ± 0.22 versus HBSS control 1.00 ± 0.10 , $p < 0.001$). Knockdown of cell surface expression of syndecan-1 and subsequent ROS treatment partially inhibits ROS-induced neutrophil chemotaxis (Figure 28A and B; migration index of syndecan-1 siRNA with ROS 1.12 ± 0.07 versus ROS alone 1.70 ± 0.22 , $p < 0.001$). Therefore, the syndecan-1 ectodomain is oxidatively shed from the surface of cells during lung injury and is highly chemotactic to neutrophils.

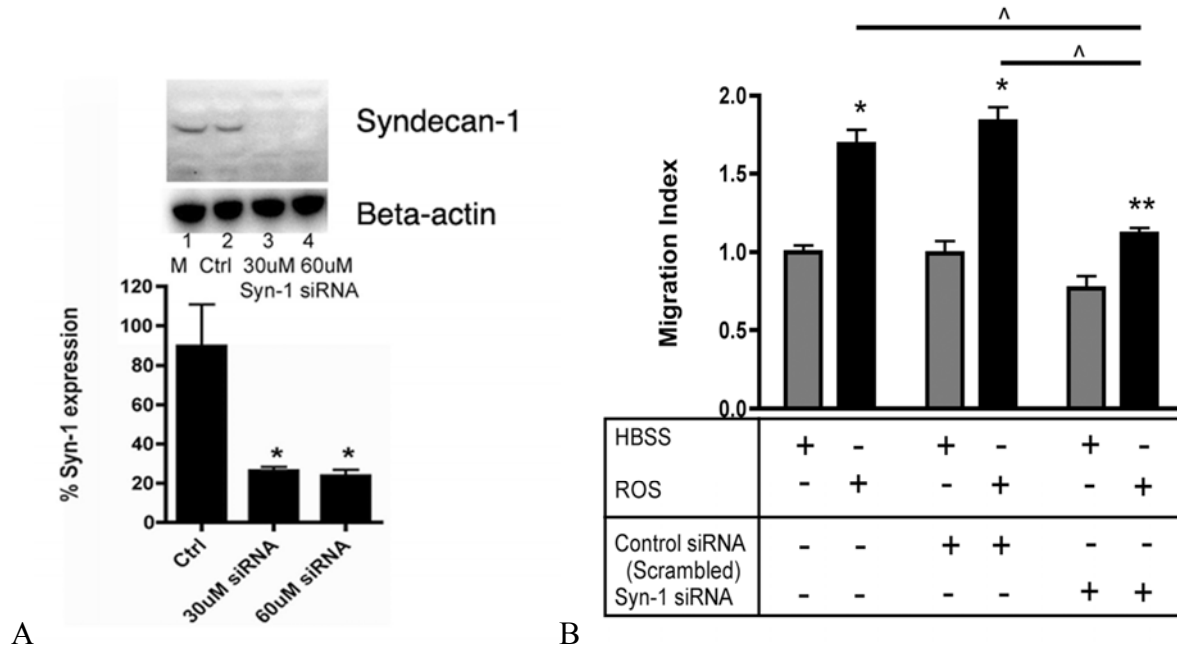


Figure 28: Oxidatively shed syndecan-1 ectodomain induces neutrophil chemotaxis. Supernatants from A549 cells treated with medium, control siRNA or syndecan-1 siRNA for 24 hours prior to experimental treatment with HBSS or ROS, were analyzed in the chemotaxis assay. A) Knock down of syndecan-1 expression in A549 cells was achieved. 30 μ M Syndecan-1 siRNA was used for subsequent experiments. B) Oxidatively shed syndecan-1, in the supernatants from A549 cells, is chemotactic to neutrophils. Knockdown of syndecan-1 protein expression inhibits chemotaxis after ROS treatment. *, $p < 0.001$ and **, $p < 0.01$ versus HBSS; ^, $p < 0.001$; $n = 6$. Grey bars: HBSS treatment; Black bars: ROS treatment.

To evaluate the direct effect of EC-SOD on neutrophil chemotaxis and syndecan-1 shedding *in vivo*, EC-SOD KO mice were co-treated with intratracheal asbestos and 50 units of purified human EC-SOD and evaluated at the 24-hour time point. EC-SOD significantly decreases the influx of neutrophils in the BALF (Fig. 29A percent BALF cells and 29B absolute cell numbers, * $p < 0.05$). Furthermore, EC-SOD results in a significant decrease in shed syndecan-1 ectodomain levels in the BALF (Fig. 29C $p < 0.01$). Human EC-SOD is detectable in the BALF of EC-SOD KO mice after 24 hours in both the TiO₂ and asbestos groups co-treated with EC-SOD (Fig. 29D). However, asbestos injury causes clearance of EC-SOD. The amount of

EC-SOD present in the BALF of this group was much lower and required longer exposure times on western blot.

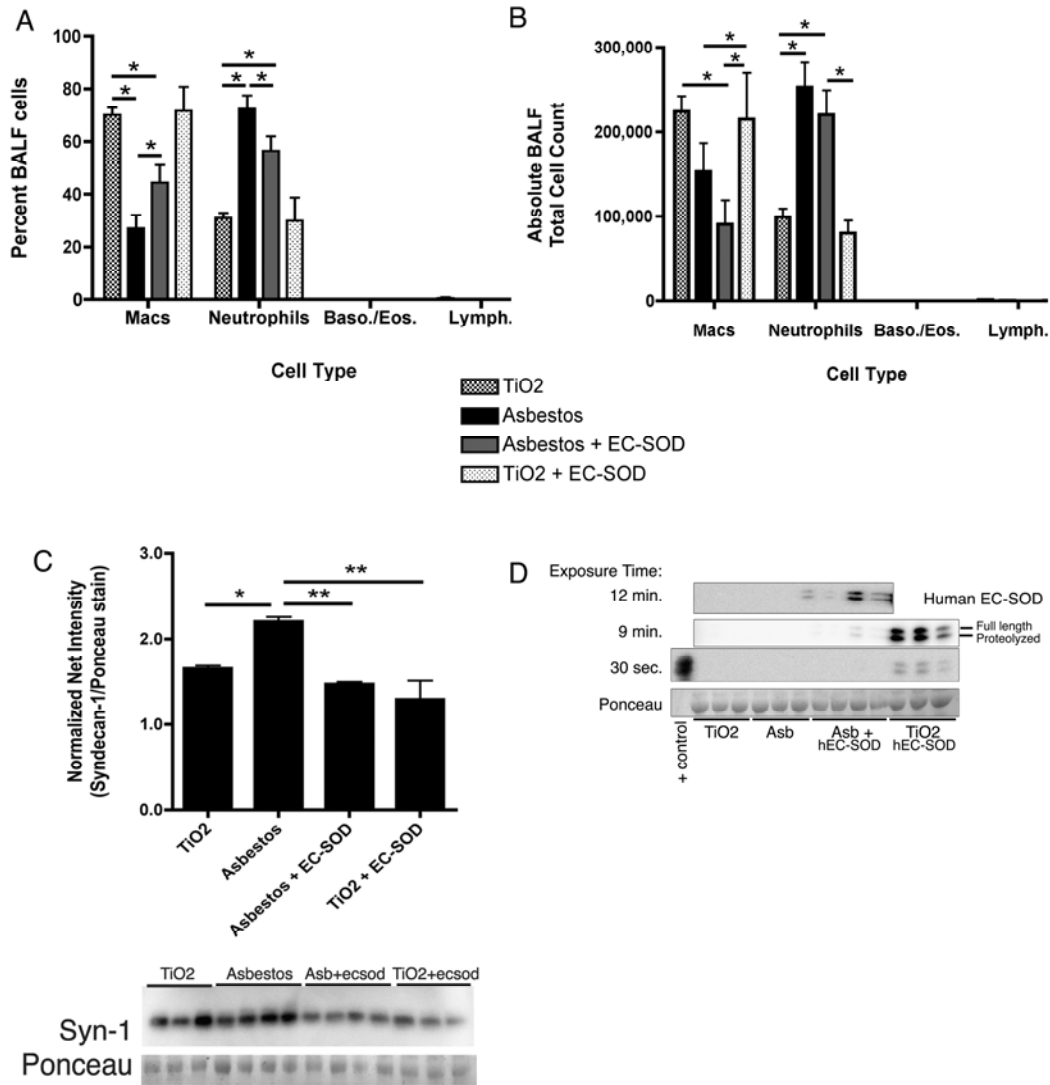


Figure 29: Intratracheal instillation of EC-SOD decreases inflammation and prevents asbestos-induced shedding of syndecan-1. EC-SOD KO mice were co-treated with purified human EC-SOD and asbestos or TiO2. BALF was collected after 24 hours. Co-treatment with EC-SOD and asbestos results in decreased neutrophils and decreased levels of shed syndecan-1 in the BALF after 24 hours. (A) Percent cell type of inflammatory cells in BALF cytopins, *, $p < 0.001$, **, $p < 0.05$; (B) Absolute cell number of inflammatory cells in BALF cytopins. *, $p < 0.05$, $n = 4$; (C) BALF levels of shed syndecan-1, assessed by western blot, *, $p < 0.05$, **, $p < 0.01$; in the BALF,

n=4. (C) Human EC-SOD is present in the BALF of EC-SOD KO mice after 24 hours. Asbestos-injured mice show less retention of EC-SOD than TiO₂ treated mice. Western blot exposure times are noted to the left.

Heparin and heparan sulfate may interact with and signal through toll like receptors, TLR-4, and integrins, both of which are present on inflammatory cells. To investigate the mechanistic roles of TLR-4 and integrins in heparan sulfate mediated neutrophil chemotaxis, we utilized blocking antibodies against TLR-4 and integrins-β1 and β3 in the chemotaxis assay. Anti-TLR4 antibody prevents chemotaxis induced by oxidatively fragmented heparin (Figure 30, *, p<0.05). LPS induction of chemotaxis via TLR-4 was used as a positive control.

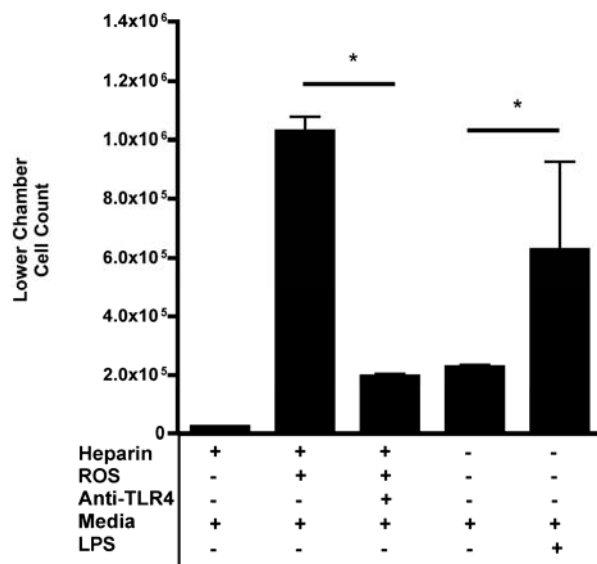


Figure 30: Toll-like receptor 4 partially mediates neutrophil chemotaxis induced by fragmented heparin. Anti-TLR4 blocking antibody was incubated with human neutrophils for 30 minutes prior to addition to the chemotaxis assay. Anti-TLR4 antibody inhibits neutrophil chemotaxis induced by ROS-fragmented heparin. *, p<0.05. Data are reported as mean lower chamber cell count ± SEM.

Incubation of neutrophils with a blocking antibody against integrin β1 prior to the chemotaxis assay, inhibits chemotaxis to oxidatively fragmented HSPG (Figure 31). An antibody against integrin β3 does not modulate chemotaxis. Species-specific IgG was used as a control for the blocking antibodies.

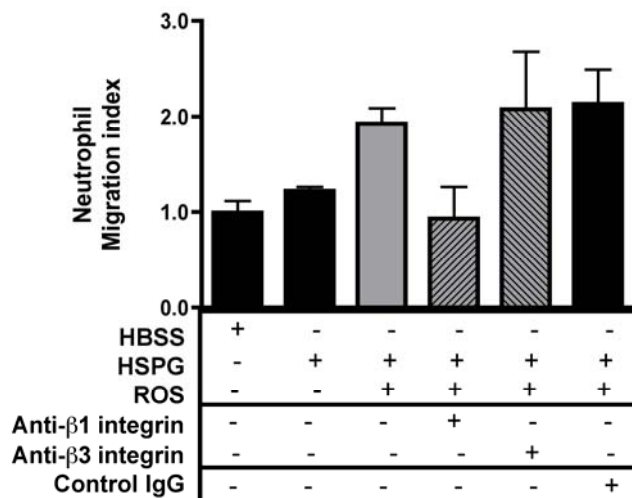


Figure 31: Chemotaxis induced by oxidatively fragmented HS is mediated through Integrin-β1.

Blocking antibodies to integrin-β1 or integrin-β3 were incubated with human neutrophils for 30 minutes prior to addition to the chemotaxis assay. Anti-integrin-β1, but not integrin-β3, inhibited neutrophil chemotaxis induced by oxidatively fragmented HSPG. Control IgG did not affect neutrophil chemotaxis. Data are reported as mean neutrophil migration index ± SEM.

5.6 OXIDATIVELY FRAGMENTED SYNDECAN-1 INDUCES ABHERRENT EPITHELIAL WOUND HEALING.

Alveolar epithelial cells are susceptible to injury and cell death in the lung. Re-epithelialization to restore areas of lost cells is critical for effective repair. Dysregulated re-epithelialization or wound healing is thought to be involved in the pathogenesis of pulmonary fibrosis²⁹. Because syndecan-1 is thought to regulate cell adhesion, we hypothesize that shed syndecan-1 ectodomains and the loss of cell surface syndecan-1 would alter wound healing in alveolar epithelial cells. To investigate this, we isolated and utilized primary mouse type I alveolar epithelial cells (AECs, Figure 32) in a wound healing “scratch” assay. Human S1ED, added at

the time of the wound, significantly inhibits re-epithelialization in primary mouse AECs after 20 hours (Figure 33, percent healing \pm SEM): medium alone, 65.0% \pm 3.7 healing *versus* hS1ED, 51.6% \pm 1.7; *, $p < 0.05$.

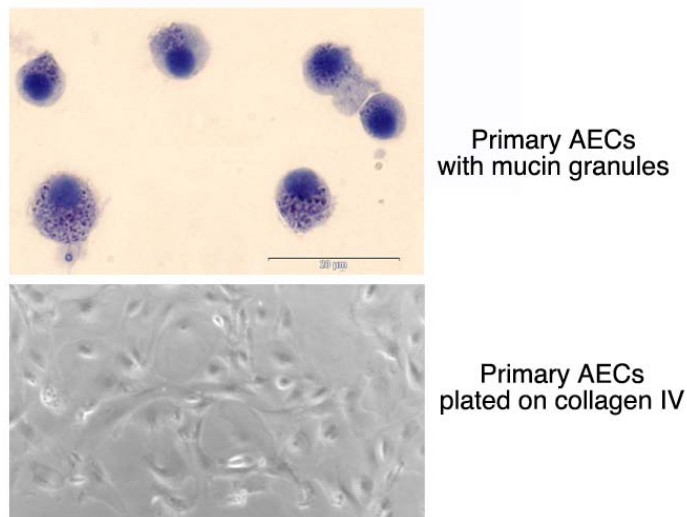


Figure 32: Primary mouse alveolar epithelial cells - type I pneumocytes. A highly pure population of primary mouse AECs was achieved. Cytopun AECs stain positive for cytoplasmic mucin granules (dark blue dots) and *in vitro* form cell-cell connections in monolayers during culture (7 days after cell harvest).

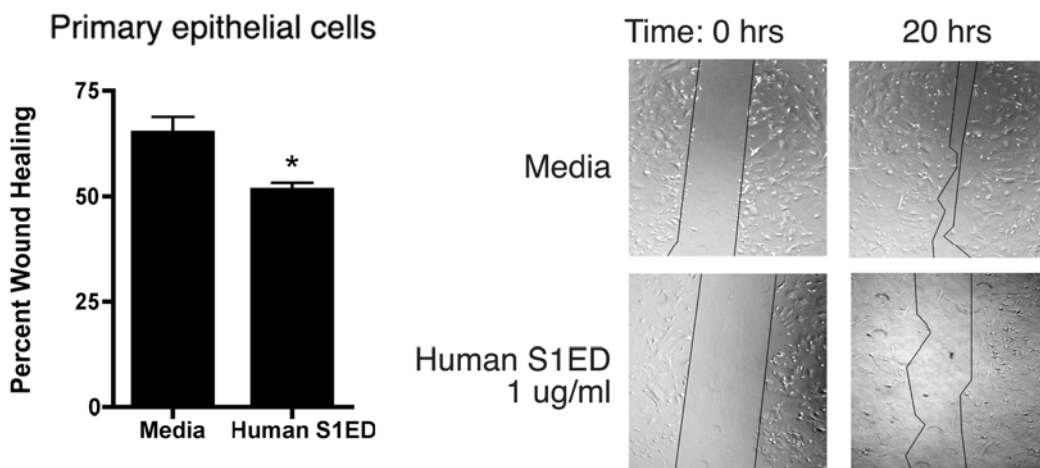


Figure 33: Human syndecan-1 ectodomain (hS1ED) inhibits re-epithelialization of primary mouse AECs. Primary AECs were grown on collagen IV, wounded and imaged at 4X magnification with phase microscopy at time 0 and 20 hours. *, $p < 0.05$. Data is reported as percent wound healing (mean \pm SEM), $n = 6$ /group.

The scratch assay was also completed using A549 cells (human alveolar epithelial cell line). Supernatants from A549 cells exposed to ROS inhibit re-epithelialization of A549 monolayers after wounding and lead to a large decrease in cell adhesion after 20 hours (data not illustrated). hS1ED added at the time of wounding, also inhibits healing of A549 cells (Figure 34): control, $92.4\% \pm 1.2$ versus hS1ED (500 ng/ml) $73.5\% \pm 3.5$; *, $p < 0.01$. After treatment with hS1ED, both A549 cells and primary AECs display a rounded, less adhered morphology. Knockdown of syndecan-1 expression in A549 cells was achieved with siRNA to human syndecan-1 (80% knockdown 24 hours after siRNA treatment, Figure 28A). The loss of cell surface syndecan-1 expression, 24 hours post-transfection, results in a significant decrease in alveolar re-epithelialization (Figure 34): negative control siRNA $80.1\% \pm 6.6$ versus syndecan-1 siRNA $49.3\% \pm 5.7$; *, $p < 0.001$. The addition of hS1ED, immediately after wounding, to siRNA treated cells partially augments the impaired healing response, however, was not a statistically significant change.

The previous chemotaxis data suggests that heparan sulfate proteoglycans, such as syndecan-1, are more chemotactic when the heparan sulfate glycosaminoglycan (GAG) side chains are oxidatively fragmented and removed. This would leave the core protein ectodomain without GAG chains, which we have shown can directly induce neutrophil chemotaxis and inhibit alveolar re-epithelialization. To confirm that the region of the protein ectodomain that contains the primary GAG attachment sites is a portion that inhibits wound healing, we created a 20 amino acid long peptide from the human syndecan-1 N-terminal amino acid sequence. The peptide sequence with the serine-glycine GAG attachment sites is shown in figure 35A. This peptide significantly inhibits wound healing in primary AECs (Figure 35B). This suggests that

oxidatively shed syndecan-1 with modification of its GAG/heparan sulfate side chains can actively alter wound healing.

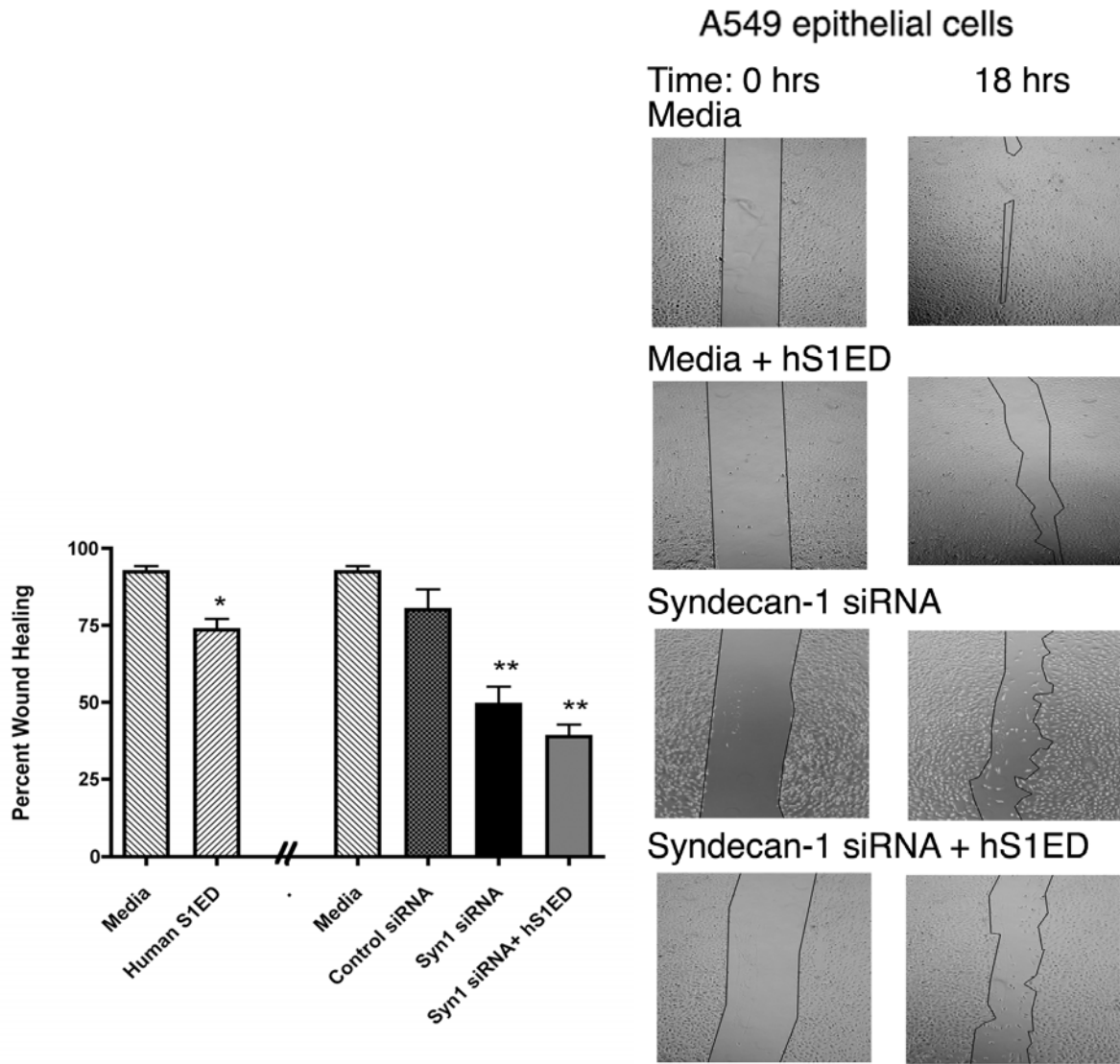


Figure 34: Human syndecan-1 ectodomain (hS1ED) inhibits wound healing while cell surface syndecan-1 promotes re-epithelialization. A549 cells were cultured on collagen IV, wounded and treated with human S1ED. Phase images were taken at 0 and 18 hours. hS1ED inhibits wound healing in A549 cells. Knockdown of syndecan-1 expression with 30 μ M siRNA (siRNA treatment was given 24 hours prior to the wound) results in impaired wound healing or re-epithelialization and changes the cell morphology from a flat, squamous cell to a rounded cell. *, $p < 0.05$; **, $p < 0.001$ versus media and control siRNA. There was no difference between baseline wound healing with medium and control siRNA. Successful knock down with siRNA is shown in figure 28A.

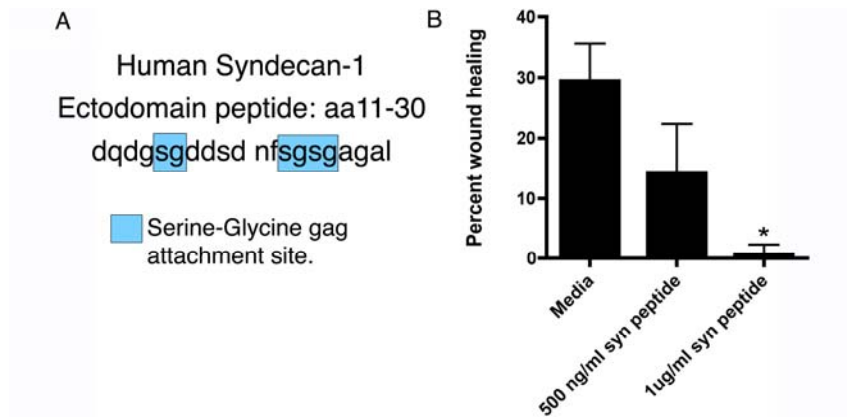


Figure 35: Syndecan-1 ectodomain peptide with GAG binding sites inhibits wound healing. A) A peptide composed of amino acids 11-30 of the syndecan-1 core protein ectodomain was synthesized. This region contains 2 of the 4 glycosaminoglycan (GAG) binding sites (serine-glycine repeats) within the ectodomain. B) This syndecan (syn) peptide inhibits wound healing in primary mouse AECs at 20 hours; *, $p < 0.05$, $n = 6$.

Finally, we investigated the effect of asbestos fibers on re-epithelialization in primary mouse AECs in the scratch assay. Crocidolite asbestos fibers ($9.5 \mu\text{g}/\text{well}$) were added immediately after wounding and significantly inhibits re-epithelialization of primary mouse AECs (Figure 36). Asbestos treatment caused a 20% reduction in wound healing by 24 hours and 33% by 48 hours. Thus, asbestos not only induces cell death through the production of reactive oxygen species, but it impairs the normal wound repair process.

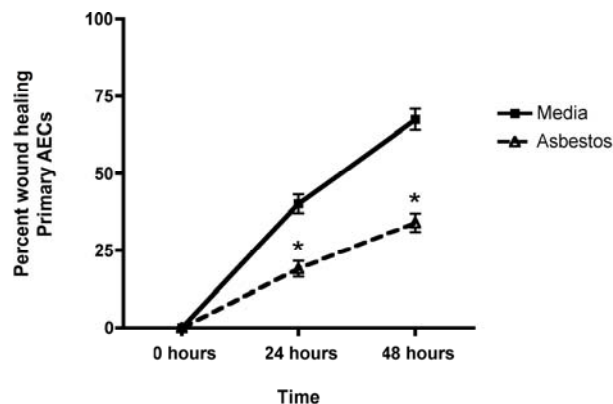


Figure 36: Asbestos fibers impair re-epithelialization of primary AECs. Cells were cultured on collagen IV, wounded and treated with asbestos. Phase images were taken at 0, 24 and 48 hours to assess wound healing. *, $p < 0.05$, $n = 6$.

5.7 SYNDECAN-1 ECTODOMAIN INDUCES FIBROGENESIS.

During wound repair, if epithelial cells fail to re-epithelialize the basement membrane of the alveolar surface, fibroblasts will proceed by proliferating and depositing extracellular matrix components such as collagen, creating fibrosis. To determine the effect shed hS1ED on fibroblasts, LL47 cells (human lung fibroblast cell line) were treated with 1 $\mu\text{g}/\text{ml}$ human S1ED or mouse S1ED (mS1ED) for 24 or 48 hours and metabolically active cells were detected as described in the methods section. hS1ED and mS1ED significantly increase the proliferation of lung fibroblasts after 24 hours (Figure 37 A and B, $p < 0.01$). Furthermore, hS1ED induces TGF- β 1 release from fibroblasts treated for 48 hours (Figure 38): TGF- β 1– medium $0.34\text{ng}/\text{ml} \pm 0.08$ versus hS1ED $0.80\text{ng}/\text{ml} \pm 0.05$; *, $p < 0.05$. There was no detectable increase in active TGF- β 1 (data not shown). hS1ED does not lead to myofibroblast differentiation of fibroblasts, as determined by α -smooth muscle actin in cell lysates after treatment for 48 hours (western blot analysis - normalized net band intensity (α -SMA/ β -actin): media 0.174 ± 0.031 versus hS1ED 0.166 ± 0.026).

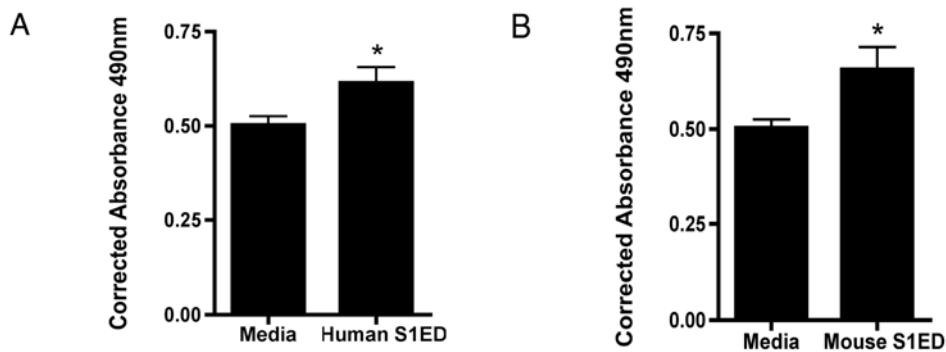


Figure 37: Human and mouse syndecan-1 ectodomains increase human lung fibroblast proliferation.

LL47 fibroblasts were treated with either human S1ED or mouse S1ED for 24 hours and cell proliferation was assayed. The absorbance at 490nm is proportional to the number of metabolically active cells. * $p < 0.01$ $n = 8$.

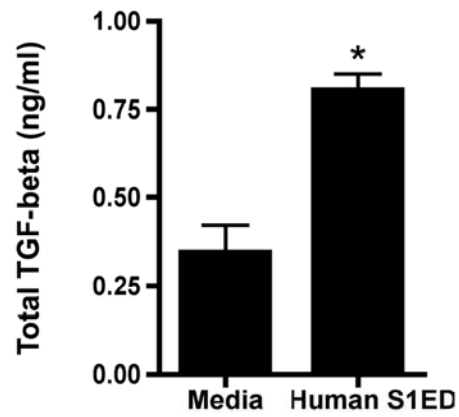


Figure 38: Syndecan-1 ectodomain induces TGF- β 1 bioavailability in human lung fibroblasts. LL47 fibroblasts were treated for 48 hours with medium or human S1ED. Supernatants were subsequently assayed for total TGF- β 1 (ng/ml). Data are reported as mean \pm SEM, *, $p < 0.01$. No differences in active TGF- β 1 levels were detected, $n = 6$.

6.0 DISCUSSION - PULMONARY FIBROSIS

Studies of pulmonary fibrosis have found that EC-SOD inhibits inflammation and fibrosis in lung injury models^{57, 63, 291}. EC-SOD is lost from the interstitium from the lung and increases in the airspaces^{60, 292}. This loss of EC-SOD may leave the extracellular matrix of the lung vulnerable to increases in oxidative stress, which is evident in idiopathic pulmonary fibrosis (IPF)^{11, 126, 176, 293}. *We hypothesized that one mechanism through which EC-SOD protects the lung from oxidant-induced damage, inflammation, and fibrosis is by preventing oxidative fragmentation of heparan sulfate (HS), specifically syndecans, in the extracellular matrix (ECM).*

Syndecans have various known functions in tissues including mediating cell adhesion and localizing cytokines and growth factors. They can be shed from the cell surface in both physiological and pathological states. MMPs, including MMP1, MMP2, MMP7 and MMP9, are various proteolytic enzymes that have been implicated in human IPF^{131, 132, 294}. Previous studies have shown a role for proteolytic cleavage of syndecan-1 by matrilysin (MMP7) in a bleomycin lung injury model and that syndecan-1 can complex with the chemokine KC to mediate inflammation²⁶³. **The role for oxidative shedding of syndecans and the effects of the shed ectodomains during injury remain unclear.** In our investigations, we have found that heparan sulfate can be fragmented by reactive oxygen species produced in a Fenton-like $\text{CuSO}_4/\text{H}_2\text{O}_2$ system. In addition, the ectodomain of syndecan-1 can be oxidatively shed from alveolar

epithelial cells, which can be prevented by EC-SOD. This suggests that heparan sulfate and syndecans in the extracellular matrix are sensitive to oxidative stress.

Oxidative shedding also occurs *in vivo* during pulmonary fibrosis. Heparan sulfate fragments can be detected in the bronchoalveolar lavage fluid (BALF) of wild type mice after a 24-hour exposure to asbestos, which generates reactive oxygen species via structural transition metals. Furthermore, EC-SOD KO mice, which display increased levels of oxidative stress, have significantly more heparan sulfate in BALF during both the inflammatory phase (24 hours) and fibrotic phases (days 14 and 28) of asbestos-induced pulmonary fibrosis. We have identified these shed species to be syndecan-1 and syndecan-4, which are expressed on alveolar epithelial cells. EC-SOD KO mice have further increases in shed syndecan-1 and syndecan-4 ectodomains into the BALF at the inflammatory and fibrotic phases of the asbestos model and in a second bleomycin model of fibrosis. The significance of these findings is further supported by increases in these syndecans in the BALF of IPF patients. Syndecan-1 levels in IPF BALF samples are significantly elevated at all stages of IPF disease severity. These data provide novel evidence implicating a role for oxidative stress in degradation of the extracellular matrix of the lung, specifically syndecan-1 and -4. Previous studies have found that EC-SOD protein expression decreases in the lung interstitium with a corresponding increase in EC-SOD in the bronchoalveolar lavage fluid (BALF). We found that EC-SOD decreases at the mRNA expression level during asbestos-induced fibrosis. The decrease in EC-SOD during pulmonary fibrosis and oxidative injury may be due to a loss of EC-SOD-producing epithelial cells in the lung interstitium. TGF- β , a growth factor important in fibrosis, has also been shown to down-regulate EC-SOD expression²¹⁶. Because EC-SOD binds to heparin species in the lung, HS

shedding may be one mechanism through which the distribution of EC-SOD changes with oxidative injury.

While present in the BALF after injury, the functions of shed syndecan-1 during pulmonary fibrosis remain unknown. Inflammation and aberrant wound healing are key pathological processes involved in IPF and were thus investigated. Neutrophil influx into the lung during injury is a characteristic of human IPF and animal models of pulmonary fibrosis. Oxidatively fragmented heparan sulfate and the syndecan-1 ectodomain (as would be shed from the matrix) are highly chemotactic to neutrophils. Oxidative damage and removal of the carbohydrate side chains of HSPG can expose the syndecan core protein. The core protein is then able to induce chemotaxis. siRNA studies in A549 epithelial cells support the direct role of the syndecan-1 ectodomain in induction of chemotaxis. Shedding of syndecan-1 and subsequent neutrophil chemotaxis can be inhibited by EC-SOD *in vivo* and *in vitro*, highlighting one mechanism through which EC-SOD is mediating inflammation. Thus, **our studies provide the first report of a novel mechanism by which oxidants induce shedding of the syndecan-1 ectodomain, which can directly promote neutrophil chemotaxis in the absence of cytokines and chemokines.**

The mechanism through which shed syndecan-1 induces chemotaxis is unknown, but toll like receptor 4 (TLR-4) and integrin- β 1 on neutrophils are likely involved based on our findings. TLR4 is known for its pathogen recognition of gram-negative bacteria. Excessive syndecan-1 shedding may also be recognized by TLR-4 as a signal of tissue injury. Integrins are intricately involved in cell-cell and cell-matrix communication and adhesion. Integrins may also utilize membrane bound syndecans as co-receptors and shed syndecans as signals of injury to trigger cellular migration and the repair process.

Wound healing studies suggest that in addition to pro-inflammatory properties, shed syndecan-1 impairs alveolar re-epithelialization. Human syndecan-1 ectodomain (hS1ED) was found to inhibit wound healing of epithelial monolayers at physiological levels of syndecan-1. siRNA studies indicate that cell surface bound syndecan-1 is important in the normal repair process, as knockdown of syndecan-1 with siRNA technology results in significant impairment of wound healing. Subsequent studies with a synthesized syndecan-1 peptide suggest that the region of the syndecan-1 protein with GAG binding sites mediates this response. Other investigators report that syndecan-1 interacts with integrins to mediate cell adhesion and activation^{252, 258}. In this study, shed syndecan-1 may be competitively binding with integrin subunits to inhibit re-epithelialization. Thus, during lung injury, syndecan-1 gains a pathologic function when it is oxidatively shed (neutrophil chemotaxis and inhibition of re-epithelialization) and loses its homeostatic function as a membrane bound protein, for the epithelium during the repair process (inhibition of re-epithelialization).

The pathogenesis of IPF also involves fibroblasts and a potential dysregulation of their function. hS1ED promotes lung fibroblast proliferation and release of TGF- β 1 from fibroblasts. This suggests that syndecan-1 may contribute to the pulmonary fibrosis by activating fibroblasts and the release of pro-fibrotic paracrine mediators like TGF- β 1. This pro-fibrotic and anti-inflammatory growth factor has also been shown to downregulate EC-SOD expression²¹⁶, which would alter levels of oxidative stress in the lung.

Tissue homogenate, immunofluorescent staining, and real time RT-PCR data indicate that syndecan-1 cell surface expression increases in areas of fibrosis while EC-SOD decreases in the lung after injury. IHC staining for syndecan-1 shows that the expression increases are unique to areas of active fibrosis because changes are not seen in areas with normal lung architecture. The

loss of interstitial EC-SOD during pulmonary fibrosis may increase the vulnerability of matrix proteins and heparan sulfate, including syndecan-1, to the increases in oxidative stress seen in human IPF and animal models of pulmonary fibrosis. The combination of the changes that occur in interstitial syndecan-1 and EC-SOD distribution may favor fibrogenesis by creating a cycle of sustained inflammatory cell recruitment, abnormal epithelial wound healing, and increased TGF- β bioavailability (Figure 39). The novel findings of this investigation show that the loss of EC-SOD in the lung leaves syndecan-1 vulnerable to oxidative stress and that oxidant-induced loss of cell surface syndecan-1 impairs re-epithelialization, induces inflammation, and promotes a fibrotic microenvironment in the lung.

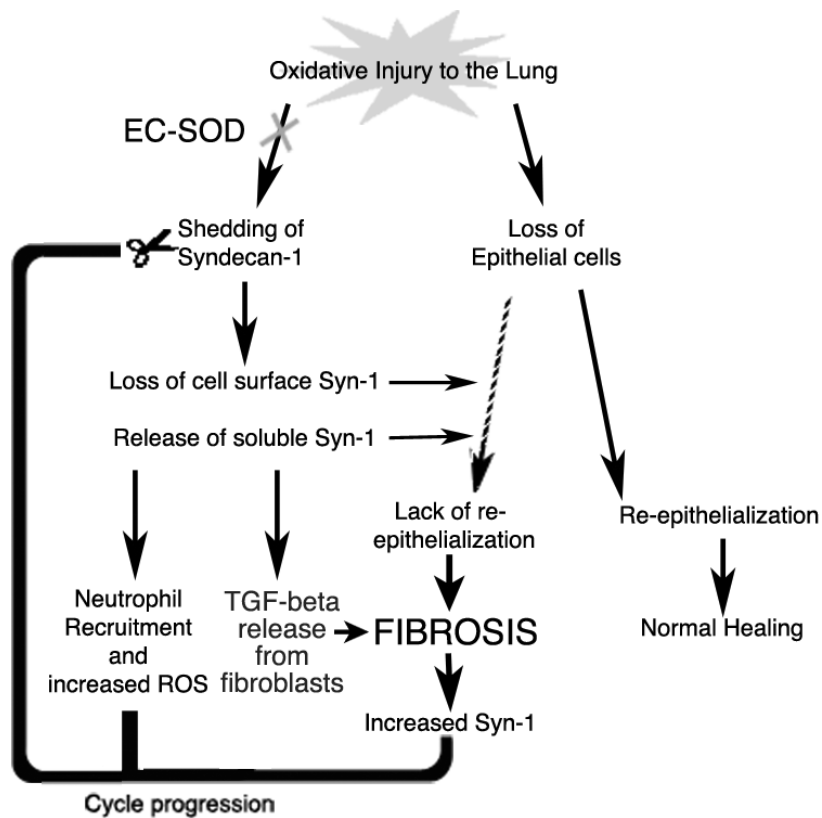


Figure 39: Summary of Oxidative Stress in the Lung. Oxidative injury to the lung can lead to loss of epithelial cells and shedding of syndecan-1. This shedding may create a damaging cycle of inflammatory cell

chemotaxis, abnormal re-epithelialization of alveolar epithelium, and increased TGF- β bioavailability that contribute to fibrosis in the lung.

6.1 CLINICAL SIGNIFICANCE AND FUTURE DIRECTIONS

A recent clinical study shows prognostic benefit for predicting early mortality in IPF by evaluating neutrophil burden in the BALF of patients⁷. Moreover, syndecan-1 shedding into BALF may provide additional clinically relevant information on inflammatory and fibrotic mediators in IPF and may be one way to follow disease presence, which is suggested by our findings of increases in syndecan-1 levels in BALF at all IPF disease severities. We are addressing this possibility in the samples from the IPF patient population we evaluated for these studies. Furthermore, data from our asbestos mouse model suggests that syndecan-1 levels do correlate with neutrophil burden of the BALF. Additional investigations are required to determine if serum or urine detection of the ectodomains is possible, as these would involve less invasive sampling procedures. The present studies show that oxidatively shed syndecan-1 promotes neutrophil chemotaxis, impairs alveolar re-epithelialization after injury, and promotes fibrogenesis. Therefore, oxidatively shed syndecan-1 may be one potential therapeutic target to control fibrosis progression in IPF lungs. Targeting of the shed syndecan-1 ectodomain with an antibody provides a potential way to aid in the clearance of the fragments and control fibrosis progression.

Our data show that intratracheal instillation of human EC-SOD inhibits syndecan-1 shedding and neutrophil influx into the lung of EC-SOD KO mice at 24 hours post-asbestos exposure. Western blot analysis of BALF and lung homogenate samples revealed the presence of

the administered human EC-SOD, however, at lower levels in asbestos treated mice. Further studies could be completed to study the pharmacokinetics of exogenously administered intratracheal EC-SOD during pulmonary injury. How long does full length human EC-SOD remains in the un-injured lung and how EC-SOD is being removed from the lung after an injury. Several mechanisms could be involved in EC-SOD clearance: removal of EC-SOD to the serum due to a “leaky” lung, removal by leukocytes and uptake by epithelial or other resident cells. With a greater understanding of the half-life of administered EC-SOD, future studies could include EC-SOD administration during the course of fibrotic injury to evaluate its role in the fibrosis phase (after approximately day 7).

Important questions remain about the biology of EC-SOD including if and how it signals in cells. Syndecan-4 is known to signal through PKC and acts as a co-receptor for growth factors such as fibroblast growth factor. Syndecans may also have a similar role for EC-SOD and how cells detect extracellular levels of EC-SOD because they are in very close proximity to one another. We have shown that EC-SOD increases in response to oxidative injury suggesting that EC-SOD levels may be detected by cells. In addition, interactions of EC-SOD with syndecans may mediate signaling if another receptor is involved. HSPG binding is required for complete signaling of FGF through its receptor. If EC-SOD does signal, a similar interaction may be required. Another aspect of EC-SOD biology that is unclear is how EC-SOD is transported into and out of cells. Heparan sulfates/syndecans are important in the endocytosis of LDL in adipocytes. Because of the high binding affinity of EC-SOD to heparan sulfate species, HSPGs may be good candidates for mediating uptake or recycling of EC-SOD by cells.

Our data shows EC-SOD and syndecan-1 distribution in the lung interstitium. Syndecan expression in pulmonary inflammatory cells during pulmonary fibrosis injury remains unclear.

Peritoneal macrophages do express syndecans^{247, 250}. However, the expression of syndecans on neutrophils and alveolar macrophages within the lung is currently unknown. Syndecans on pulmonary inflammatory cells may be involved in docking EC-SOD to the surface of leukocytes that are producing large amounts of reactive oxygen species. Macrophage syndecan expression and shedding may be key factors in the regulation of cytokine/growth factor signals in the lung.

While not the focus of the current study, syndecan-4 clearly has a role in oxidative injury in the lung. The ubiquitous expression of syndecan-4 suggests that it is also expressed on leukocytes and fibroblasts. The function of syndecan-4 in fibroblasts is thought to involve cell migration, however additional functions in inflammation and fibrosis remain unclear. Our data shows that syndecan-4 increases in the lavage fluid during pulmonary fibrosis however, no significant changes in the lung homogenates are seen. The shed syndecan-4 could be coming from recruited neutrophils or resident macrophages.

While this study focused on syndecans, the heparan sulfate glypican family should be investigated to determine their interactions with EC-SOD, susceptibility to oxidative stress and how they may mediate pulmonary injury and repair.

7.0 RESULTS – CARDIAC FIBROSIS

7.1 LACK OF EC-SOD MODULATES CARDIAC MORPHOLOGY.

We hypothesized that EC-SOD protects the heart from oxidant-induced fibrosis and loss of function by mediating normal cardiac function, inflammation and preventing oxidative ECM shedding. The significance of a lack of EC-SOD in normal cardiac morphology and during oxidant injury and fibrosis was determined utilizing wild type (WT) and EC-SOD KO mice. Echocardiography was utilized to assess cardiac dimensions and function. Control EC-SOD KO mice have a significant decrease in left ventricular posterior wall thickness (LVPWT, mm) compared to control WT mice (Figure 40A and relative thickness 40B; data in Table 2) and a significant increase in intra-ventricular end diastolic dimension (LVEDD, Figure 39C, * $p < 0.05$; data in Table 2). While significant changes occur in the morphology of the LV, EC-SOD KO mice appear to functionally compensate as they have similar cardiac function compared to control WT mice (Figure 41A percent fractional shortening; Figure 41B percent ejection fraction; * $p < 0.05$).

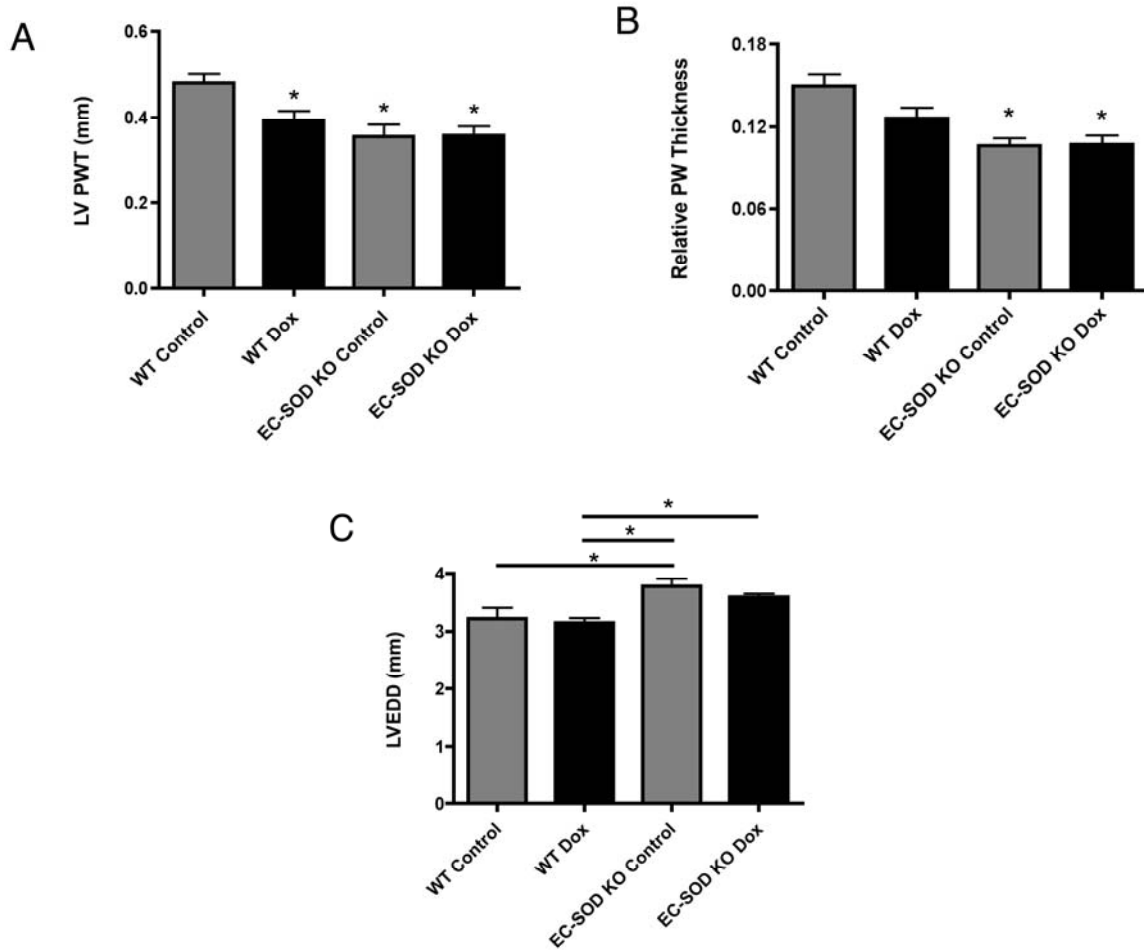


Figure 40: Changes in left ventricular morphology are present in control EC-SOD KO mice and after doxorubicin treatment. Cardiac dimensions were collected using echocardiography. A) LV posterior wall thickness (LVPWT, mm), *, $p < 0.05$ compared to WT control. B) Relative posterior wall thickness (LVPWT / LVEDD), *, $p < 0.05$ compared to WT control. C) LV end diastolic dimension (LVEDD, mm), *, $p < 0.05$. All data is reported as mean \pm SEM.

Table 2: Anatomic and Functional Cardiac Data for Wild type and EC-SOD KO mice.

Parameters	Strain	Control (day 15)	Doxorubicin (day 15)
Body Weight (g)	WT	20.51 ± 0.44	18.75 ± 0.20*
	EC-SOD KO	20.35 ± 0.43	18.05 ± 0.52**
% Weight Change	WT		-1.90 ± 1.50
	EC-SOD KO		-11.38 ± 2.03 [§]
Heart Mass (mg)	WT	127.51 ± 0.007	113.76 ± 0.004*
	EC-SOD KO	121.26 ± 0.005	105.16 ± 0.004**
Heart rate (bpm)	WT	397 ± 25.7	380 ± 27.6
	EC-SOD KO	416 ± 29.1	420 ± 22.2
Fractional Shortening (%)	WT	28.46 ± 2.73	23.47 ± 2.39
	EC-SOD KO	33.45 ± 2.90	18.11 ± 2.07**
LVEDD (mm)	WT	3.20 ± 0.19	3.14 ± 0.08
	EC-SOD KO	3.77 ± 0.13*	3.59 ± 0.06 [§]
LVESD (mm)	WT	2.37 ± 0.19	2.41 ± 0.12
	EC-SOD KO	2.39 ± 0.32	2.94 ± 0.11
LVPWT (mm)	WT	0.481 ± 0.021	0.393 ± 0.023*
	EC-SOD KO	0.355 ± 0.028*	0.357 ± 0.023*
Relative PWT (LVEDD/LVPWT)	WT	0.149 ± 0.009	0.125 ± 0.007
	EC-SOD KO	0.106 ± 0.005*	0.107 ± 0.006*
*p<0.05 versus WT control; **p<0.05 versus EC-SOD KO control; §p<0.05 versus WT Doxorubicin;			

7.2 LACK OF EC-SOD EXACERBATES LOSS OF CARDIAC FUNCTION.

The functional significance of cardiovascular EC-SOD after oxidant injury was determined by utilizing WT and EC-SOD KO mice given a single intraperitoneal injection of control saline or doxorubicin, with echocardiography assessment on day 15. Exposure to doxorubicin causes a significant decrease in the posterior wall thickness of the left ventricle (LVPWT) in wild type mice by echocardiography (Figure 39A; Relative posterior wall thickness 40B). No additional decreases were seen in the LVPWT of doxorubicin-treated EC-SOD KO mice, however functional impairment was evident. EC-SOD KO mice have a significant decrease in myocardial fractional shortening (figure 41A, *p<0.05; data shown in table 2) and ejection fraction (figure

41B, * $p < 0.05$; EC-SOD KO control $62.70\% \pm 4.28$; doxorubicin $38.06\% \pm 3.94$). Doxorubicin-treated WT mice have a trend towards decreases in FS and EF but do not reach significance. Figure 41C shows representative images for wild type and EC-SOD KO groups, including H&E of a cardiac section, and B-mode and M-mode cardiac images from echocardiography. These functional findings suggest that the lack of EC-SOD exacerbates systolic (contractile) dysfunction associated with doxorubicin-induced left ventricular injury.

Weight loss was used as a marker of overall health and injury status in the doxorubicin model. In both wild type and EC-SOD KO mice, doxorubicin treatment led to a significant decrease in body weight compared to control mice ($p < 0.05$, Table 2 - percent weight change). Notably, EC-SOD KO mice lost significantly more weight (9.48%) compared to wild type mice after doxorubicin administration (* $p < 0.05$, Table 2).

In addition, the lack of EC-SOD results in oxidative damage to membrane proteins in cardiomyocytes. Carbonyl modifications on proteins were detected in the membrane fraction of left ventricle homogenates in control and doxorubicin-treated wild type and EC-SOD KO mice. The lack of EC-SOD causes a significant increase in carbonyl modifications to proteins in control EC-SOD KO mice (Figure 42). Furthermore, doxorubicin treatment causes a significant increase in carbonyl groups in wild type animals. No further increase was seen in dox-treated EC-SOD KO mice. This data suggests that doxorubicin is producing extracellular oxidative stress leading to modifications in membrane proteins and that EC-SOD protects against this oxidative stress.

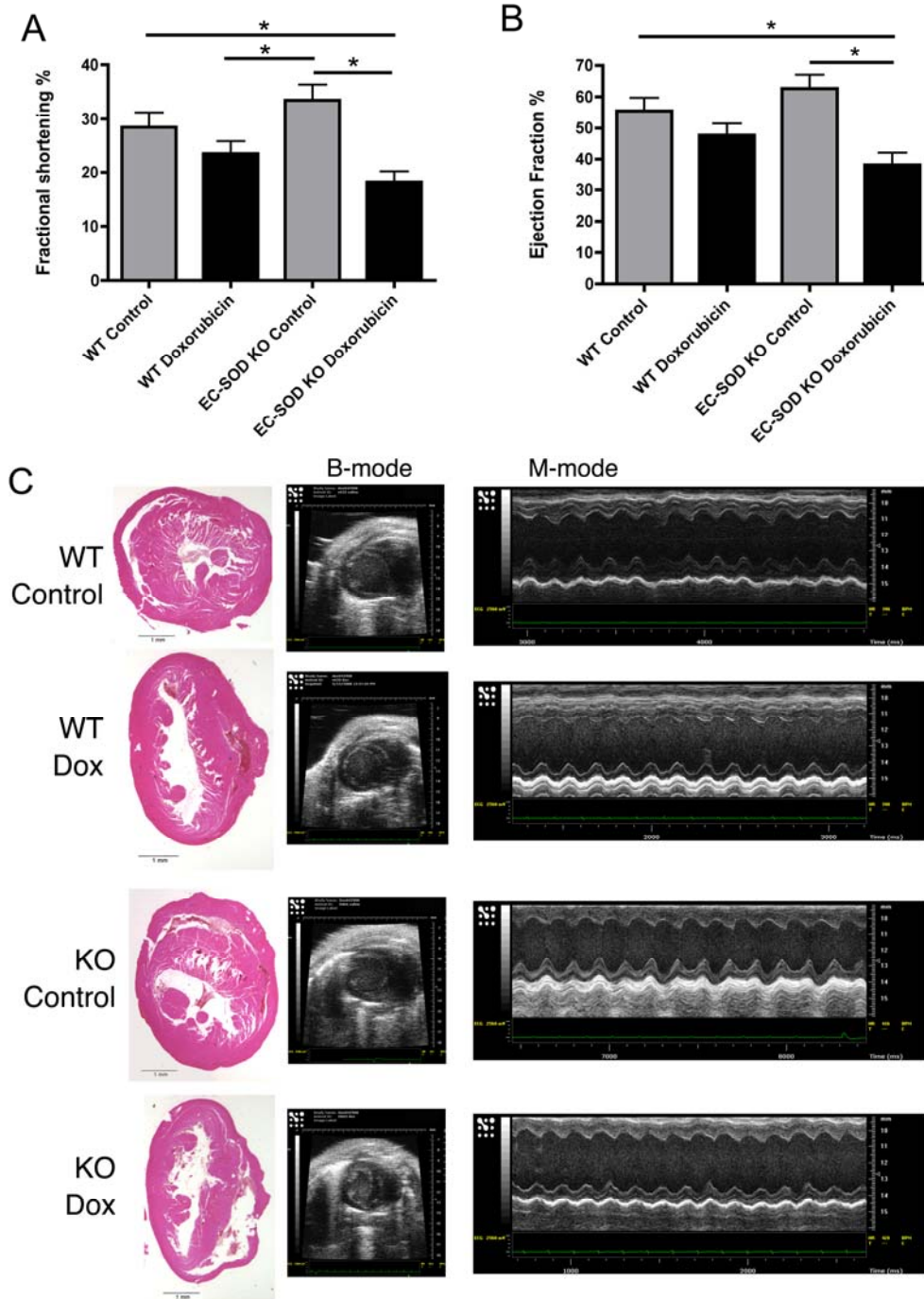


Figure 41: Lack of EC-SOD results in a significant decrease in cardiac function after doxorubicin. Cardiac function was determined by echocardiography. A) Percent fractional shortening in wild type and EC-SOD KO mice. *, $p < 0.05$; $n = 7-8$; B) Percent ejection fraction of the left ventricle *, $p < 0.05$; $n = 7-8$; C) Representative images for wild type and EC-SOD KO groups depicting $4\mu\text{m}$ H&E-stained cardiac section at 1.6X magnification and B- and M-mode images of the left ventricle from echocardiography, $n = 7-8$. Methods section 3.4.1 and Figure 5.

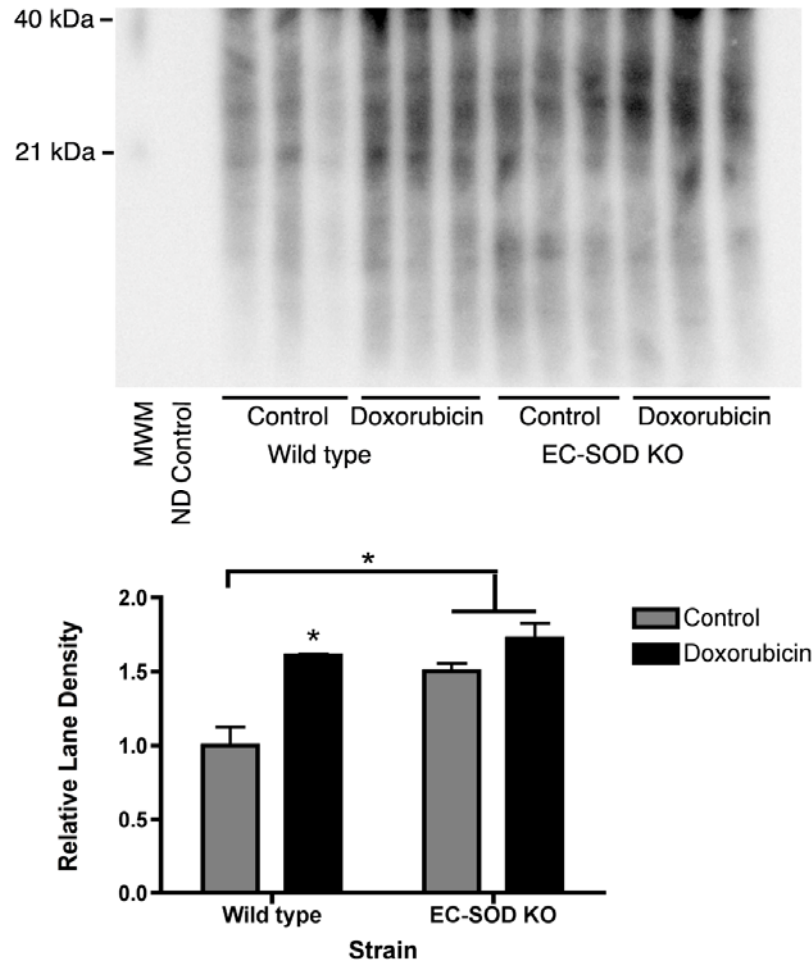


Figure 42: Lack of EC-SOD and doxorubicin treatment lead to increases in extracellular oxidative stress. An oxyblot kit was used to detect carbonyl group formation on proteins in the membrane fraction of LV homogenates. Samples were run on western blot and the membrane was probed for derivatized carbonyl groups. A MWM of derivatized proteins (MWM) and a non-derivatized control sample (ND Control) were included. The Lack of EC-SOD and doxorubicin treatment cause increased carbonyl modifications in membrane proteins, *, $p < 0.05$.

7.3 LACK OF EC-SOD RESULTS IN INCREASED FIBROSIS AFTER DOXORUBICIN.

Lack of cardiac EC-SOD results in increased fibrosis in left ventricular tissue, as shown by increased Sirius red staining of collagen fibers (Figure 43 C,D versus A,B) and increased collagen via trichrome staining (Figure 44 C,D versus A,B; Blue staining of collagen fibers). Deposition of acellular collagen is present between cardiomyocytes within the left ventricle (Figure 44-E, blue staining of collagen fibers), as well as, typical cellular pathology caused by doxorubicin including cytoplasmic vacuolization (Figure 44-F and 44-E, black arrows). Doxorubicin exposure caused a significant increase in LV hydroxyproline in wild type mice (Figure 45, WT control 0.76 ± 0.04 $\mu\text{g}/\text{mg}$ LV tissue; WT doxorubicin 0.89 ± 0.03 $\mu\text{g}/\text{mg}$, $*p < 0.05$). EC-SOD KO mice treated with doxorubicin had a significant increase in hydroxyproline compared to controls (Figure 45, EC-SOD KO control: 0.80 ± 0.02 $\mu\text{g}/\text{mg}$ LV tissue; EC-SOD KO dox 1.0 ± 0.04 $\mu\text{g}/\text{mg}$ LV tissue, $*p < 0.05$) and a significant increase compared to similarly treated wild type mice (WT dox: 0.89 ± 0.03 $\mu\text{g}/\text{mg}$ LV tissue; EC-SOD KO dox 1.0 ± 0.04 $\mu\text{g}/\text{mg}$ LV tissue, $*p < 0.05$). Control WT and EC-SOD KO mice had similar hydroxyproline levels in mice 8 weeks of age.

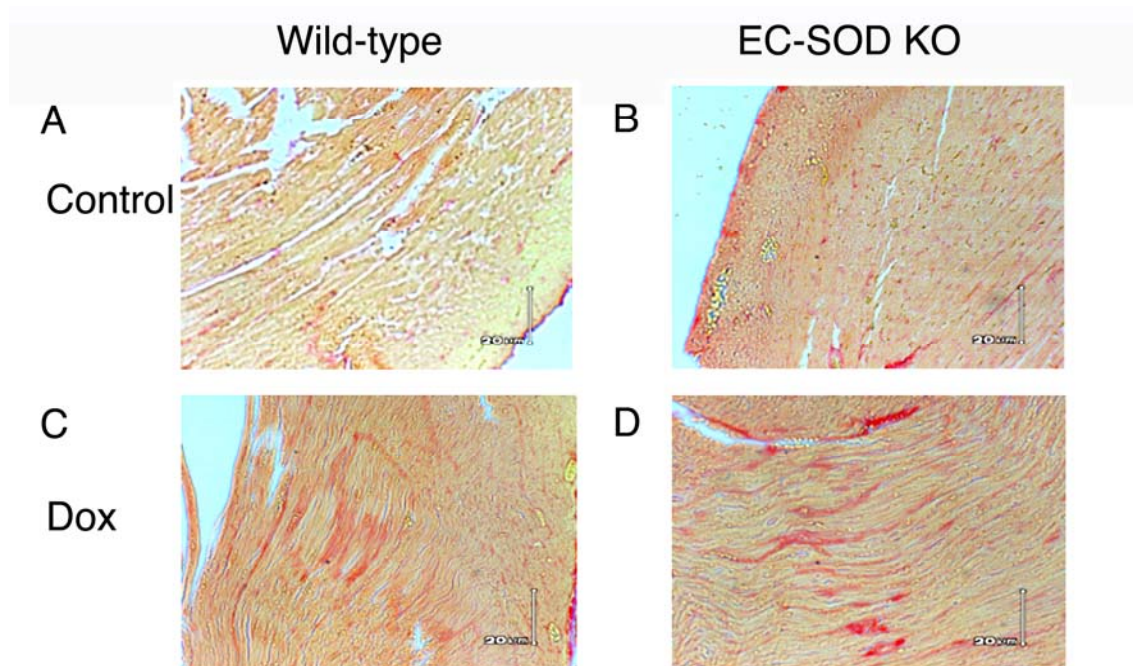


Figure 43: Sirius red staining for collagen fibers in LV tissue. Collagen fibers are stained orange/red by sirius red. EC-SOD KO mice have significantly more LV fibrosis after doxorubicin (D) compared to WT dox mice (C). Images are representative of staining from each group.

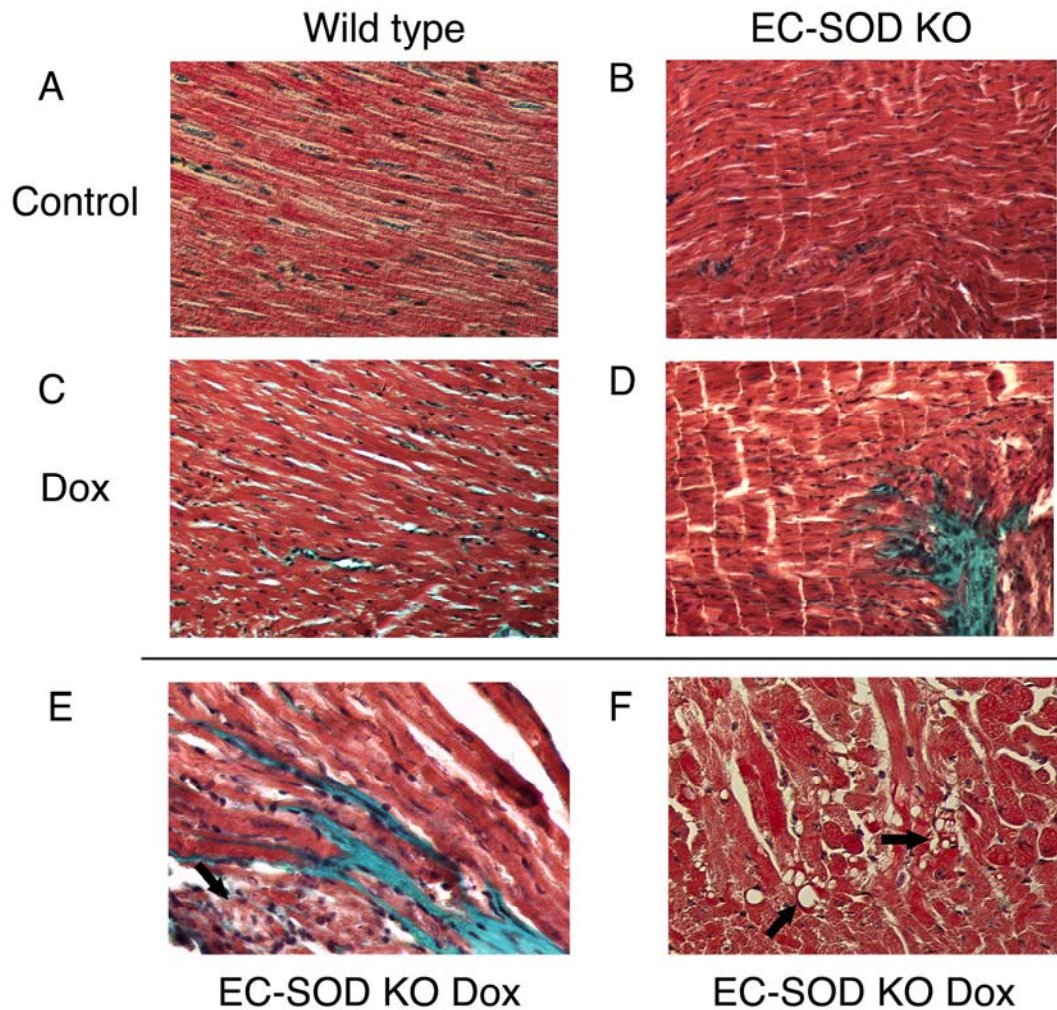


Figure 44: Trichrome staining for collagen deposition in LV cardiac tissue. LV tissue sections were stained with Masson's trichrome. Collagen fibers stain blue, nuclei are dark brown and cell cytoplasm stain red. EC-SOD KO mice have extensive collagen deposition after doxorubicin treatment (D) compared to WT dox mice (C). E) Collagen deposition (blue staining) at higher magnification in the LV tissue of a doxorubicin-treated EC-SOD KO mouse. F) Cellular ultra-structural pathology can be appreciated by cytoplasmic vacuolization (arrows) in a cardiac section from a doxorubicin-treated EC-SOD KO mouse. These are also noted on section E with an arrow.

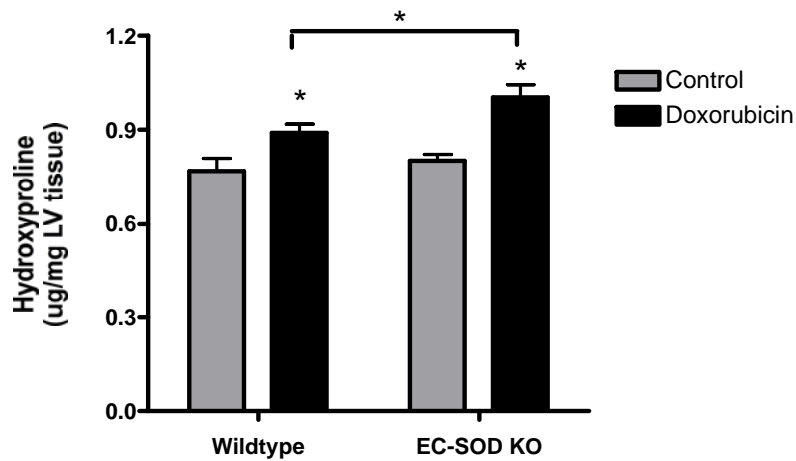


Figure 45: Hydroxyproline analysis of collagen content in LV tissue. EC-SOD KO mice develop significantly more fibrosis as assessed by hydroxyproline content after doxorubicin compared to WT dox mice. *, $p < 0.05$ WT dox or KO dox compared to respective control mice; Bar with *, $p < 0.05$ EC-SOD KO dox versus WT dox, $n = 6-8$.

7.4 LACK OF EC-SOD AND OXIDATIVE INJURY INCREASES SHEDDING OF SYNDECAN-1, MYOCARDIAL INFLAMMATION, AND APOPTOSIS.

In wild type mice, doxorubicin exposure leads to an increase in total protein expression of EC-SOD in LV tissue homogenates (Figure 46A). Proteolyzed EC-SOD increases in serum after doxorubicin (Figure 46B, $p < 0.05$) while there is no change in EC-SOD mRNA expression by quantitative real time RT-PCR (Figure 46C, percent relative ddCT expression). Syndecan-1 is a major component of the extracellular matrix and anchors EC-SOD to cell surfaces. Serum levels of shed syndecan-1 increase in WT mice after doxorubicin and high serum levels are also seen in control EC-SOD KO mice with no further increase after doxorubicin (Figure 46D). In left ventricle homogenates, syndecan-1 membrane bound protein decreases after doxorubicin in both

WT and EC-SOD KO mice (Figure 46E) corresponding to the increase in serum syndecan-1 levels. Syndecan-1 mRNA expression significantly decreases in EC-SOD KO mice after doxorubicin by day 15 (Figure 46F, $p < 0.05$) but does not in WT mice. Inflammatory cell infiltration, shown by CD45-(+) cell staining in LV tissue, is evident in WT dox mice and is further enhanced with the lack of EC-SOD and dox treatment (Figure 47; red staining = CD45, blue = nuclei).

Doxorubicin results in increased cell death shown by a trend in increased serum lactate dehydrogenase (LDH) (Figure 48A). Furthermore, WT and EC-SOD KO mice have significant decreases in total heart mass by day 15 after doxorubicin treatment (Table 2, $*p < 0.05$). We determined if this decrease in heart mass was due to apoptotic cell death. The lack of EC-SOD results in increased apoptosis in the LV after oxidative injury, as evident by a significant increase in active caspase-3 in soluble heart homogenates after doxorubicin (Figure 48B, activated caspase-3, 12-17kDa form; KO control 0.11 ± 0.02 ; KO dox 0.57 ± 0.10 , $*p < 0.05$). The ratio of active to inactive caspase-3 is significantly higher in doxorubicin-treated EC-SOD KO mice compared to control KO mice and both WT treatment groups (Figure 48C, Caspase-3 ratio (active/inactive): EC-SOD KO control 0.11 ± 0.01 and EC-SOD KO dox 0.64 ± 0.13 , $*p < 0.05$; WT control 0.12 ± 0.04 ; WT dox 0.19 ± 0.05 , $*p < 0.05$ versus KO dox). There were no changes in the inactive pro-form of caspase-3 (Figure 48B, 37kDa) suggesting that there is an increase in caspase-3 activation with a lack of EC-SOD and doxorubicin treatment. By TUNEL analysis, the lack of EC-SOD further modulates the number of apoptotic cells in both control and doxorubicin-treated groups, as shown by the presence of TUNEL-positive cells (Figure 48C, TUNEL (red), DAPI nuclear stain (blue), overlay).

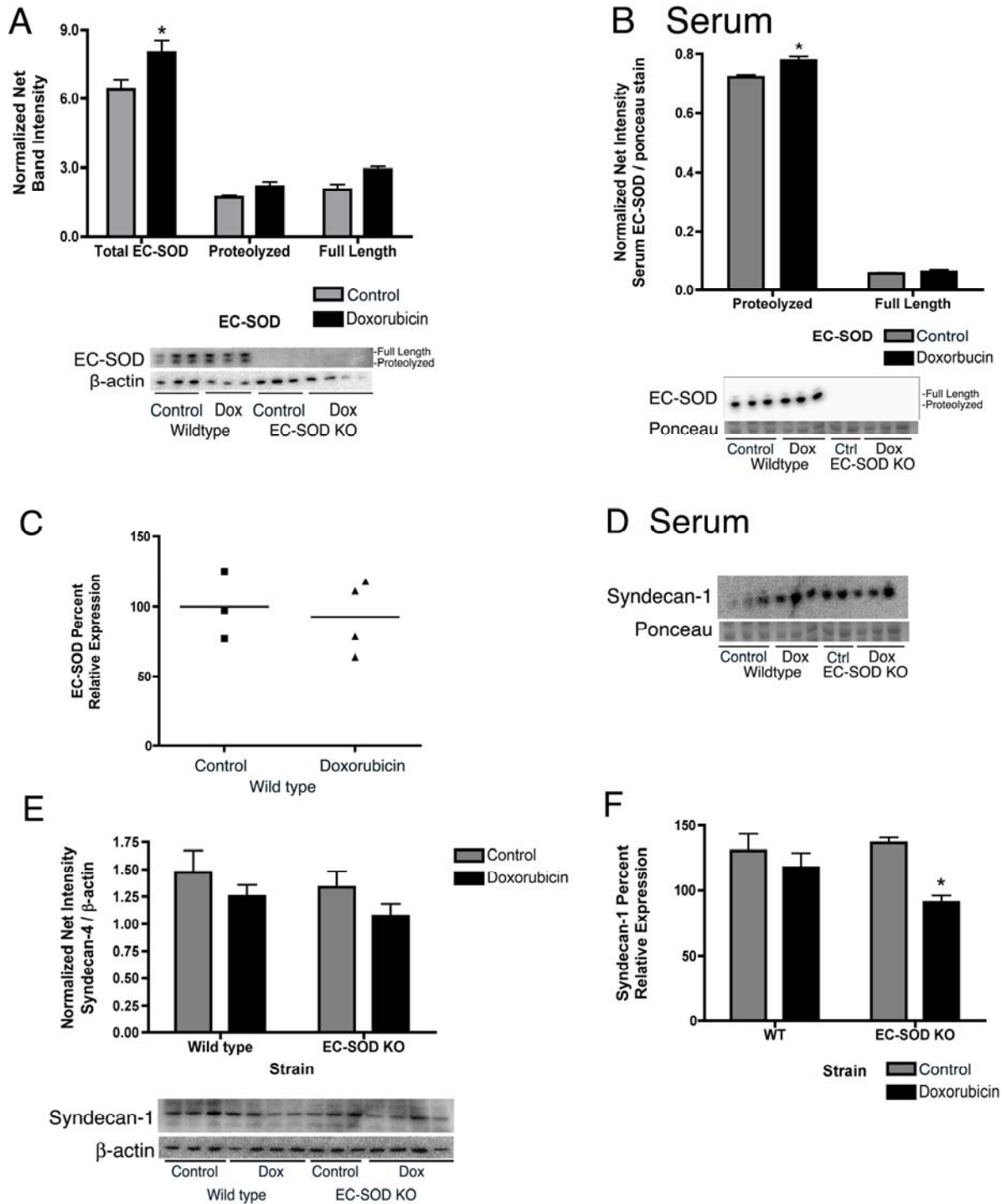


Figure 46: Doxorubicin treatment cause alterations in antioxidant EC-SOD and syndecan-1 of the ECM. A) EC-SOD in left ventricular (LV) homogenates after doxorubicin-treatment. Band intensity normalized to β -actin, mean \pm SEM. * $p < 0.05$ B) Serum EC-SOD after doxorubicin-treatment. Band intensity normalized to ponceau red, * $p < 0.05$. C) Left ventricular EC-SOD mRNA expression after doxorubicin in wild-type mice,

presented as percent relative ddCT expression, mean \pm SEM. n=4 D) Syndecan-1 ectodomains are shed from tissue into the serum due to doxorubicin-treatment and the lack of EC-SOD. Band intensity was normalized to ponceau red. E) Syndecan-1 in left ventricular (LV) homogenates after doxorubicin-treatment. Band intensity normalized to β -actin, mean \pm SEM. F) Left ventricular syndecan-1 mRNA expression after doxorubicin in wild-type and EC-SOD KO mice, percent relative ddCT expression, normalized to endogenous GAPDH expression. *p<0.05. n=4.

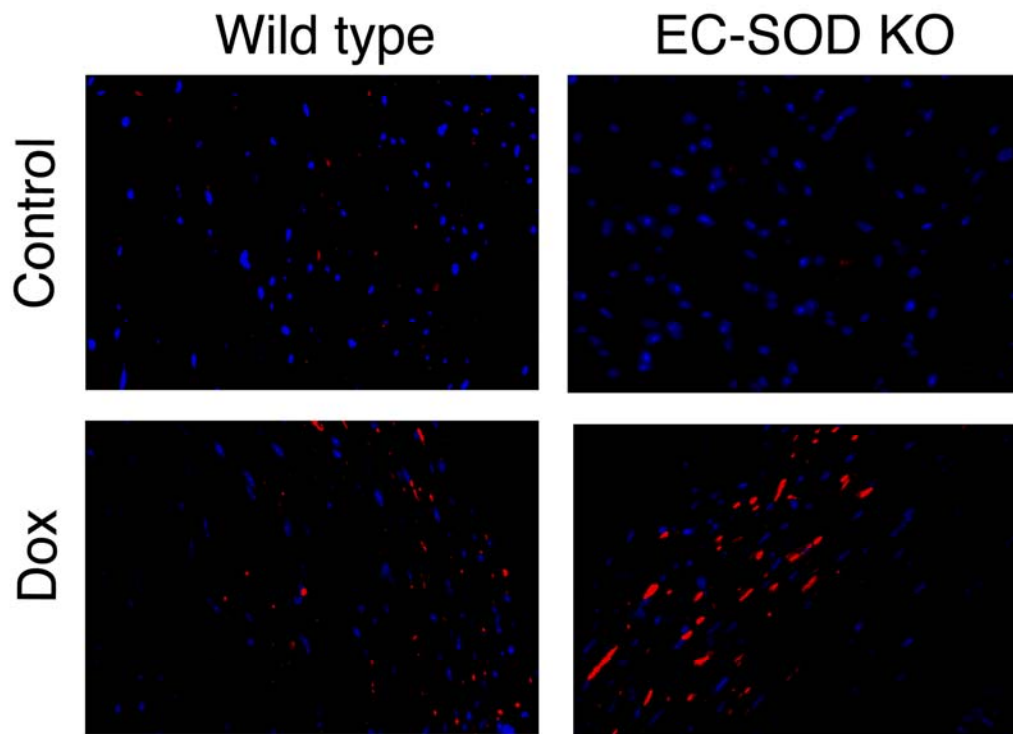


Figure 47: Lack of EC-SOD exacerbates inflammatory cell infiltration after oxidative injury due to doxorubicin. LV tissue sections were fluorescently stained for CD45 (leukocyte marker) and DAPI nuclear stain and imaged by standard immunofluorescence. Red = CD45, Blue = nuclei.

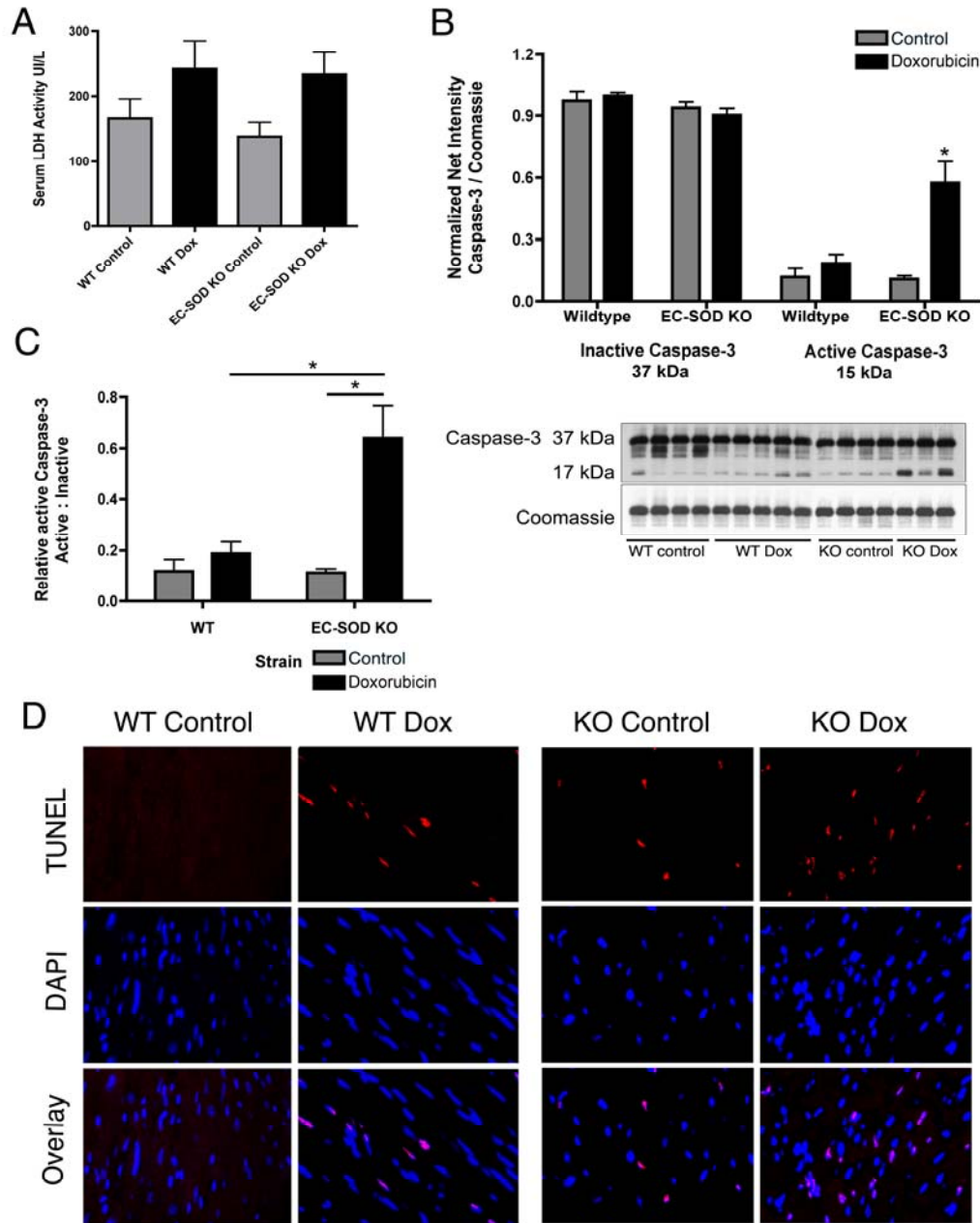


Figure 48: Lack of EC-SOD exacerbates apoptotic cell death in LV tissue. A) Serum lactate dehydrogenase (LDH) in serum from wild type and EC-SOD KO mice. B) Caspase-3, Inactive (37kDa pro-form) and active (12-17kDa form), in the soluble protein fractions of LV homogenates. Grey bars: Control group, Black bars: Doxorubicin group. Normalized to coomassie blue staining. * $p < 0.05$, $n = 3-5$. C) Relative active caspase-3 (active form to inactive form). * $p < 0.05$. D) Immunofluorescent TUNEL staining for DNA strand breaks in left ventricular tissue sections from each treatment group. Top panel: TUNEL (red staining), middle panel: DAPI nuclear stain (blue), bottom panel: overlay of TUNEL and DAPI.

8.0 DISCUSSION – CARDIAC FIBROSIS

EC-SOD is an important antioxidant in the cardiovascular system for its protective role against oxidative stress mediated by superoxide and other free radicals^{197, 198}. *We hypothesized that EC-SOD protects the heart from oxidant-induced fibrosis and loss of function by mediating normal cardiac function, inflammation and preventing oxidative shedding of the ECM.*

In this investigation, we found novel data supporting an important role for EC-SOD in cardiac morphology in the normal state, in addition to, protection against oxidative cardiac injury, including left ventricular (LV) fibrosis, inflammation, apoptosis, and loss of cardiac function. We utilized wild type and EC-SOD KO mice to evaluate the functional significance of a lack of EC-SOD in a baseline state and under oxidative stress. Doxorubicin-induced oxidant production¹³⁸ and subsequent cardiac fibrosis was utilized as our injury model.

Our data show that a lack of EC-SOD leads to changes in the morphology of the left ventricle including significant posterior wall thinning and increased LV end diastolic dimensions at baseline compared to age and gender matched control wild type (WT) mice (Figure 40). Interestingly, control EC-SOD KO mice do not have detectible functional impairment with these changes (Figure 41A, B) until they are challenged with an injury, such as oxidative stress via doxorubicin. In WT mice, doxorubicin causes a significant decrease in the LV posterior wall thickness (Figure 40A). In EC-SOD KO mice, doxorubicin does not cause an additional decrease in LVPWT however, it does cause a significant loss of cardiac function in the KO mice that does

not occur in the WT mice. This suggests that lack of EC-SOD exacerbates systolic dysfunction associated with doxorubicin cardio-toxicity. In addition, this suggests that EC-SOD is critical for maintaining a normal ventricular morphology and that the lack of EC-SOD increases sensitivity to oxidative stress and damage to the heart, which results in enhanced functional impairment. This is the first study examining the role of EC-SOD in maintaining cardiac morphology. EC-SOD KO mice also had significant increases in oxidative carbonyl modifications in membrane proteins suggesting increased extracellular oxidative stress. Control treated EC-SOD KO mice appear to develop spontaneous cardiac fibrosis at baseline compared to control WT mice by Trichrome staining (data not shown).

A primary pathological feature of doxorubicin cardio-toxicity is cardiac fibrosis that leads to non-ischemic dilated cardiomyopathy and congestive heart failure¹⁹⁸. Our *in vivo* histological and biochemical data show that doxorubicin causes significantly more left ventricular (LV) fibrosis and collagen deposition in EC-SOD KO mice compared to wild type mice (Figure 42-44). The pathological findings include remodeling of the LV myocardium through the deposition of collagen (Figure 43E) and the presence of cytoplasmic vacuolization (Figure 43F, black arrows), which together alter the functional capacity of the tissue.

It has been reported that syndecan-1 may protect against ventricular dilation and dysfunction in ischemic cardiac injury²⁵⁵. Our studies in pulmonary fibrosis show that EC-SOD prevents oxidative shedding of syndecan-1 from the lung epithelium and that the syndecan-1 ectodomain induces inflammation and may also contribute to pulmonary fibrosis²⁷⁸. Doxorubicin treatment results in increased shed syndecan-1 in the serum of wild type mice. EC-SOD KO mice have increased syndecan-1 shedding with control treatment and no further increase with doxorubicin (Figure 46). Furthermore, there are corresponding decreases in membrane bound

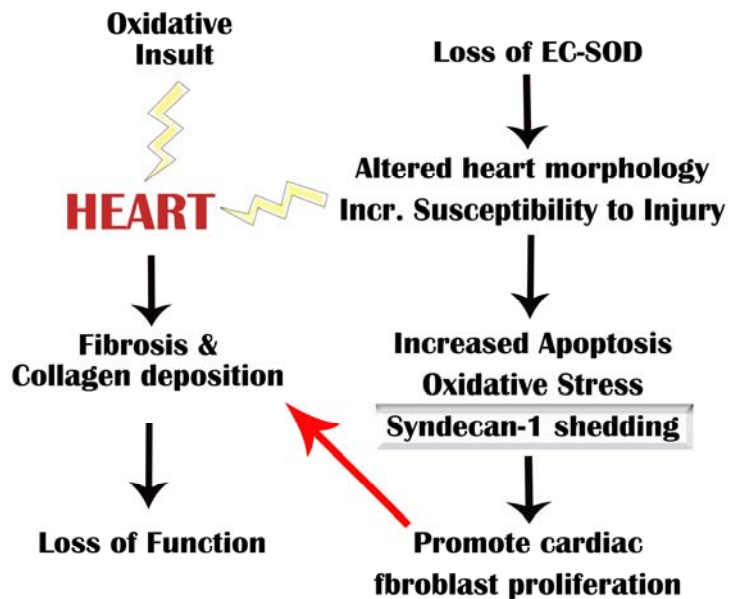
syndecan-1 in the LV of both WT and EC-SOD KO mice after doxorubicin treatment. EC-SOD KO mice also have significantly lower syndecan-1 mRNA expression after doxorubicin compared to WT mice (Figure 46). These findings suggest that the lack of EC-SOD and the increase in oxidative stress in EC-SOD KO mice leads to syndecan-1 shedding and decreases in tissue expression after injury. The lack of cardiac EC-SOD also results in enhanced inflammatory cell infiltration after doxorubicin oxidative injury (Figure 47), which may be due to the increases in syndecan-1 shedding. Our studies in the lung show that shed syndecan-1 promotes inflammatory cell recruitment. This may be a mechanism involved in oxidant damage to the heart. These findings support a novel role for EC-SOD in protecting the cardiac extracellular matrix and regulating inflammation. In addition, the data show that the lack of EC-SOD results in a loss of membrane-bound syndecan-1 and cardiac remodeling consistent with dilation, which correlates with other investigations showing that a lack of syndecan-1 in ischemic heart injury exacerbates ventricular dilation. Based on this prior study, we would predict that shedding of syndecan-1 in EC-SOD KO mice and doxorubicin-induced oxidative shedding would exacerbate cardiac remodeling, leading to thinning of the left ventricle and dilation. Furthermore, this suggests that administration of EC-SOD or an SOD-like compound in these settings would protect against the ventricular remodeling and subsequent loss in cardiac function.

The doxorubicin-induced oxidative cardiac injury that is seen in both wild type and EC-SOD KO mice leads to a loss in LV tissue mass. This injury involves apoptotic cell death. Doxorubicin-treated EC-SOD KO mice have a significant increase in apoptosis compared to doxorubicin-treated WT mice (Figure 48). EC-SOD KO mice have significantly more caspase-3 activation compared to wild type mice after doxorubicin treatment (Figure 48B and C, increased ratio of active to inactive caspase-3). EC-SOD KO mice also have increased TUNEL staining in

both the control and doxorubicin treatment groups compared to wild type mice. This data suggests that, mechanistically, EC-SOD functions in regulating apoptosis after exposure to doxorubicin by limiting caspase-3 activation. Moreover, EC-SOD protects against cardiomyocyte cell death, replacement of LV tissue with collagen, and subsequent loss of cardiac function, in part, by regulating oxidant-induced apoptosis. To investigate the interactions involved between the scavenging of extracellular superoxide by EC-SOD and intracellular apoptosis signaling, cardiomyocytes could be treated with a superoxide generating system. Apoptosis could be evaluated by caspase activation in cell lysates. If the addition of EC-SOD prevented apoptosis induction, this would suggest that superoxide mediates the signaling. If exogenous EC-SOD does not alter apoptosis induction, catalase should be utilized to determine if membrane-permeable H₂O₂ is mediating apoptotic signaling.

The pharmacological activity of doxorubicin has 2 levels: first doxorubicin enters into cells to bind with DNA causing cellular dysregulation and second, it can undergo quinone-semiquinone reduction-oxidation reactions to produce reactive oxygen species. Studies suggest that doxorubicin can generate intracellular and extracellular oxidants. The current findings that EC-SOD has such profound effects on the injury caused by doxorubicin are novel in the pathogenesis of doxorubicin-induced injury. Several mechanisms may explain these findings. EC-SOD may be preventing inflammation and fibrosis in the heart by protecting the ECM, specifically syndecan-1, on cardiac cells from oxidants. Shed syndecan-1 may be promoting leukocyte recruitment. Our pulmonary fibrosis studies confirm that the shed syndecan-1 ectodomain is chemotactic to leukocytes. The loss of membrane bound syndecan-1 could then promote dilation of the left ventricle. In addition, our findings suggest that EC-SOD regulates

apoptosis by limiting caspase-3 activation. Increased apoptosis of LV cardiomyocytes can lead to LV wall thinning, ventricle dilation and loss of cardiac function.



8.1 CLINICAL SIGNIFICANCE AND FUTURE DIRECTIONS

This data highlights the implications of a lack of EC-SOD in the heart, which has a relevant clinical correlate. An EC-SOD gene variant has been implicated in increased risk for cardiovascular and ischemic heart disease. Studies report that an amino acid modification, EC-SOD^{R213G} arginine-213 to glycine substitution, in the matrix-binding domain of EC-SOD results in decreased binding affinity of EC-SOD for the tissue matrix^{208, 210}. Individuals with this mutation have increased serum levels of EC-SOD^{209, 211}. Population studies suggest that 2-6% of individuals may carry this mutation, thus it is considered to be a common gene variant^{211, 212}. A study from Denmark reports a 2.3 fold increase in the risk of ischemic heart disease in heterozygous individuals for EC-SOD^{R213G}²¹³. Our present data suggest that EC-SOD is

effective in protecting the heart against oxidant-induced cardiac fibrosis, LV posterior wall thinning and dilation, cardiomyocyte apoptosis, and loss of function. These findings raise interesting questions about the potential effects of the EC-SOD^{R213G} gene variant on an individual's susceptibility to oxidative insults to the heart and further developing fibrosis and loss of cardiac function.

This study shows that EC-SOD is important in the maintenance of normal cardiac morphology, the development of cardiac fibrosis, inflammation, and the loss of function associated with oxidative injury, as modeled by doxorubicin. These findings warrant additional studies on the utilization of antioxidants, potentially EC-SOD, for the prevention of oxidant-induced cardiac injury. We are currently completing a study analyzing the efficacy of a superoxide dismutase-like agent, AEOL10150. This compound is a small porphyrin antioxidant analog and has been successful in limiting NF- κ B activation and lipid peroxidation in hemorrhagic lung injury in mice²²⁷, protected against oxidative stress and apoptosis²⁹⁷, reducing infarct size by 43% in a brain ischemia model of middle cerebral artery occlusion²⁹⁸, and oxidative neurotoxicity²⁹⁹. WT and EC-SOD KO mice will be treated with saline or doxorubicin on day 0, as in prior experiments, with administration of AEOL10150 or vehicle twice daily for 15 days. Cardiac function will be evaluated by echocardiography and cardiac fibrosis will be assessed by hydroxyproline. We hypothesize that AEOL10150 will decrease fibrosis and improve cardiac function in both WT and EC-SOD KO mice treated with doxorubicin.

We are also completing aging studies in EC-SOD KO mice to evaluate their cardiac morphology and function compared to similarly aged WT mice. We have evaluated 5 week old, 9 week old and 5 month old, untreated WT and EC-SOD KO mice. Our initial study shows that WT mice lose some cardiac function with age (percent ejection fraction and fractional shortening

of the LV). Interestingly, EC-SOD KO mice appear to lose cardiac function in a more drastic manner and earlier. Furthermore, EC-SOD KO mice have evident cardiac fibrosis already by 6 weeks of age, which would predict progressed with age. A lack of EC-SOD has surprising effects on the heart and additional studies should be done to evaluate how EC-SOD protects the heart. Our current studies suggest that regulation of caspase activation and protecting the extracellular matrix are important functions of EC-SOD. The lack of EC-SOD may also be leading to uncoupling of NOS enzymes, such as eNOS. The uncoupling of eNOS would lead to increased superoxide production and a decrease in NO production, which has cardiovascular benefits when present.

In our pulmonary fibrosis studies, we show that EC-SOD protects syndecan-1 from oxidative fragmentation and that the shed ectodomain of syndecan-1 promotes abnormal wound healing and fibrosis. The effect of the syndecan-1 ectodomain could be investigated in cardiac cell models including cardiomyocytes and cardiac fibroblasts. Structurally, syndecans are linked to the actin cytoskeleton, thus, disruption of membrane bound syndecan-1 could alter the contractile ability of cardiomyocytes. We are currently completing studies to determine syndecan-1 is shed proteolytically or oxidatively from neonatal rat cardiomyocytes.

9.0 FINAL DISCUSSION

Tissue fibrosis of the lung and heart are thought to involve oxidant and anti-oxidant imbalances. The current literature on the pathogenesis of tissue fibrosis focuses primarily on the roles of epithelial, mesenchymal and inflammatory cells. The importance of oxidative modifications to the extracellular matrix and how this alters cellular responses remains an open and under-investigated area. Specifically, the role for oxidative shedding of syndecans and the effects of the shed ectodomains during tissue injury remain unclear. Extracellular superoxide dismutase (EC-SOD) is the most abundant antioxidant in the extracellular space of many tissues where it is localized through binding to matrix components such as heparan sulfates, or syndecans. We provide novel evidence that oxidative shedding of syndecan-1 occurs in multiple organ systems and that EC-SOD has a primary role in protecting the matrix and down-stream consequences. While there are unique differences found in EC-SOD and syndecan-1 biology between the lungs and cardiovascular system during fibrosis, as discussed in previous sections, several novel biological themes over-arch the pathogenesis of inflammation and fibrosis.

First, EC-SOD is a key anti-oxidant enzyme that protects the extracellular matrix of a tissue from increases in oxidative stress. We have shown that a lack of EC-SOD results in increased syndecan-1 shedding from the epithelium of the lung and into the serum, potentially from the endothelium of the vasculature. While tissue proteases are critical to tissue remodeling and the repair process, oxidative stress plays an important role. Potential therapeutic targets that

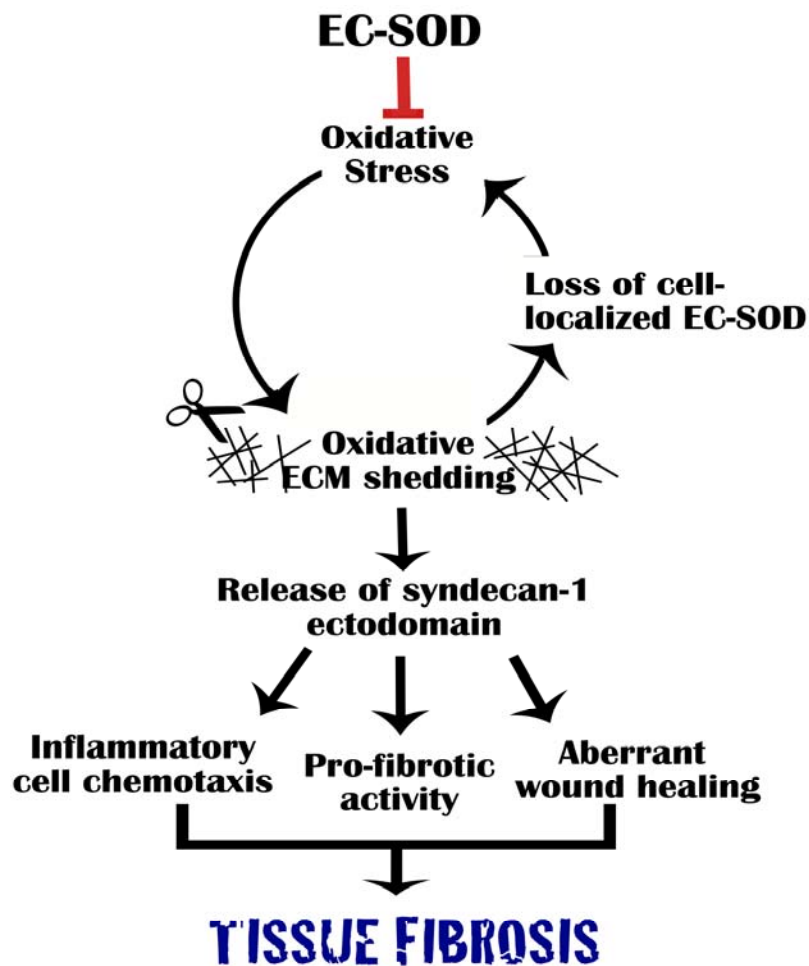
may be of use in controlling fibrogenesis include utilizing antioxidants to modulate the oxidative stress levels in a tissue, as well as, matrix fragments may have negative effects within the cellular microenvironment.

Second, syndecan-1 gains a pathological function when shed from the cell surface. Our data provides novel evidence that the shed syndecan-1 ectodomain is chemotactic to neutrophils, which is independent of chemokines, and impairs epithelial wound healing. Shed syndecan-1 also gains a pro-fibrotic functions through its ability to induce proliferation of both lung and cardiac fibroblasts and to stimulate TGF- β release from lung fibroblasts. These findings suggest that shed syndecan-1 has a pathologic gain of function during the inflammatory and fibrotic phasis of fibrosis development.

Finally, membrane-bound syndecan-1 functions by mediating cell-cell and cell-matrix adhesion, as well as, regulating growth factor and cytokine gradients and receptor activation. Our data suggests that when syndecan-1 is oxidative shed and lost from the epithelial cell surface, there is a loss of function that occurs. Epithelial wound healing is dysregulated and inhibited when membrane-bound syndecan-1 is lost. Therefore, oxidatively shed syndecan-1 may promote a fibrotic path for a tissue due to the loss of membrane-bound syndecan-1 during the initial injury. Without the appropriate re-epithelialization repair response, the cells are driven toward matrix deposition and fibrosis.

In summary, the extracellular matrix creates a complex and critical microenvironment for the cells that make up a tissue. The pulmonary and cardiovascular systems are constantly challenged by oxidative insults that require well-coordinated repair responses. Extracellular superoxide dismutase is the primary antioxidant enzyme that protects this microenvironment. Through our studies of the pulmonary and cardiac fibrosis show that EC-SOD has a role in

maintaining the appropriate repair response. Oxidative stress, in addition to proteolytic fragmentation, leads to shedding of the extracellular matrix. Syndecan-1, which binds EC-SOD, is one of the affected matrix components. The loss of syndecan-1 from the cell surface leads to de-localization of EC-SOD, which promotes additional oxidative stress. The function of shed matrix components is unclear but important in aiding the understanding how to modulate disease development and progression. The syndecan-1 ectodomain gains pathological functions including leukocyte recruitment, pro-fibrotic actions such as the induction of fibroblast proliferation and TGF- bioavailability, and inhibiting re-epithelialization. Each of these functions, which appear to be conserved among cell types in various tissues, push a tissue away from normal wound healing toward fibrosis development.



REFERENCES

1. Raghu G, Weycker D, Edelsberg J, Bradford WZ, Oster G. Incidence and prevalence of idiopathic pulmonary fibrosis. *American journal of respiratory and critical care medicine*. 2006;**174**(7):810-816.
2. Gross TJ, Hunninghake GW. Idiopathic pulmonary fibrosis. *The New England journal of medicine*. 2001;**345**(7):517-525.
3. American Thoracic Society. Idiopathic pulmonary fibrosis: diagnosis and treatment. International consensus statement. American Thoracic Society (ATS), and the European Respiratory Society (ERS). *American journal of respiratory and critical care medicine*. 2000;**161**(2 Pt 1):646-664.
4. Oury TD, Schaefer LM, Fattman CL, Choi A, Weck KE, Watkins SC. Depletion of pulmonary EC-SOD after exposure to hyperoxia. *American journal of physiology*. 2002;**283**(4):L777-784.
5. Daniil ZD, Papageorgiou E, Koutsokera A, Kostikas K, Kiropoulos T, Papaioannou AI, Gourgoulisanis KI. Serum levels of oxidative stress as a marker of disease severity in idiopathic pulmonary fibrosis. *Pulmonary pharmacology & therapeutics*. 2008;**21**(1):26-31.
6. MacNee W, Rahman I. Oxidants/antioxidants in idiopathic pulmonary fibrosis. *Thorax*. 1995;**50 Suppl 1**:S53-58.
7. Kinder BW, Brown KK, Schwarz MI, Ix JH, Kervitsky A, King TE, Jr. Baseline BAL neutrophilia predicts early mortality in idiopathic pulmonary fibrosis. *Chest*. 2008;**133**(1):226-232.
8. Ryu YJ, Chung MP, Han J, Kim TS, Lee KS, Chun EM, Kyung SY, Jeong SH, Colby TV, Kim H, Kwon OJ. Bronchoalveolar lavage in fibrotic idiopathic interstitial pneumonias. *Respiratory medicine*. 2007;**101**(3):655-660.
9. Strausz J, Muller-Quernheim J, Stepling H, Ferlinz R. Oxygen radical production by alveolar inflammatory cells in idiopathic pulmonary fibrosis. *The American review of respiratory disease*. 1990;**141**(1):124-128.
10. Teramoto S, Fukuchi Y, Uejima Y, Shu CY, Orimo H. Superoxide anion formation and glutathione metabolism of blood in patients with idiopathic pulmonary fibrosis. *Biochem Mol Med*. 1995;**55**(1):66-70.
11. Rahman I, Skwarska E, Henry M, Davis M, O'Connor CM, FitzGerald MX, Greening A, MacNee W. Systemic and pulmonary oxidative stress in idiopathic pulmonary fibrosis. *Free Radic Biol Med*. 1999;**27**(1-2):60-68.
12. Katzenstein AA, Askin FB. Surgical pathology of non-neoplastic lung disease. *Major Probl Pathol*. 1982;**13**:1-430.

13. Panos RJ, Mortenson RL, Niccoli SA, King TE, Jr. Clinical deterioration in patients with idiopathic pulmonary fibrosis: causes and assessment. *Am J Med.* 1990;**88**(4):396-404.
14. Walter N, Collard HR, King TE, Jr. Current perspectives on the treatment of idiopathic pulmonary fibrosis. *Proceedings of the American Thoracic Society.* 2006;**3**(4):330-338.
15. Flaherty KR, Toews GB, Lynch JP, 3rd, Kazerooni EA, Gross BH, Strawderman RL, Hariharan K, Flint A, Martinez FJ. Steroids in idiopathic pulmonary fibrosis: a prospective assessment of adverse reactions, response to therapy, and survival. *Am J Med.* 2001;**110**(4):278-282.
16. Flaherty KR, Toews GB, Travis WD, Colby TV, Kazerooni EA, Gross BH, Jain A, Strawderman RL, 3rd, Paine R, Flint A, Lynch JP, 3rd, Martinez FJ. Clinical significance of histological classification of idiopathic interstitial pneumonia. *Eur Respir J.* 2002;**19**(2):275-283.
17. Raghu G, Depaso WJ, Cain K, Hammar SP, Wetzel CE, Dreis DF, Hutchinson J, Pardee NE, Winterbauer RH. Azathioprine combined with prednisone in the treatment of idiopathic pulmonary fibrosis: a prospective double-blind, randomized, placebo-controlled clinical trial. *The American review of respiratory disease.* 1991;**144**(2):291-296.
18. Zisman DA, Lynch JP, 3rd, Toews GB, Kazerooni EA, Flint A, Martinez FJ. Cyclophosphamide in the treatment of idiopathic pulmonary fibrosis: a prospective study in patients who failed to respond to corticosteroids. *Chest.* 2000;**117**(6):1619-1626.
19. Collard HR, Ryu JH, Douglas WW, Schwarz MI, Curran-Everett D, King TE, Jr., Brown KK. Combined corticosteroid and cyclophosphamide therapy does not alter survival in idiopathic pulmonary fibrosis. *Chest.* 2004;**125**(6):2169-2174.
20. Rennard SI, Bitterman PB, Ozaki T, Rom WN, Crystal RG. Colchicine suppresses the release of fibroblast growth factors from alveolar macrophages in vitro. The basis of a possible therapeutic approach of the fibrotic disorders. *The American review of respiratory disease.* 1988;**137**(1):181-185.
21. Zhang L, Zhu Y, Luo W, Xi P, Yan Y. The protective effect of colchicine on bleomycin-induced pulmonary fibrosis in rats. *Chin Med Sci J.* 1992;**7**(1):58-60.
22. Douglas WW, Ryu JH, Schroeder DR. Idiopathic pulmonary fibrosis: Impact of oxygen and colchicine, prednisone, or no therapy on survival. *American journal of respiratory and critical care medicine.* 2000;**161**(4 Pt 1):1172-1178.
23. Douglas WW, Ryu JH, Swensen SJ, Offord KP, Schroeder DR, Caron GM, DeRemee RA. Colchicine versus prednisone in the treatment of idiopathic pulmonary fibrosis. A randomized prospective study. Members of the Lung Study Group. *American journal of respiratory and critical care medicine.* 1998;**158**(1):220-225.
24. Fiorucci E, Lucantoni G, Paone G, Zotti M, Li BE, Serpilli M, Regimenti P, Cammarella I, Puglisi G, Schmid G. Colchicine, cyclophosphamide and prednisone in the treatment of mild-moderate idiopathic pulmonary fibrosis: comparison of three currently available therapeutic regimens. *Eur Rev Med Pharmacol Sci.* 2008;**12**(2):105-111.
25. Iyer SN, Gurujeyalakshmi G, Giri SN. Effects of pirfenidone on transforming growth factor-beta gene expression at the transcriptional level in bleomycin hamster model of lung fibrosis. *J Pharmacol Exp Ther.* 1999;**291**(1):367-373.
26. Iyer SN, Margolin SB, Hyde DM, Giri SN. Lung fibrosis is ameliorated by pirfenidone fed in diet after the second dose in a three-dose bleomycin-hamster model. *Exp Lung Res.* 1998;**24**(1):119-132.

27. Raghu G, Johnson WC, Lockhart D, Mageto Y. Treatment of idiopathic pulmonary fibrosis with a new antifibrotic agent, pirfenidone: results of a prospective, open-label Phase II study. *American journal of respiratory and critical care medicine*. 1999;**159**(4 Pt 1):1061-1069.
28. Thabut G, Mal H, Castier Y, Groussard O, Brugiere O, Marrash-Chahla R, Leseche G, Fournier M. Survival benefit of lung transplantation for patients with idiopathic pulmonary fibrosis. *J Thorac Cardiovasc Surg*. 2003;**126**(2):469-475.
29. Selman M, Pardo A. Idiopathic pulmonary fibrosis: an epithelial/fibroblastic cross-talk disorder. *Respiratory research*. 2002;**3**:3.
30. Manning CB, Vallyathan V, Mossman BT. Diseases caused by asbestos: mechanisms of injury and disease development. *International immunopharmacology*. 2002;**2**(2-3):191-200.
31. Murphy RL, Jr. The diagnosis of nonmalignant diseases related to asbestos. *The American review of respiratory disease*. 1987;**136**(6):1516-1517.
32. Sporn TA, Roggli, V.L. Asbestosis. In: Roggli V, Oury, TD, Sporn, TA., ed. *Pathology of Asbestos-Associated Diseases*. Second ed. New York: Springer-Verlag; 2005:34-70.
33. Niklinski J, Niklinska W, Chyczewska E, Laudanski J, Naumnik W, Chyczewski L, Pluygers E. The epidemiology of asbestos-related diseases. *Lung Cancer*. 2004;**45 Suppl 1**:S7-S15.
34. Darcey DJ, Alleman, T. Occupational and Environmental Exposure to Asbestos. In: Roggli V, Oury, TD, Sporn, TA., ed. *Pathology of Asbestos-Associated Diseases*. Second ed. New York: Springer-Verlag; 2005:17-33.
35. Roggli VL, Coin, P. Mineralogy of Asbestos. In: Roggli V, Oury, TD, Sporn, TA., ed. *Pathology of Asbestos-Associated Diseases*. Second ed. New York: Springer-Verlag; 2005:1-16.
36. Roggli VL, Sanders LL. Asbestos content of lung tissue and carcinoma of the lung: a clinicopathologic correlation and mineral fiber analysis of 234 cases. *Ann Occup Hyg*. 2000;**44**(2):109-117.
37. Roggli VL. Asbestos Bodies and Nonasbestos Ferruginous Bodies. *Pathology of Asbestos-Associated Diseases*. Second ed. New York: Springer-Verlag; 2005:71-103.
38. Governa M, Amati M, Fontana S, Visona I, Botta GC, Mollo F, Bellis D, Bo P. Role of iron in asbestos-body-induced oxidant radical generation. *J Toxicol Environ Health A*. 1999;**58**(5):279-287.
39. Schapira RM, Ghio AJ, Effros RM, Morrisey J, Dawson CA, Hacker AD. Hydroxyl radicals are formed in the rat lung after asbestos instillation in vivo. *Am J Respir Cell Mol Biol*. 1994;**10**(5):573-579.
40. Shukla A, Gulumian M, Hei TK, Kamp D, Rahman Q, Mossman BT. Multiple roles of oxidants in the pathogenesis of asbestos-induced diseases. *Free Radic Biol Med*. 2003;**34**(9):1117-1129.
41. Shukla A, Ramos-Nino M, Mossman B. Cell signaling and transcription factor activation by asbestos in lung injury and disease. *Int J Biochem Cell Biol*. 2003;**35**(8):1198-1209.
42. Hansen K, Mossman BT. Generation of superoxide (O₂⁻) from alveolar macrophages exposed to asbestiform and nonfibrous particles. *Cancer Res*. 1987;**47**(6):1681-1686.
43. Rola-Pleszczynski M, Gouin S, Begin R. Asbestos-induced lung inflammation. Role of local macrophage-derived chemotactic factors in accumulation of neutrophils in the lungs. *Inflammation*. 1984;**8**(1):53-62.

44. Peterson MW, Kirschbaum J. Asbestos-induced lung epithelial permeability: potential role of nonoxidant pathways. *Am J Physiol.* 1998;**275**(2 Pt 1):L262-268.
45. Shukla A, Stern M, Lounsbury KM, Flanders T, Mossman BT. Asbestos-induced apoptosis is protein kinase C delta-dependent. *Am J Respir Cell Mol Biol.* 2003;**29**(2):198-205.
46. Buder-Hoffmann SA, Shukla A, Barrett TF, MacPherson MB, Lounsbury KM, Mossman BT. A protein kinase Cdelta-dependent protein kinase D pathway modulates ERK1/2 and JNK1/2 phosphorylation and Bim-associated apoptosis by asbestos. *Am J Pathol.* 2009;**174**(2):449-459.
47. Haegens A, Barrett TF, Gell J, Shukla A, Macpherson M, Vacek P, Poynter ME, Butnor KJ, Janssen-Heininger YM, Steele C, Mossman BT. Airway epithelial NF-kappaB activation modulates asbestos-induced inflammation and mucin production in vivo. *J Immunol.* 2007;**178**(3):1800-1808.
48. Dostert C, Petrilli V, Van Bruggen R, Steele C, Mossman BT, Tschopp J. Innate immune activation through Nalp3 inflammasome sensing of asbestos and silica. *Science.* 2008;**320**(5876):674-677.
49. Liu JY, Brody AR. Increased TGF-beta1 in the lungs of asbestos-exposed rats and mice: reduced expression in TNF-alpha receptor knockout mice. *J Environ Pathol Toxicol Oncol.* 2001;**20**(2):97-108.
50. Pociask DA, Sime PJ, Brody AR. Asbestos-derived reactive oxygen species activate TGF-beta1. *Lab Invest.* 2004;**84**(8):1013-1023.
51. Lazo JS, Hoyt DG, Sebti SM, Pitt BR. Bleomycin: a pharmacologic tool in the study of the pathogenesis of interstitial pulmonary fibrosis. *Pharmacol Ther.* 1990;**47**(3):347-358.
52. Thrall RS, Scalise, P.J. Bleomycin. In: Phan SH, Thrall, R.S., ed. *Lung Biology in Health and Disease: Pulmonary Fibrosis*. First ed. New York: Marcel Dekker; 1995:231-292.
53. Sugiura Y. The production of hydroxyl radical from copper(I) complex systems of bleomycin and tallysomylin: comparison with copper(II) and iron(II) systems. *Biochem Biophys Res Commun.* 1979;**90**(1):375-383.
54. Teixeira KC, Soares FS, Rocha LG, Silveira PC, Silva LA, Valenca SS, Dal Pizzol F, Streck EL, Pinho RA. Attenuation of bleomycin-induced lung injury and oxidative stress by N-acetylcysteine plus deferoxamine. *Pulm Pharmacol Ther.* 2008;**21**(2):309-316.
55. Bowler RP, Nicks M, Warnick K, Crapo JD. Role of extracellular superoxide dismutase in bleomycin-induced pulmonary fibrosis. *Am J Physiol Lung Cell Mol Physiol.* 2002;**282**(4):L719-726.
56. Manoury B, Nenan S, Leclerc O, Guenon I, Boichot E, Planquois JM, Bertrand CP, Lagente V. The absence of reactive oxygen species production protects mice against bleomycin-induced pulmonary fibrosis. *Respir Res.* 2005;**6**:11.
57. Fattman CL, Chang LY, Termin TA, Petersen L, Enghild JJ, Oury TD. Enhanced bleomycin-induced pulmonary damage in mice lacking extracellular superoxide dismutase. *Free radical biology & medicine.* 2003;**35**(7):763-771.
58. Izbicki G, Segel MJ, Christensen TG, Conner MW, Breuer R. Time course of bleomycin-induced lung fibrosis. *Int J Exp Pathol.* 2002;**83**(3):111-119.
59. Venkatesan N, Roughley PJ, Ludwig MS. Proteoglycan expression in bleomycin lung fibroblasts: role of transforming growth factor-beta(1) and interferon-gamma. *Am J Physiol Lung Cell Mol Physiol.* 2002;**283**(4):L806-814.

60. Tan RJ, Fattman CL, Watkins SC, Oury TD. Redistribution of pulmonary EC-SOD after exposure to asbestos. *J Appl Physiol.* 2004;**97**(5):2006-2013.
61. Kinnula VL, Hodgson UA, Lakari EK, Tan RJ, Sormunen RT, Soini YM, Kakko SJ, Laitinen TH, Oury TD, Paakko PK. Extracellular superoxide dismutase has a highly specific localization in idiopathic pulmonary fibrosis/usual interstitial pneumonia. *Histopathology.* 2006;**49**(1):66-74.
62. Fattman CL, Chu, C.T., Oury, T.D. Experimental Models of Asbestos-Related Diseases. In: Roggli V, Oury, TD, Sporn, TA., ed. *Pathology of Asbestos Associated Diseases.* Second ed. New York: Springer-Verlag; 2005:256-308.
63. Fattman CL, Tan RJ, Tobolewski JM, Oury TD. Increased sensitivity to asbestos-induced lung injury in mice lacking extracellular superoxide dismutase. *Free radical biology & medicine.* 2006;**40**(4):601-607.
64. McLemore TL, Mace ML, Jr., Roggli V, Marshall MV, Lawrence EC, Wilson RK, Martin RR, Brinkley BR, Greenberg SD. Asbestos body phagocytosis by human free alveolar macrophages. *Cancer Lett.* 1980;**9**(2):85-93.
65. Barry BE, Wong KC, Brody AR, Crapo JD. Reaction of rat lungs to inhaled chrysotile asbestos following acute and subchronic exposures. *Exp Lung Res.* 1983;**5**(1):1-21.
66. Dai J, Gilks B, Price K, Churg A. Mineral dusts directly induce epithelial and interstitial fibrogenic mediators and matrix components in the airway wall. *American journal of respiratory and critical care medicine.* 1998;**158**(6):1907-1913.
67. Hirano S, Ono M, Aimoto A. Functional and biochemical effects on rat lung following instillation of crocidolite and chrysotile asbestos. *J Toxicol Environ Health.* 1988;**24**(1):27-39.
68. Lemaire I. Silica- and Asbestos-induced Pulmonary Fibrosis. In: Phan SH, Thrall, R.S., ed. *Lung Biology in Health and Disease: Pulmonary Fibrosis.* Vol 80. First ed. New York: Marcel Dekker; 1995:319-362.
69. Adamson IY, Bowden DH. Role of polymorphonuclear leukocytes in silica-induced pulmonary fibrosis. *Am J Pathol.* 1984;**117**(1):37-43.
70. Adamson IY, Letourneau HL, Bowden DH. Enhanced macrophage-fibroblast interactions in the pulmonary interstitium increases fibrosis after silica injection to monocyte-depleted mice. *Am J Pathol.* 1989;**134**(2):411-418.
71. Bowden DH, Hedgecock C, Adamson IY. Silica-induced pulmonary fibrosis involves the reaction of particles with interstitial rather than alveolar macrophages. *J Pathol.* 1989;**158**(1):73-80.
72. Porter DW, Ramsey D, Hubbs AF, Battelli L, Ma J, Barger M, Landsittel D, Robinson VA, McLaurin J, Khan A, Jones W, Teass A, Castranova V. Time course of pulmonary response of rats to inhalation of crystalline silica: histological results and biochemical indices of damage, lipidosis, and fibrosis. *J Environ Pathol Toxicol Oncol.* 2001;**20** Suppl 1:1-14.
73. Adamson IY, Prieditis H. Silica deposition in the lung during epithelial injury potentiates fibrosis and increases particle translocation to lymph nodes. *Exp Lung Res.* 1998;**24**(3):293-306.
74. Mariani TJ, Roby JD, Mecham RP, Parks WC, Crouch E, Pierce RA. Localization of type I procollagen gene expression in silica-induced granulomatous lung disease and implication of transforming growth factor-beta as a mediator of fibrosis. *Am J Pathol.* 1996;**148**(1):151-164.

75. Poole A. Collagen synthesis in rats with silica-induced pulmonary fibrosis. *Arch Toxicol Suppl.* 1987;**11**:285-287.
76. Vuorio EI, Makela JK, Vuorio TK, Poole A, Wagner JC. Characterization of excessive collagen production during development of pulmonary fibrosis induced by chronic silica inhalation in rats. *Br J Exp Pathol.* 1989;**70**(3):305-315.
77. Velan GM, Kumar RK, Cohen DD. Pulmonary inflammation and fibrosis following subacute inhalational exposure to silica: determinants of progression. *Pathology.* 1993;**25**(3):282-290.
78. Barbarin V, Nihoul A, Misson P, Arras M, Delos M, Leclercq I, Lison D, Huaux F. The role of pro- and anti-inflammatory responses in silica-induced lung fibrosis. *Respir Res.* 2005;**6**:112.
79. Cassel SL, Eisenbarth SC, Iyer SS, Sadler JJ, Colegio OR, Tephly LA, Carter AB, Rothman PB, Flavell RA, Sutterwala FS. The Nalp3 inflammasome is essential for the development of silicosis. *Proc Natl Acad Sci U S A.* 2008;**105**(26):9035-9040.
80. Kuhlmann UC, Chwieralski CE, van den Brule S, Rocken C, Reinhold D, Welte T, Buhling F. Modulation of cytokine production and silica-induced lung fibrosis by inhibitors of aminopeptidase N and of dipeptidyl peptidase-IV-related proteases. *Life Sci.* 2009;**84**(1-2):1-11.
81. Pulmonary Fibrosis. In: Phan SH, Thrall, R.S., ed. *Lung Biology in Health and Disease.* Vol 80. New York: Marcel Dekker; 1995.
82. Kumar V, Robbins SL. *Robbins basic pathology.* 8th ed. Philadelphia, PA: Saunders/Elsevier; 2007.
83. Baptista AL, Parra ER, Filho JV, Kairalla RA, de Carvalho CR, Capelozzi VL. Structural features of epithelial remodeling in usual interstitial pneumonia histologic pattern. *Lung.* 2006;**184**(4):239-244.
84. Budinger GR, Mutlu GM, Eisenbart J, Fuller AC, Bellmeyer AA, Baker CM, Wilson M, Ridge K, Barrett TA, Lee VY, Chandel NS. Proapoptotic Bid is required for pulmonary fibrosis. *Proc Natl Acad Sci U S A.* 2006;**103**(12):4604-4609.
85. Maeyama T, Kuwano K, Kawasaki M, Kunitake R, Hagimoto N, Matsuba T, Yoshimi M, Inoshima I, Yoshida K, Hara N. Upregulation of Fas-signalling molecules in lung epithelial cells from patients with idiopathic pulmonary fibrosis. *Eur Respir J.* 2001;**17**(2):180-189.
86. Koth LL, Sheppard, D. Integrins and Pulmonary Fibrosis. In: Lynch JP, ed. *Idiopathic Pulmonary Fibrosis: Lung Biology in Health and Disease.* Vol 185. First ed. New York: Marcel Dekker; 2005:359-378.
87. Levine D, Rockey DC, Milner TA, Breuss JM, Fallon JT, Schnapp LM. Expression of the integrin alpha8beta1 during pulmonary and hepatic fibrosis. *Am J Pathol.* 2000;**156**(6):1927-1935.
88. Xia H, Diebold D, Nho R, Perlman D, Kleidon J, Kahm J, Avdulov S, Peterson M, Nerva J, Bitterman P, Henke C. Pathological integrin signaling enhances proliferation of primary lung fibroblasts from patients with idiopathic pulmonary fibrosis. *J Exp Med.* 2008;**205**(7):1659-1672.
89. Kim KK, Wei Y, Szekeres C, Kugler MC, Wolters PJ, Hill ML, Frank JA, Brumwell AN, Wheeler SE, Kreidberg JA, Chapman HA. Epithelial cell alpha3beta1 integrin links beta-catenin and Smad signaling to promote myofibroblast formation and pulmonary fibrosis. *J Clin Invest.* 2009;**119**(1):213-224.

90. Sheppard D. Integrin-mediated activation of transforming growth factor-beta(1) in pulmonary fibrosis. *Chest*. 2001;**120**(1 Suppl):49S-53S.
91. Wang Q, Wang Y, Hyde DM, Gotwals PJ, Lobb RR, Ryan ST, Giri SN. Effect of antibody against integrin alpha4 on bleomycin-induced pulmonary fibrosis in mice. *Biochem Pharmacol*. 2000;**60**(12):1949-1958.
92. Horan GS, Wood S, Ona V, Li DJ, Lukashev ME, Weinreb PH, Simon KJ, Hahm K, Allaire NE, Rinaldi NJ, Goyal J, Feghali-Bostwick CA, Matteson EL, O'Hara C, Lafyatis R, Davis GS, Huang X, Sheppard D, Violette SM. Partial inhibition of integrin alpha(v)beta6 prevents pulmonary fibrosis without exacerbating inflammation. *Am J Respir Crit Care Med*. 2008;**177**(1):56-65.
93. Munger JS, Huang X, Kawakatsu H, Griffiths MJ, Dalton SL, Wu J, Pittet JF, Kaminski N, Garat C, Matthay MA, Rifkin DB, Sheppard D. The integrin alpha v beta 6 binds and activates latent TGF beta 1: a mechanism for regulating pulmonary inflammation and fibrosis. *Cell*. 1999;**96**(3):319-328.
94. Rudd RM, Haslam PL, Turner-Warwick M. Cryptogenic fibrosing alveolitis. Relationships of pulmonary physiology and bronchoalveolar lavage to response to treatment and prognosis. *Am Rev Respir Dis*. 1981;**124**(1):1-8.
95. Boomars KA, Wagenaar SS, Mulder PG, van Velzen-Blad H, van den Bosch JM. Relationship between cells obtained by bronchoalveolar lavage and survival in idiopathic pulmonary fibrosis. *Thorax*. 1995;**50**(10):1087-1092.
96. Bergeron A, Soler P, Kambouchner M, Loiseau P, Milleron B, Valeyre D, Hance AJ, Tazi A. Cytokine profiles in idiopathic pulmonary fibrosis suggest an important role for TGF-beta and IL-10. *Eur Respir J*. 2003;**22**(1):69-76.
97. Waghray M, Cui Z, Horowitz JC, Subramanian IM, Martinez FJ, Toews GB, Thannickal VJ. Hydrogen peroxide is a diffusible paracrine signal for the induction of epithelial cell death by activated myofibroblasts. *FASEB J*. 2005;**19**(7):854-856.
98. Obayashi Y, Yamadori I, Fujita J, Yoshinouchi T, Ueda N, Takahara J. The role of neutrophils in the pathogenesis of idiopathic pulmonary fibrosis. *Chest*. 1997;**112**(5):1338-1343.
99. Ozaki T, Hayashi H, Tani K, Ogushi F, Yasuoka S, Ogura T. Neutrophil chemotactic factors in the respiratory tract of patients with chronic airway diseases or idiopathic pulmonary fibrosis. *The American review of respiratory disease*. 1992;**145**(1):85-91.
100. Khalil N, O'Connor RN, Flanders KC, Unruh H. TGF-beta 1, but not TGF-beta 2 or TGF-beta 3, is differentially present in epithelial cells of advanced pulmonary fibrosis: an immunohistochemical study. *Am J Respir Cell Mol Biol*. 1996;**14**(2):131-138.
101. Li H, He B, Que C, Weng B. Expression of TGF-beta 1, PDGF and IGF-1 mRNA in lung of bleomycin-A5-induced pulmonary fibrosis in rats. *Chin Med J (Engl)*. 1996;**109**(7):533-536.
102. Xu YD, Hua J, Mui A, O'Connor R, Grotendorst G, Khalil N. Release of biologically active TGF-beta1 by alveolar epithelial cells results in pulmonary fibrosis. *Am J Physiol Lung Cell Mol Physiol*. 2003;**285**(3):L527-539.
103. Zhao Y, Geverd DA. Regulation of Smad3 expression in bleomycin-induced pulmonary fibrosis: a negative feedback loop of TGF-beta signaling. *Biochem Biophys Res Commun*. 2002;**294**(2):319-323.

104. Song M, He B, Qiu Z. [Expressions of TNF alpha, PDGF in alveolar type II epithelial cells of rats with bleomycin-induced pulmonary fibrosis]. *Zhonghua Jie He He Hu Xi Za Zhi*. 1998;**21**(4):221-223.
105. Antoniadou HN, Bravo MA, Avila RE, Galanopoulos T, Neville-Golden J, Maxwell M, Selman M. Platelet-derived growth factor in idiopathic pulmonary fibrosis. *J Clin Invest*. 1990;**86**(4):1055-1064.
106. Zhang K, Gharaee-Kermani M, McGarry B, Remick D, Phan SH. TNF-alpha-mediated lung cytokine networking and eosinophil recruitment in pulmonary fibrosis. *J Immunol*. 1997;**158**(2):954-959.
107. Gauldie J, Sime PJ, Xing Z, Marr B, Tremblay GM. Transforming growth factor-beta gene transfer to the lung induces myofibroblast presence and pulmonary fibrosis. *Curr Top Pathol*. 1999;**93**:35-45.
108. Mangan PR, Harrington LE, O'Quinn DB, Helms WS, Bullard DC, Elson CO, Hatton RD, Wahl SM, Schoeb TR, Weaver CT. Transforming growth factor-beta induces development of the T(H)17 lineage. *Nature*. 2006;**441**(7090):231-234.
109. Tsunawaki S, Sporn M, Ding A, Nathan C. Deactivation of macrophages by transforming growth factor-beta. *Nature*. 1988;**334**(6179):260-262.
110. Venkatesan N, Pini L, Ludwig MS. Changes in Smad expression and subcellular localization in bleomycin-induced pulmonary fibrosis. *Am J Physiol Lung Cell Mol Physiol*. 2004;**287**(6):L1342-1347.
111. Bonniaud P, Kolb M, Galt T, Robertson J, Robbins C, Stampfli M, Lavery C, Margetts PJ, Roberts AB, Gauldie J. Smad3 null mice develop airspace enlargement and are resistant to TGF-beta-mediated pulmonary fibrosis. *J Immunol*. 2004;**173**(3):2099-2108.
112. Ouellet S, Yang H, Aubin RA, Hawley RG, Wenckebach GF, Lemaire I. Bidirectional modulation of TNF-alpha production by alveolar macrophages in asbestos-induced pulmonary fibrosis. *J Leukoc Biol*. 1993;**53**(3):279-286.
113. Piguet PF, Collart MA, Grau GE, Kapanci Y, Vassalli P. Tumor necrosis factor/cachectin plays a key role in bleomycin-induced pneumopathy and fibrosis. *J Exp Med*. 1989;**170**(3):655-663.
114. Miyazaki Y, Araki K, Vesin C, Garcia I, Kapanci Y, Whitsett JA, Piguet PF, Vassalli P. Expression of a tumor necrosis factor-alpha transgene in murine lung causes lymphocytic and fibrosing alveolitis. A mouse model of progressive pulmonary fibrosis. *J Clin Invest*. 1995;**96**(1):250-259.
115. Cheng N, Shi X, Ye J, Castranova V, Chen F, Leonard SS, Vallyathan V, Rojanasakul Y. Role of transcription factor NF-kappaB in asbestos-induced TNFalpha response from macrophages. *Exp Mol Pathol*. 1999;**66**(3):201-210.
116. Kuhn C, 3rd, Boldt J, King TE, Jr., Crouch E, Vartio T, McDonald JA. An immunohistochemical study of architectural remodeling and connective tissue synthesis in pulmonary fibrosis. *Am Rev Respir Dis*. 1989;**140**(6):1693-1703.
117. Kuhn C, McDonald JA. The roles of the myofibroblast in idiopathic pulmonary fibrosis. Ultrastructural and immunohistochemical features of sites of active extracellular matrix synthesis. *Am J Pathol*. 1991;**138**(5):1257-1265.
118. Phan SH. The myofibroblast in pulmonary fibrosis. *Chest*. 2002;**122**(6 Suppl):286S-289S.

119. Uhal BD, Joshi I, True AL, Mundle S, Raza A, Pardo A, Selman M. Fibroblasts isolated after fibrotic lung injury induce apoptosis of alveolar epithelial cells in vitro. *Am J Physiol*. 1995;**269**(6 Pt 1):L819-828.
120. Wu Z, Yang L, Cai L, Zhang M, Cheng X, Yang X, Xu J. Detection of epithelial to mesenchymal transition in airways of a bleomycin induced pulmonary fibrosis model derived from an alpha-smooth muscle actin-Cre transgenic mouse. *Respir Res*. 2007;**8**:1.
121. Kasai H, Allen JT, Mason RM, Kamimura T, Zhang Z. TGF-beta1 induces human alveolar epithelial to mesenchymal cell transition (EMT). *Respir Res*. 2005;**6**:56.
122. Spees JL, Pociask DA, Sullivan DE, Whitney MJ, Lasky JA, Prockop DJ, Brody AR. Engraftment of bone marrow progenitor cells in a rat model of asbestos-induced pulmonary fibrosis. *Am J Respir Crit Care Med*. 2007;**176**(4):385-394.
123. Tan RJ, Fattman CL, Niehouse LM, Tobolewski JM, Hanford LE, Li Q, Monzon FA, Parks WC, Oury TD. Matrix metalloproteinases promote inflammation and fibrosis in asbestos-induced lung injury in mice. *American journal of respiratory cell and molecular biology*. 2006;**35**(3):289-297.
124. Yaguchi T, Fukuda Y, Ishizaki M, Yamanaka N. Immunohistochemical and gelatin zymography studies for matrix metalloproteinases in bleomycin-induced pulmonary fibrosis. *Pathol Int*. 1998;**48**(12):954-963.
125. Selman M, Pardo A. Matrix Metalloproteinases and Tissue Inhibitors. In: Lynch JP, ed. *Lung Biology in Health and Disease: Idiopathic Pulmonary Fibrosis*. Vol 185. New York: Marcel Dekker, Inc.; 2004:451-480.
126. Kinnula VL, Fattman CL, Tan RJ, Oury TD. Oxidative stress in pulmonary fibrosis: a possible role for redox modulatory therapy. *American journal of respiratory and critical care medicine*. 2005;**172**(4):417-422.
127. Fu X, Kassim SY, Parks WC, Heinecke JW. Hypochlorous acid generated by myeloperoxidase modifies adjacent tryptophan and glycine residues in the catalytic domain of matrix metalloproteinase-7 (matrilysin): an oxidative mechanism for restraining proteolytic activity during inflammation. *J Biol Chem*. 2003;**278**(31):28403-28409.
128. Nelson KK, Melendez JA. Mitochondrial redox control of matrix metalloproteinases. *Free Radic Biol Med*. 2004;**37**(6):768-784.
129. Hayashi T, Stetler-Stevenson WG, Fleming MV, Fishback N, Koss MN, Liotta LA, Ferrans VJ, Travis WD. Immunohistochemical study of metalloproteinases and their tissue inhibitors in the lungs of patients with diffuse alveolar damage and idiopathic pulmonary fibrosis. *Am J Pathol*. 1996;**149**(4):1241-1256.
130. McKeown S, Richter AG, O'Kane C, McAuley DF, Thickett DR. MMP expression and abnormal lung permeability are important determinants of outcome in IPF. *Eur Respir J*. 2009;**33**(1):77-84.
131. Rosas IO, Richards TJ, Konishi K, Zhang Y, Gibson K, Lokshin AE, Lindell KO, Cisneros J, Macdonald SD, Pardo A, Sciruba F, Dauber J, Selman M, Gochoico BR, Kaminski N. MMP1 and MMP7 as potential peripheral blood biomarkers in idiopathic pulmonary fibrosis. *PLoS Med*. 2008;**5**(4):e93.
132. Zuo F, Kaminski N, Eugui E, Allard J, Yakhini Z, Ben-Dor A, Lollini L, Morris D, Kim Y, DeLustro B, Sheppard D, Pardo A, Selman M, Heller RA. Gene expression analysis reveals matrilysin as a key regulator of pulmonary fibrosis in mice and humans. *Proc Natl Acad Sci U S A*. 2002;**99**(9):6292-6297.

133. Cabrera S, Gaxiola M, Arreola JL, Ramirez R, Jara P, D'Armiento J, Richards T, Selman M, Pardo A. Overexpression of MMP9 in macrophages attenuates pulmonary fibrosis induced by bleomycin. *Int J Biochem Cell Biol.* 2007;**39**(12):2324-2338.
134. Kukin ML, Fuster V. *Oxidative stress and cardiac failure.* Armonk, NY: Futura Pub.; 2003.
135. Richardson P, McKenna W, Bristow M, Maisch B, Mautner B, O'Connell J, Olsen E, Thiene G, Goodwin J, Gyarsfas I, Martin I, Nordet P. Report of the 1995 World Health Organization/International Society and Federation of Cardiology Task Force on the Definition and Classification of cardiomyopathies. *Circulation.* 1996;**93**(5):841-842.
136. Singal PK, Iliskovic N. Doxorubicin-induced cardiomyopathy. *N Engl J Med.* 1998;**339**(13):900-905.
137. Swain SM, Whaley FS, Ewer MS. Congestive heart failure in patients treated with doxorubicin: a retrospective analysis of three trials. *Cancer.* 2003;**97**(11):2869-2879.
138. Kalyanaraman B, Joseph J, Kalivendi S, Wang S, Konorev E, Kotamraju S. Doxorubicin-induced apoptosis: implications in cardiotoxicity. *Mol Cell Biochem.* 2002;**234-235**(1-2):119-124.
139. Singal PK, Li T, Kumar D, Danelisen I, Iliskovic N. Adriamycin-induced heart failure: mechanism and modulation. *Mol Cell Biochem.* 2000;**207**(1-2):77-86.
140. Lefrak EA, Pitha J, Rosenheim S, Gottlieb JA. A clinicopathologic analysis of adriamycin cardiotoxicity. *Cancer.* 1973;**32**(2):302-314.
141. Kaiserova H, Simunek T, van der Vijgh WJ, Bast A, Kvasnickova E. Flavonoids as protectors against doxorubicin cardiotoxicity: role of iron chelation, antioxidant activity and inhibition of carbonyl reductase. *Biochim Biophys Acta.* 2007;**1772**(9):1065-1074.
142. Santos RV, Batista ML, Jr., Caperuto EC, Costa Rosa LF. Chronic supplementation of creatine and vitamins C and E increases survival and improves biochemical parameters after Doxorubicin treatment in rats. *Clin Exp Pharmacol Physiol.* 2007;**34**(12):1294-1299.
143. Singal PK, Iliskovic N, Li T, Kumar D. Adriamycin cardiomyopathy: pathophysiology and prevention. *FASEB J.* 1997;**11**(12):931-936.
144. Doroshov JH, Locker GY, Baldinger J, Myers CE. The effect of doxorubicin on hepatic and cardiac glutathione. *Res Commun Chem Pathol Pharmacol.* 1979;**26**(2):285-295.
145. Kalivendi SV, Kotamraju S, Zhao H, Joseph J, Kalyanaraman B. Doxorubicin-induced apoptosis is associated with increased transcription of endothelial nitric-oxide synthase. Effect of antiapoptotic antioxidants and calcium. *J Biol Chem.* 2001;**276**(50):47266-47276.
146. Wang S, Konorev EA, Kotamraju S, Joseph J, Kalivendi S, Kalyanaraman B. Doxorubicin induces apoptosis in normal and tumor cells via distinctly different mechanisms. Intermediacy of H(2)O(2)- and p53-dependent pathways. *J Biol Chem.* 2004;**279**(24):25535-25543.
147. Bernuzzi F, Recalcati S, Alberghini A, Cairo G. Reactive oxygen species-independent apoptosis in doxorubicin-treated H9c2 cardiomyocytes: role for heme oxygenase-1 down-modulation. *Chem Biol Interact.* 2009;**177**(1):12-20.
148. Winyard PG, Blake DR, Evans CH. *Free radicals and inflammation.* Basel ; Boston: Birkhäuser Verlag; 2000.
149. Kinnula VL, Crapo JD. Superoxide dismutases in the lung and human lung diseases. *American journal of respiratory and critical care medicine.* 2003;**167**(12):1600-1619.

150. Kinnula VL. Oxidant and antioxidant mechanisms of lung disease caused by asbestos fibres. *Eur Respir J*. 1999;**14**(3):706-716.
151. Petersen SV, Oury TD, Ostergaard L, Valnickova Z, Wegrzyn J, Thogersen IB, Jacobsen C, Bowler RP, Fattman CL, Crapo JD, Enghild JJ. Extracellular superoxide dismutase (EC-SOD) binds to type I collagen and protects against oxidative fragmentation. *The Journal of biological chemistry*. 2004;**279**(14):13705-13710.
152. Chambers DE, Parks DA, Patterson G, Roy R, McCord JM, Yoshida S, Parmley LF, Downey JM. Xanthine oxidase as a source of free radical damage in myocardial ischemia. *J Mol Cell Cardiol*. 1985;**17**(2):145-152.
153. McCord JM, Roy RS, Schaffer SW. Free radicals and myocardial ischemia. The role of xanthine oxidase. *Adv Myocardiol*. 1985;**5**:183-189.
154. Patt A, Harken AH, Burton LK, Rodell TC, Piermattei D, Schorr WJ, Parker NB, Berger EM, Horesh IR, Terada LS, et al. Xanthine oxidase-derived hydrogen peroxide contributes to ischemia reperfusion-induced edema in gerbil brains. *The Journal of clinical investigation*. 1988;**81**(5):1556-1562.
155. Ghio AJ, Kennedy TP, Stonehuerner J, Carter JD, Skinner KA, Parks DA, Hoidal JR. Iron regulates xanthine oxidase activity in the lung. *American journal of physiology*. 2002;**283**(3):L563-572.
156. Lynch MJ, Grum CM, Gallagher KP, Bolling SF, Deeb GM, Morganroth ML. Xanthine oxidase inhibition attenuates ischemic-reperfusion lung injury. *J Surg Res*. 1988;**44**(5):538-544.
157. Terada LS, Dormish JJ, Shanley PF, Leff JA, Anderson BO, Repine JE. Circulating xanthine oxidase mediates lung neutrophil sequestration after intestinal ischemia-reperfusion. *Am J Physiol*. 1992;**263**(3 Pt 1):L394-401.
158. Dahlgren C, Karlsson A. Respiratory burst in human neutrophils. *J Immunol Methods*. 1999;**232**(1-2):3-14.
159. Swain SD, Rohn TT, Quinn MT. Neutrophil priming in host defense: role of oxidants as priming agents. *Antioxidants & redox signaling*. 2002;**4**(1):69-83.
160. Derevianko A, D'Amico R, Graeber T, Keeping H, Simms HH. Endogenous PMN-derived reactive oxygen intermediates provide feedback regulation on respiratory burst signal transduction. *J Leukoc Biol*. 1997;**62**(2):268-276.
161. Hawkins CL, Rees MD, Davies MJ. Superoxide radicals can act synergistically with hypochlorite to induce damage to proteins. *FEBS Lett*. 2002;**510**(1-2):41-44.
162. Woods AA, Linton SM, Davies MJ. Detection of HOCl-mediated protein oxidation products in the extracellular matrix of human atherosclerotic plaques. *Biochem J*. 2003;**370**(Pt 2):729-735.
163. Hawkins CL, Davies MJ. Degradation of hyaluronic acid, poly- and monosaccharides, and model compounds by hypochlorite: evidence for radical intermediates and fragmentation. *Free Radic Biol Med*. 1998;**24**(9):1396-1410.
164. Rees MD, Hawkins CL, Davies MJ. Hypochlorite and superoxide radicals can act synergistically to induce fragmentation of hyaluronan and chondroitin sulphates. *Biochem J*. 2004;**381**(Pt 1):175-184.
165. Rees MD, Pattison DI, Davies MJ. Oxidation of heparan sulphate by hypochlorite: role of N-chloro derivatives and dichloramine-dependent fragmentation. *Biochem J*. 2005;**391**(Pt 1):125-134.

166. Eiserich JP, Baldus S, Brennan ML, Ma W, Zhang C, Tousson A, Castro L, Lusis AJ, Nauseef WM, White CR, Freeman BA. Myeloperoxidase, a leukocyte-derived vascular NO oxidase. *Science*. 2002;**296**(5577):2391-2394.
167. Bruckdorfer R. The basics about nitric oxide. *Mol Aspects Med*. 2005;**26**(1-2):3-31.
168. Hsu YC, Wang LF, Chien YW. Nitric oxide in the pathogenesis of diffuse pulmonary fibrosis. *Free Radic Biol Med*. 2007;**42**(5):599-607.
169. Zeidler P, Hubbs A, Battelli L, Castranova V. Role of inducible nitric oxide synthase-derived nitric oxide in silica-induced pulmonary inflammation and fibrosis. *J Toxicol Environ Health A*. 2004;**67**(13):1001-1026.
170. Aldieri E, Bergandi L, Riganti C, Costamagna C, Bosia A, Ghigo D. Doxorubicin induces an increase of nitric oxide synthesis in rat cardiac cells that is inhibited by iron supplementation. *Toxicol Appl Pharmacol*. 2002;**185**(2):85-90.
171. Sayed-Ahmed MM, Khattab MM, Gad MZ, Osman AM. Increased plasma endothelin-1 and cardiac nitric oxide during doxorubicin-induced cardiomyopathy. *Pharmacol Toxicol*. 2001;**89**(3):140-144.
172. Pfeilschifter J, Eberhardt W, Beck KF. Regulation of gene expression by nitric oxide. *Pflugers Arch*. 2001;**442**(4):479-486.
173. Qin Z, Reszka KJ, Fukai T, Weintraub NL. Extracellular superoxide dismutase (ecSOD) in vascular biology: an update on exogenous gene transfer and endogenous regulators of ecSOD. *Transl Res*. 2008;**151**(2):68-78.
174. Zelko IN, Mariani TJ, Folz RJ. Superoxide dismutase multigene family: a comparison of the CuZn-SOD (SOD1), Mn-SOD (SOD2), and EC-SOD (SOD3) gene structures, evolution, and expression. *Free radical biology & medicine*. 2002;**33**(3):337-349.
175. Rees MD, Kennett EC, Whitelock JM, Davies MJ. Oxidative damage to extracellular matrix and its role in human pathologies. *Free Radic Biol Med*. 2008;**44**(12):1973-2001.
176. Psathakis K, Mermigkis D, Papatheodorou G, Loukides S, Panagou P, Polychronopoulos V, Siafakas NM, Bouros D. Exhaled markers of oxidative stress in idiopathic pulmonary fibrosis. *European journal of clinical investigation*. 2006;**36**(5):362-367.
177. Chen EP, Bittner HB, Davis RD, Folz RJ, Van Trigt P. Extracellular superoxide dismutase transgene overexpression preserves postischemic myocardial function in isolated murine hearts. *Circulation*. 1996;**94**(9 Suppl):II412-417.
178. Chu CT. Eaten alive: autophagy and neuronal cell death after hypoxia-ischemia. *Am J Pathol*. 2008;**172**(2):284-287.
179. Dias-Santagata D, Fulga TA, Duttaroy A, Feany MB. Oxidative stress mediates tau-induced neurodegeneration in Drosophila. *J Clin Invest*. 2007;**117**(1):236-245.
180. Droge W, Schipper HM. Oxidative stress and aberrant signaling in aging and cognitive decline. *Aging Cell*. 2007;**6**(3):361-370.
181. Levine RL, Stadtman ER. Oxidative modification of proteins during aging. *Exp Gerontol*. 2001;**36**(9):1495-1502.
182. Marmol F, Sanchez J, Lopez D, Martinez N, Rosello-Catafau J, Mitjavila MT, Puig-Parellada P. Loss of adaptation to oxidative stress as a mechanism for aortic damage in aging rats. *J Physiol Biochem*. 2007;**63**(3):239-247.
183. Montuschi P, Ciabattoni G, Paredi P, Pantelidis P, du Bois RM, Kharitonov SA, Barnes PJ. 8-Isoprostane as a biomarker of oxidative stress in interstitial lung diseases. *American journal of respiratory and critical care medicine*. 1998;**158**(5 Pt 1):1524-1527.

184. Cantin AM, Hubbard RC, Crystal RG. Glutathione deficiency in the epithelial lining fluid of the lower respiratory tract in idiopathic pulmonary fibrosis. *The American review of respiratory disease*. 1989;**139**(2):370-372.
185. Bowler RP, Crapo JD. Oxidative stress in airways: is there a role for extracellular superoxide dismutase? *American journal of respiratory and critical care medicine*. 2002;**166**(12 Pt 2):S38-43.
186. Gao F, Koenitzer JR, Tobolewski JM, Jiang D, Liang J, Noble PW, Oury TD. Extracellular superoxide dismutase inhibits inflammation by preventing oxidative fragmentation of hyaluronan. *The Journal of biological chemistry*. 2008;**283**(10):6058-6066.
187. Harris RN, Doroshov JH. Effect of doxorubicin-enhanced hydrogen peroxide and hydroxyl radical formation on calcium sequestration by cardiac sarcoplasmic reticulum. *Biochem Biophys Res Commun*. 1985;**130**(2):739-745.
188. Kalyanaraman B, Perez-Reyes E, Mason RP. Spin-trapping and direct electron spin resonance investigations of the redox metabolism of quinone anticancer drugs. *Biochim Biophys Acta*. 1980;**630**(1):119-130.
189. Qin F, Shite J, Liang CS. Antioxidants attenuate myocyte apoptosis and improve cardiac function in CHF: association with changes in MAPK pathways. *Am J Physiol Heart Circ Physiol*. 2003;**285**(2):H822-832.
190. Konorev EA, Kennedy MC, Kalyanaraman B. Cell-permeable superoxide dismutase and glutathione peroxidase mimetics afford superior protection against doxorubicin-induced cardiotoxicity: the role of reactive oxygen and nitrogen intermediates. *Arch Biochem Biophys*. 1999;**368**(2):421-428.
191. Behr J. Oxidants and Antioxidants in Idiopathic Pulmonary Fibrosis. In: Lynch JP, ed. *Idiopathic Pulmonary Fibrosis: Lung Biology in Health and Disease*. Vol 185. First ed. New York: Marcel Dekker; 2005:379-396.
192. Murrell GA, Francis MJ, Bromley L. Modulation of fibroblast proliferation by oxygen free radicals. *Biochem J*. 1990;**265**(3):659-665.
193. McCord JM, Fridovich I. The reduction of cytochrome c by milk xanthine oxidase. *The Journal of biological chemistry*. 1968;**243**(21):5753-5760.
194. McCord JM, Fridovich I. Superoxide dismutase. An enzymic function for erythrocyte (hemocuprein). *The Journal of biological chemistry*. 1969;**244**(22):6049-6055.
195. Marklund SL. Human copper-containing superoxide dismutase of high molecular weight. *Proceedings of the National Academy of Sciences of the United States of America*. 1982;**79**(24):7634-7638.
196. Marklund SL, Holme E, Hellner L. Superoxide dismutase in extracellular fluids. *Clin Chim Acta*. 1982;**126**(1):41-51.
197. Fattman CL, Schaefer LM, Oury TD. Extracellular superoxide dismutase in biology and medicine. *Free radical biology & medicine*. 2003;**35**(3):236-256.
198. Nozik-Grayck E, Suliman HB, Piantadosi CA. Extracellular superoxide dismutase. *The international journal of biochemistry & cell biology*. 2005;**37**(12):2466-2471.
199. Fattman CL, Enghild JJ, Crapo JD, Schaefer LM, Valnickova Z, Oury TD. Purification and characterization of extracellular superoxide dismutase in mouse lung. *Biochemical and biophysical research communications*. 2000;**275**(2):542-548.
200. Oury TD, Crapo JD, Valnickova Z, Enghild JJ. Human extracellular superoxide dismutase is a tetramer composed of two disulphide-linked dimers: a simplified, high-

- yield purification of extracellular superoxide dismutase. *The Biochemical journal*. 1996;**317** (Pt 1):51-57.
201. Petersen SV, Oury TD, Valnickova Z, Thogersen IB, Hojrup P, Crapo JD, Enghild JJ. The dual nature of human extracellular superoxide dismutase: one sequence and two structures. *Proceedings of the National Academy of Sciences of the United States of America*. 2003;**100**(24):13875-13880.
 202. Tainer JA, Getzoff ED, Beem KM, Richardson JS, Richardson DC. Determination and analysis of the 2 A-structure of copper, zinc superoxide dismutase. *J Mol Biol*. 1982;**160**(2):181-217.
 203. Due AV, Petersen SV, Valnickova Z, Ostergaard L, Oury TD, Crapo JD, Enghild JJ. Extracellular superoxide dismutase exists as an octamer. *FEBS Lett*. 2006;**580**(5):1485-1489.
 204. Adachi T, Kodera T, Ohta H, Hayashi K, Hirano K. The heparin binding site of human extracellular-superoxide dismutase. *Archives of biochemistry and biophysics*. 1992;**297**(1):155-161.
 205. Adachi T, Yamnamoto M, Hara H. Heparin-Affinity of human extracellular-superoxide dismutase in the brain. *Biological & pharmaceutical bulletin*. 2001;**24**(2):191-193.
 206. Karlsson K, Lindahl U, Marklund SL. Binding of human extracellular superoxide dismutase C to sulphated glycosaminoglycans. *The Biochemical journal*. 1988;**256**(1):29-33.
 207. Karlsson K, Marklund SL. Extracellular-superoxide dismutase association with cell surface-bound sulfated glucosaminoglycans. *Basic life sciences*. 1988;**49**:647-650.
 208. Adachi T, Yamada H, Yamada Y, Morihara N, Yamazaki N, Murakami T, Futenma A, Kato K, Hirano K. Substitution of glycine for arginine-213 in extracellular-superoxide dismutase impairs affinity for heparin and endothelial cell surface. *Biochem J*. 1996;**313** (Pt 1):235-239.
 209. Adachi T, Yamazaki N, Tasaki H, Toyokawa T, Yamashita K, Hirano K. Changes in the heparin affinity of extracellular-superoxide dismutase in patients with coronary artery atherosclerosis. *Biol Pharm Bull*. 1998;**21**(10):1090-1093.
 210. Folz RJ, Peno-Green L, Crapo JD. Identification of a homozygous missense mutation (Arg to Gly) in the critical binding region of the human EC-SOD gene (SOD3) and its association with dramatically increased serum enzyme levels. *Hum Mol Genet*. 1994;**3**(12):2251-2254.
 211. Adachi T, Ohta H, Yamada H, Futenma A, Kato K, Hirano K. Quantitative analysis of extracellular-superoxide dismutase in serum and urine by ELISA with monoclonal antibody. *Clin Chim Acta*. 1992;**212**(3):89-102.
 212. Sandstrom J, Nilsson P, Karlsson K, Marklund SL. 10-fold increase in human plasma extracellular superoxide dismutase content caused by a mutation in heparin-binding domain. *J Biol Chem*. 1994;**269**(29):19163-19166.
 213. Juul K, Tybjaerg-Hansen A, Marklund S, Heegaard NH, Steffensen R, Sillesen H, Jensen G, Nordestgaard BG. Genetically reduced antioxidative protection and increased ischemic heart disease risk: The Copenhagen City Heart Study. *Circulation*. 2004;**109**(1):59-65.
 214. Brady TC, Chang LY, Day BJ, Crapo JD. Extracellular superoxide dismutase is upregulated with inducible nitric oxide synthase after NF-kappa B activation. *Am J Physiol*. 1997;**273**(5 Pt 1):L1002-1006.

215. Stralin P, Marklund SL. Vasoactive factors and growth factors alter vascular smooth muscle cell EC-SOD expression. *Am J Physiol Heart Circ Physiol*. 2001;**281**(4):H1621-1629.
216. Marklund SL. Regulation by cytokines of extracellular superoxide dismutase and other superoxide dismutase isoenzymes in fibroblasts. *The Journal of biological chemistry*. 1992;**267**(10):6696-6701.
217. Marklund SL. Extracellular superoxide dismutase in human tissues and human cell lines. *The Journal of clinical investigation*. 1984;**74**(4):1398-1403.
218. Marklund SL. Properties of extracellular superoxide dismutase from human lung. *The Biochemical journal*. 1984;**220**(1):269-272.
219. Sandstrom J, Karlsson K, Edlund T, Marklund SL. Heparin-affinity patterns and composition of extracellular superoxide dismutase in human plasma and tissues. *The Biochemical journal*. 1993;**294** (Pt 3):853-857.
220. Karlsson K, Marklund SL. Extracellular superoxide dismutase in the vascular system of mammals. *The Biochemical journal*. 1988;**255**(1):223-228.
221. Karlsson K, Sandstrom J, Edlund A, Marklund SL. Turnover of extracellular-superoxide dismutase in tissues. *Laboratory investigation; a journal of technical methods and pathology*. 1994;**70**(5):705-710.
222. Adachi T, Ohta H, Hayashi K, Hirano K, Marklund SL. The site of nonenzymic glycation of human extracellular-superoxide dismutase in vitro. *Free radical biology & medicine*. 1992;**13**(3):205-210.
223. Oury TD, Chang LY, Marklund SL, Day BJ, Crapo JD. Immunocytochemical localization of extracellular superoxide dismutase in human lung. *Laboratory investigation; a journal of technical methods and pathology*. 1994;**70**(6):889-898.
224. Oury TD, Day BJ, Crapo JD. Extracellular superoxide dismutase in vessels and airways of humans and baboons. *Free radical biology & medicine*. 1996;**20**(7):957-965.
225. Loenders B, Van Mechelen E, Nicolai S, Buysens N, Van Osselaer N, Jorens PG, Willems J, Herman AG, Slegers H. Localization of extracellular superoxide dismutase in rat lung: neutrophils and macrophages as carriers of the enzyme. *Free radical biology & medicine*. 1998;**24**(7-8):1097-1106.
226. Tan RJ, Lee JS, Manni ML, Fattman CL, Tobolewski JM, Zheng M, Kolls JK, Martin TR, Oury TD. Inflammatory cells as a source of airspace extracellular superoxide dismutase after pulmonary injury. *American journal of respiratory cell and molecular biology*. 2006;**34**(2):226-232.
227. Bowler RP, Arcaroli J, Abraham E, Patel M, Chang LY, Crapo JD. Evidence for extracellular superoxide dismutase as a mediator of hemorrhage-induced lung injury. *American journal of physiology*. 2003;**284**(4):L680-687.
228. Bowler RP, Nicks M, Tran K, Tanner G, Chang LY, Young SK, Worthen GS. Extracellular superoxide dismutase attenuates lipopolysaccharide-induced neutrophilic inflammation. *American journal of respiratory cell and molecular biology*. 2004;**31**(4):432-439.
229. Lu Z, Xu X, Hu X, Zhu G, Zhang P, van Deel ED, French JP, Fassett JT, Oury TD, Bache RJ, Chen Y. Extracellular superoxide dismutase deficiency exacerbates pressure overload-induced left ventricular hypertrophy and dysfunction. *Hypertension*. 2008;**51**(1):19-25.

230. Sharma S, Dewald O, Adroque J, Salazar RL, Razeghi P, Crapo JD, Bowler RP, Entman ML, Taegtmeier H. Induction of antioxidant gene expression in a mouse model of ischemic cardiomyopathy is dependent on reactive oxygen species. *Free Radic Biol Med.* 2006;**40**(12):2223-2231.
231. van Deel ED, Lu Z, Xu X, Zhu G, Hu X, Oury TD, Bache RJ, Duncker DJ, Chen Y. Extracellular superoxide dismutase protects the heart against oxidative stress and hypertrophy after myocardial infarction. *Free Radic Biol Med.* 2008;**44**(7):1305-1313.
232. Chu Y, Alwahdani A, Iida S, Lund DD, Faraci FM, Heistad DD. Vascular effects of the human extracellular superoxide dismutase R213G variant. *Circulation.* 2005;**112**(7):1047-1053.
233. Iida S, Chu Y, Weiss RM, Kang YM, Faraci FM, Heistad DD. Vascular effects of a common gene variant of extracellular superoxide dismutase in heart failure. *Am J Physiol Heart Circ Physiol.* 2006;**291**(2):H914-920.
234. Petersen SV, Olsen DA, Kenney JM, Oury TD, Valnickova Z, Thogersen IB, Crapo JD, Enghild JJ. The high concentration of Arg213-->Gly extracellular superoxide dismutase (EC-SOD) in plasma is caused by a reduction of both heparin and collagen affinities. *Biochem J.* 2005;**385**(Pt 2):427-432.
235. Dewald O, Frangogiannis NG, Zoerlein M, Duerr GD, Klemm C, Knuefermann P, Taffet G, Michael LH, Crapo JD, Welz A, Entman ML. Development of murine ischemic cardiomyopathy is associated with a transient inflammatory reaction and depends on reactive oxygen species. *Proc Natl Acad Sci U S A.* 2003;**100**(5):2700-2705.
236. Landmesser U, Merten R, Spiekermann S, Buttner K, Drexler H, Hornig B. Vascular extracellular superoxide dismutase activity in patients with coronary artery disease: relation to endothelium-dependent vasodilation. *Circulation.* 2000;**101**(19):2264-2270.
237. Laurila JP, Castellone MD, Curcio A, Laatikainen LE, Haaparanta-Solin M, Gronroos TJ, Marjamaki P, Martikainen S, Santoro M, Laukkanen MO. Extracellular Superoxide Dismutase Is a Growth Regulatory Mediator of Tissue Injury Recovery. *Mol Ther.* 2008.
238. Varki A, Chrispeels MJ. *Essentials of glycobiology.* Cold Spring Harbor, N.Y.: Cold Spring Harbor Laboratory Press; 1999.
239. Bernfield M, Gotte M, Park PW, Reizes O, Fitzgerald ML, Lincecum J, Zako M. Functions of cell surface heparan sulfate proteoglycans. *Annual review of biochemistry.* 1999;**68**:729-777.
240. Wang L, Fuster M, Sriramarao P, Esko JD. Endothelial heparan sulfate deficiency impairs L-selectin- and chemokine-mediated neutrophil trafficking during inflammatory responses. *Nature immunology.* 2005;**6**(9):902-910.
241. Gotte M. Syndecans in inflammation. *FASEB J.* 2003;**17**(6):575-591.
242. Bernfield M, Kokenyesi R, Kato M, Hinkes MT, Spring J, Gallo RL, Lose EJ. Biology of the syndecans: a family of transmembrane heparan sulfate proteoglycans. *Annual review of cell biology.* 1992;**8**:365-393.
243. Taylor KR, Gallo RL. Glycosaminoglycans and their proteoglycans: host-associated molecular patterns for initiation and modulation of inflammation. *FASEB J.* 2006;**20**(1):9-22.
244. Gotte M, Echtermeyer F. Syndecan-1 as a regulator of chemokine function. *ScientificWorldJournal.* 2003;**3**:1327-1331.

245. Kainulainen V, Wang H, Schick C, Bernfield M. Syndecans, heparan sulfate proteoglycans, maintain the proteolytic balance of acute wound fluids. *The Journal of biological chemistry*. 1998;**273**(19):11563-11569.
246. Chen Y, Leask A, Abraham DJ, Pala D, Shiwen X, Khan K, Liu S, Carter DE, Wilcox-Adelman S, Goetinck P, Denton CP, Black CM, Pitsillides AA, Sarraf CE, Eastwood M. Heparan sulfate-dependent ERK activation contributes to the overexpression of fibrotic proteins and enhanced contraction by scleroderma fibroblasts. *Arthritis Rheum*. 2008;**58**(2):577-585.
247. Yeaman C, Rapraeger AC. Membrane-anchored proteoglycans of mouse macrophages: P388D1 cells express a syndecan-4-like heparan sulfate proteoglycan and a distinct chondroitin sulfate form. *J Cell Physiol*. 1993;**157**(2):413-425.
248. Derksen PW, Keehnen RM, Evers LM, van Oers MH, Spaargaren M, Pals ST. Cell surface proteoglycan syndecan-1 mediates hepatocyte growth factor binding and promotes Met signaling in multiple myeloma. *Blood*. 2002;**99**(4):1405-1410.
249. Parish CR. Heparan sulfate and inflammation. *Nature immunology*. 2005;**6**(9):861-862.
250. Yeaman C, Rapraeger AC. Post-transcriptional regulation of syndecan-1 expression by cAMP in peritoneal macrophages. *The Journal of cell biology*. 1993;**122**(4):941-950.
251. Ojeh N, Hiilesvuo K, Warri A, Salmivirta M, Henttinen T, Maatta A. Ectopic expression of syndecan-1 in basal epidermis affects keratinocyte proliferation and wound re-epithelialization. *J Invest Dermatol*. 2008;**128**(1):26-34.
252. Stepp MA, Gibson HE, Gala PH, Iglesia DD, Pajoohesh-Ganji A, Pal-Ghosh S, Brown M, Aquino C, Schwartz AM, Goldberger O, Hinkes MT, Bernfield M. Defects in keratinocyte activation during wound healing in the syndecan-1-deficient mouse. *Journal of cell science*. 2002;**115**(Pt 23):4517-4531.
253. Hayashida K, Johnston DR, Goldberger O, Park PW. Syndecan-1 expression in epithelial cells is induced by transforming growth factor beta through a PKA-dependent pathway. *The Journal of biological chemistry*. 2006;**281**(34):24365-24374.
254. Finsen AV, Woldbaek PR, Li J, Wu J, Lyberg T, Tonnessen T, Christensen G. Increased syndecan expression following myocardial infarction indicates a role in cardiac remodeling. *Physiol Genomics*. 2004;**16**(3):301-308.
255. Vanhoutte D, Schellings MW, Gotte M, Swinnen M, Herias V, Wild MK, Vestweber D, Chorianopoulos E, Cortes V, Rigotti A, Stepp MA, Van de Werf F, Carmeliet P, Pinto YM, Heymans S. Increased expression of syndecan-1 protects against cardiac dilatation and dysfunction after myocardial infarction. *Circulation*. 2007;**115**(4):475-482.
256. Fan J, Malik AB. Toll-like receptor-4 (TLR4) signaling augments chemokine-induced neutrophil migration by modulating cell surface expression of chemokine receptors. *Nat Med*. 2003;**9**(3):315-321.
257. Johnson GB, Brunn GJ, Platt JL. Cutting edge: an endogenous pathway to systemic inflammatory response syndrome (SIRS)-like reactions through Toll-like receptor 4. *J Immunol*. 2004;**172**(1):20-24.
258. Vuoriluoto K, Jokinen J, Kallio K, Salmivirta M, Heino J, Ivaska J. Syndecan-1 supports integrin alpha2beta1-mediated adhesion to collagen. *Exp Cell Res*. 2008;**314**(18):3369-3381.
259. Heit B, Colarusso P, Kubes P. Fundamentally different roles for LFA-1, Mac-1 and alpha4-integrin in neutrophil chemotaxis. *Journal of cell science*. 2005;**118**(Pt 22):5205-5220.

260. Mollinedo F, Nakajima M, Llorens A, Barbosa E, Callejo S, Gajate C, Fabra A. Major co-localization of the extracellular-matrix degradative enzymes heparanase and gelatinase in tertiary granules of human neutrophils. *The Biochemical journal*. 1997;**327** (Pt 3):917-923.
261. Yang Y, Macleod V, Miao HQ, Theus A, Zhan F, Shaughnessy JD, Jr., Sawyer J, Li JP, Zcharia E, Vlodavsky I, Sanderson RD. Heparanase enhances syndecan-1 shedding: a novel mechanism for stimulation of tumor growth and metastasis. *The Journal of biological chemistry*. 2007;**282**(18):13326-13333.
262. Yu WH, Woessner JF, Jr. Heparan sulfate proteoglycans as extracellular docking molecules for matrilysin (matrix metalloproteinase 7). *The Journal of biological chemistry*. 2000;**275**(6):4183-4191.
263. Li Q, Park PW, Wilson CL, Parks WC. Matrilysin shedding of syndecan-1 regulates chemokine mobilization and transepithelial efflux of neutrophils in acute lung injury. *Cell*. 2002;**111**(5):635-646.
264. Bartlett AH, Hayashida K, Park PW. Molecular and cellular mechanisms of syndecans in tissue injury and inflammation. *Mol Cells*. 2007;**24**(2):153-166.
265. Fitzgerald ML, Wang Z, Park PW, Murphy G, Bernfield M. Shedding of syndecan-1 and -4 ectodomains is regulated by multiple signaling pathways and mediated by a TIMP-3-sensitive metalloproteinase. *The Journal of cell biology*. 2000;**148**(4):811-824.
266. Raats CJ, Bakker MA, van den Born J, Berden JH. Hydroxyl radicals depolymerize glomerular heparan sulfate in vitro and in experimental nephrotic syndrome. *The Journal of biological chemistry*. 1997;**272**(42):26734-26741.
267. Raats CJ, Van Den Born J, Berden JH. Glomerular heparan sulfate alterations: mechanisms and relevance for proteinuria. *Kidney international*. 2000;**57**(2):385-400.
268. Hawkins CL, Davies MJ. Generation and propagation of radical reactions on proteins. *Biochimica et biophysica acta*. 2001;**1504**(2-3):196-219.
269. Enghild JJ, Thogersen IB, Oury TD, Valnickova Z, Hojrup P, Crapo JD. The heparin-binding domain of extracellular superoxide dismutase is proteolytically processed intracellularly during biosynthesis. *The Journal of biological chemistry*. 1999;**274**(21):14818-14822.
270. Konorev EA, Kotamraju S, Zhao H, Kalivendi S, Joseph J, Kalyanaraman B. Paradoxical effects of metalloporphyrins on doxorubicin-induced apoptosis: scavenging of reactive oxygen species versus induction of heme oxygenase-1. *Free Radic Biol Med*. 2002;**33**(7):988.
271. Cohen HJ, Chovaniec ME. Superoxide generation by digitonin-stimulated guinea pig granulocytes. A basis for a continuous assay for monitoring superoxide production and for the study of the activation of the generating system. *The Journal of clinical investigation*. 1978;**61**(4):1081-1087.
272. Carlsson LM, Jonsson J, Edlund T, Marklund SL. Mice lacking extracellular superoxide dismutase are more sensitive to hyperoxia. *Proceedings of the National Academy of Sciences of the United States of America*. 1995;**92**(14):6264-6268.
273. Kliment CR, Tobolewski JM, Manni ML, Tan RJ, Enghild J, Oury TD. Extracellular superoxide dismutase protects against matrix degradation of heparan sulfate in the lung. *Antioxidants & redox signaling*. 2008;**10**(2):261-268.

274. Pardo A, Gibson K, Cisneros J, Richards TJ, Yang Y, Becerril C, Yousem S, Herrera I, Ruiz V, Selman M, Kaminski N. Up-regulation and profibrotic role of osteopontin in human idiopathic pulmonary fibrosis. *PLoS medicine*. 2005;**2**(9):e251.
275. Kadokami T, McTiernan CF, Kubota T, Frye CS, Feldman AM. Sex-related survival differences in murine cardiomyopathy are associated with differences in TNF-receptor expression. *J Clin Invest*. 2000;**106**(4):589-597.
276. McGaffin KR, Sun CK, Rager JJ, Romano LC, Zou B, Mathier MA, O'Doherty RM, McTiernan CF, O'Donnell CP. Leptin signalling reduces the severity of cardiac dysfunction and remodelling after chronic ischaemic injury. *Cardiovasc Res*. 2008;**77**(1):54-63.
277. Janczewski AM, Zahid M, Lemster BH, Frye CS, Gibson G, Higuchi Y, Kranias EG, Feldman AM, McTiernan CF. Phospholamban gene ablation improves calcium transients but not cardiac function in a heart failure model. *Cardiovasc Res*. 2004;**62**(3):468-480.
278. Kliment CR, Englert JM, Gochuico BR, Yu G, Kaminski N, Rosas IO, Oury TD. Oxidative stress alters syndecan-1 distribution in lungs with pulmonary fibrosis. *J Biol Chem*. 2008.
279. Woessner JF, Jr. The determination of hydroxyproline in tissue and protein samples containing small proportions of this imino acid. *Arch Biochem Biophys*. 1961;**93**:440-447.
280. Englert JM, Hanford LE, Kaminski N, Tobolewski JM, Tan RJ, Fattman CL, Ramsgaard L, Richards TJ, Loutaev I, Nawroth PP, Kasper M, Bierhaus A, Oury TD. A role for the receptor for advanced glycation end products in idiopathic pulmonary fibrosis. *The American journal of pathology*. 2008;**172**(3):583-591.
281. Junqueira LC, Bignolas G, Brentani RR. Picrosirius staining plus polarization microscopy, a specific method for collagen detection in tissue sections. *Histochem J*. 1979;**11**(4):447-455.
282. Whittaker P, Kloner RA, Boughner DR, Pickering JG. Quantitative assessment of myocardial collagen with picrosirius red staining and circularly polarized light. *Basic Res Cardiol*. 1994;**89**(5):397-410.
283. Piantadosi CA, Carraway MS, Babiker A, Suliman HB. Heme oxygenase-1 regulates cardiac mitochondrial biogenesis via Nrf2-mediated transcriptional control of nuclear respiratory factor-1. *Circ Res*. 2008;**103**(11):1232-1240.
284. McQuade KJ, Beauvais DM, Burbach BJ, Rapraeger AC. Syndecan-1 regulates alphavbeta5 integrin activity in B82L fibroblasts. *J Cell Sci*. 2006;**119**(Pt 12):2445-2456.
285. Zen K, Reaves TA, Soto I, Liu Y. Response to genistein: assaying the activation status and chemotaxis efficacy of isolated neutrophils. *Journal of immunological methods*. 2006;**309**(1-2):86-98.
286. Sergejeva S, Ivanov S, Lotvall J, Linden A. Interleukin-17 as a recruitment and survival factor for airway macrophages in allergic airway inflammation. *American journal of respiratory cell and molecular biology*. 2005;**33**(3):248-253.
287. Rice WR, Conkright JJ, Na CL, Ikegami M, Shannon JM, Weaver TE. Maintenance of the mouse type II cell phenotype in vitro. *American journal of physiology*. 2002;**283**(2):L256-264.
288. Dobbs LG. Isolation and culture of alveolar type II cells. *Am J Physiol*. 1990;**258**(4 Pt 1):L134-147.

289. Liang CC, Park AY, Guan JL. In vitro scratch assay: a convenient and inexpensive method for analysis of cell migration in vitro. *Nature protocols*. 2007;**2**(2):329-333.
290. Hunninghake GW, Gadek JE, Lawley TJ, Crystal RG. Mechanisms of neutrophil accumulation in the lungs of patients with idiopathic pulmonary fibrosis. *The Journal of clinical investigation*. 1981;**68**(1):259-269.
291. Folz RJ, Abushamaa AM, Suliman HB. Extracellular superoxide dismutase in the airways of transgenic mice reduces inflammation and attenuates lung toxicity following hyperoxia. *The Journal of clinical investigation*. 1999;**103**(7):1055-1066.
292. Fattman CL, Chu CT, Kulich SM, Enghild JJ, Oury TD. Altered expression of extracellular superoxide dismutase in mouse lung after bleomycin treatment. *Free radical biology & medicine*. 2001;**31**(10):1198-1207.
293. Cantin AM, North SL, Fells GA, Hubbard RC, Crystal RG. Oxidant-mediated epithelial cell injury in idiopathic pulmonary fibrosis. *The Journal of clinical investigation*. 1987;**79**(6):1665-1673.
294. Fukuda Y, Ishizaki M, Kudoh S, Kitaichi M, Yamanaka N. Localization of matrix metalloproteinases-1, -2, and -9 and tissue inhibitor of metalloproteinase-2 in interstitial lung diseases. *Lab Invest*. 1998;**78**(6):687-698.
295. Bai P, Mabley JG, Liaudet L, Virag L, Szabo C, Pacher P. Matrix metalloproteinase activation is an early event in doxorubicin-induced cardiotoxicity. *Oncol Rep*. 2004;**11**(2):505-508.
296. Kizaki K, Ito R, Okada M, Yoshioka K, Uchide T, Temma K, Mutoh K, Uechi M, Hara Y. Enhanced gene expression of myocardial matrix metalloproteinases 2 and 9 after acute treatment with doxorubicin in mice. *Pharmacol Res*. 2006;**53**(4):341-346.
297. Chen P, Li A, Zhang M, He M, Chen Z, Wu X, Zhao C, Wang S, Liang L. Protective effects of a new metalloporphyrin on paraquat-induced oxidative stress and apoptosis in N27 cells. *Acta Biochim Biophys Sin (Shanghai)*. 2008;**40**(2):125-132.
298. Sheng H, Enghild JJ, Bowler R, Patel M, Batinic-Haberle I, Calvi CL, Day BJ, Pearlstein RD, Crapo JD, Warner DS. Effects of metalloporphyrin catalytic antioxidants in experimental brain ischemia. *Free radical biology & medicine*. 2002;**33**(7):947-961.
299. Chen P, Chen Z, Li A, Lou XC, Wu XK, Zhao CJ, Wang SL, Liang LP. Catalytic metalloporphyrin protects against paraquat neurotoxicity in vivo. *Biomed Environ Sci*. 2008;**21**(3):233-238.

APPENDIX A: Curriculum Vitae

CORRINE R. KLIMENT
kliment.corrine@medstudent.pitt.edu

Education: University of Pittsburgh – School of Medicine
 Medical Scientist Training Program, MD/PhD Candidate May 2011
 PhD: Department of Cellular and Molecular Pathology

University of Nebraska - Lincoln Major: Biochemistry
 Bachelor of Science Minors: Sociology and Chemistry
 Graduated: May 2004

Appointments

OCCUPATION	START DATE (mm/yy)	END DATE (mm/yy)	FIELD	INSTITUTION	SUPERVISOR/ EMPLOYER
Graduate Student	09/06	08/09	Pathology	Univ. of Pittsburgh	Tim Oury, MD PhD
MSTP Student	05/04	Present	MD/PhD	Univ. of Pittsburgh	Clayton Wiley, MD PhD
Kaplan MCAT Teacher/Tutor	05/05	Present	MCAT Test Preparation	Kaplan, Inc.	Gregory Vaslowski
Human Anatomy TA	09/05	11/05	Anatomy	Univ. of Pittsburgh School of Medicine	Jack Schumann, PhD
Physiology TA	08/03	05/04	Human Physiology	Univ. of Nebraska	Dept. of Biology
Biology TA	09/01	05/03	Introductory Biology	Univ. of Nebraska	Ted Pardy, PhD
Research Internship	05/03	08/03	Pulmonary Division	Univ. of Pittsburgh	Steven Duncan, MD
Summer Research Internships (2)	05/01	05/03	Pulmonary & Critical Care	Univ. of Nebraska Medical Center	Debra Romberger, MD

Academic and Professional Honors

Medical Scientist Training Program (MSTP) Grant Recipient (Institutional, T32) - National Institutes of Health
Sept. 2004-Sept. 2005, University of Pittsburgh School of Medicine
Society for Free Radical Biology and Medicine, Travel Grant Recipient, Nov. 2008.
(chosen by 225+ faculty members)
McGowan Institute for Regenerative Medicine – Travel grant to the American Thoracic Society Meeting 2008
Univ. of Pittsburgh Interdisciplinary Graduate Biomedical Training Program Travel Grants, 2006-2009.
Univ. of Pittsburgh Biomedical Graduate Student Association Student Spotlight Winner, Spring, 2009.
University of Nebraska College of Arts and Sciences Dean’s List – six of eight semesters.
2003 Max John and Pauline H. Stuermer Scholarship Recipient for an undergraduate female in premedicine.
UNL Research Poster Presented at the Natl. Conf. for Undergraduate Research (NCUR) March 2003.

Speaking Engagements and Talks

Invited Instructor/Speaker, Molecular Pathobiology Graduate Student Course, Department of Pathology “Animal Models of Pulmonary Fibrosis”, Spring 2008.

Dept. of Pathology, University of Pittsburgh – Annual Retreat – Selected graduate student speaker during oral research session. “Heparin/Heparan sulfate and EC-SOD Interactions in Pulmonary Fibrosis”, May 2007.

Duke University Hyperbaric Research Center – Invited Guest Speaker, “Asbestos Model of Pulmonary Fibrosis”, Feb. 12, 2007.

Individual Grants and Funding

Source: National Institutes of Health – NRSA MD/PhD Individual Fellowship; F30ES016483
National Institute of Environmental Health Sciences
Title: “Extracellular Matrix Components, Oxidants and Antioxidants in Pulmonary Fibrosis.”
Role in Project: Principal Investigator
Funding period: September 2007-September 2012

Reviewer Participation

Invited reviewer for the journal *Antioxidant and Redox Signaling*.

<u>Organizational Activities and Leadership</u>		
Organization	Position/Role	Year(s)
Univ. of Pittsburgh - Medical Scientist Training Program (MSTP)	Applicant Screening Committee	2009-2010
	Student Interviewer Interdisciplinary Biomedical Program	2008-2009
	Student Committee Chair Student Guidebook Chair	2007-2008
	Second Look Applicant Weekend Planning Committee	Spring 2007
	Student Mentoring Co-Chair	2006-2007
	Annual Retreat Coordinator	2005-2006
Bach Choir of Pittsburgh www.bachchoirpittsburgh.org	Choir member, (80 members by audition)	2008-2009
Honor Council - Univ. of Pittsburgh School of Medicine	Student Representative - Class of 2008 & MSTP	2004-current
	Academic Hearing Board Member -Formal Student Solicitor/Case Representative (Dean of Student Affairs-selected representative)	2006 (Informal) 2007 (Formal)
Univ. of Pittsburgh School of Medicine	Interviewer for the SOM Guaranteed Admit Program	Spring 2009
American Physician Scientists Assoc.	Institutional Representative Membership Committee member	2008-2009
Duke Univ. Hyperbaric Research Center	Guest Speaker—"Asbestos Model of Pulmonary Fibrosis"	Feb. 12, 2007
Dept. of Pathology – Univ. of Pittsburgh Department Retreat Planning Committee	Student Representative	2007-current
Dept. of Pathology – Annual Retreat	Dept. of Pathology Graduate Student Top Poster Award Winner	May 2008
	Student speaker during oral research session.	June 2007
	Retreat Committee Member	2007
Biomedical Graduate Student Association	Secretary	2006-2007
	Symposium Planning Committee	2007
American Medical Students Association (AMSA)	National Officer – Region 3 Associate Trustee	2005-2006
	Co-President, Univ. of Pittsburgh Chapter Community & Public Health Committee Chair	2005-2006
	National Conference Credentials Committee	2005
Pittsburgh Women's Abuse Shelter	Medical Student Volunteer	2004-2005
University of Nebraska (UNL) Honors Program	Honors Thesis Research – Biology & Biochemistry	Sept. 2000 – May 2004
Honors Program Ambassador	Secretary	2002-2003
UNL Mortar Board Senior Honors Society	Class Induction Chairperson	2003-2004
NU MEDS – Pre-medicine Group	President	2002-2003
- 4 year member	Treasurer/ Consult	2003-2004
National Society of Collegiate Scholars	Vice Pres. of Community Service	2003-2004

Medical and Science Memberships:			
American Society of Investigational Pathology	Member		2007-present
Society for Free Radical Biology and Medicine	Member, Student member of the Women in Science Group		2006-present
American Medical Association	Member		2006-present
American Medical Students Association	Member		2004-present
Pennsylvania Medical Society	Member		2004-present

Publications

Peer Reviewed Publications:

Kliment, CR, Englert, JM. Gochuico, BR., Yu, G., Kaminski, N., Rosas, IO., Oury, TD. "Oxidative Stress Alters Syndecan-1 Distribution in the Lung During Pulmonary Fibrosis." J Biol Chem, 2009 Feb 6; 284(6):3537-45. PMID: 19073610

Kliment, CR, Clemens, K, Oury, TD. Case Report: North American Erionite-associated Mesothelioma with Pleural Plaques and Pulmonary Fibrosis. Int J Clin Exp Pathol, 2009; 2(4), 407-410. PMID: 19158938

Kliment, CR, Tobolewski, J, Manni, M, Tan, R, Enghild, J, Oury, T. "Extracellular Superoxide Dismutase protects against matrix degradation of heparan sulfate in the lung." Antioxid Redox Signal. 2008 Feb;10(2):261-8. PMID: 17961072

Myllärniemi, M, Lindholm P, Ryyänänen M, **Kliment, C**, Salmenkivi K, Keski-Oja, J, Kinnula, V, Oury , T, Koli, K. "Gremlin-mediated decrease in BMP signaling promotes pulmonary fibrosis", Am J Respir Crit Care Med. 2008 Feb 1;177(3):321-9. PMID: 17975199

Carraway, MS, Suliman, HB, **Kliment, CR**, Oury, TD, Welty-Wolf, KE, Piantadosi, CA. "Mitochondrial Biogenesis in the Pulmonary Vasculature during Inhalational Lung Injury and Fibrosis", Antioxid Redox Signal. 2008 Feb;10(2):269-75. PMID: 17999632

Zheng M., Ramsay, A., Robichaux, M., Norris, K., **Kliment, C.**, Crowe, C., Rapaka, R., Steele, C., McAllister, F., Shellito, J., Marrero, L., Schwarzenberger, P., Zhong, Q., Kolls, J., "CD4+ T cell-independent DNA vaccination against opportunistic infections," J. Clin. Invest., 2005 Dec 1;115(12):3536-3544.

Abstract Publications and Conference Presentations:

1. **Kliment, CR**, Gochuico, B, Piganelli, J, Rosas, I, Oury, T. Contrasts Between IPF and Mouse Models of Pulmonary Fibrosis. Am J of Resp. Crit. Care Med, April 2000; 179: A2716. Abstract (poster discussion session).
2. **Kliment, CR**, Englert, J, Yu, G., Rosas, I, Oury, T. Oxidative Stress and EC-SOD Alter Syndecan-1 Distribution in Lungs with Pulmonary Fibrosis. Am J of Resp. Crit. Care Med, April 2009; 179: A3022. Abstract.
3. **Kliment, CR**, Tobolewski, JM, McGaffin, KR, McTiernan, CF, Oury, TD. Lack of Extracellular Superoxide Dismutase leads to increased Doxorubicin-induced Cardiac Injury. American Heart Association Fellow Research Day, Pittsburgh, PA February 2009, Abstract.
4. **Kliment, CR**, Englert, J, Yu, G., Rosas, I, Oury, T. Lack of EC-SOD leads to syndecan shedding in pulmonary fibrosis. *FRBM*, 45(1): S47. Abstract (Oral presentation)
5. **Kliment, CR**, Tobolewski, JM, McGaffin, KR, McTiernan, CF, Oury, TD. Lack of Extracellular Superoxide Dismutase leads to increased Doxorubicin-induced Cardiac Injury. *FRBM*, 45(1): S86. Abstract
6. **Kliment, CR**, Englert, J, Yu, G., Rosas, I, Oury, T. Lack of EC-SOD leads to syndecan shedding in pulmonary fibrosis. 15th International Colloquium on Lung and Airway Fibrosis, Sunset Beach, NC, September, 2008. Abstract
7. **Kliment, CR**, Englert, J, Yu, G., Rosas, I, Oury, T. Lack of EC-SOD leads to syndecan shedding in pulmonary fibrosis. University of Pittsburgh Department of Pathology Annual Retreat, May 2008, and Medical Scientist Training Program Annual Retreat, August 2008. Abstract
8. **Kliment, CR**, Rosas, I, Oury, TD. The Role of Heparan Sulfate, Oxidants, and Antioxidant EC-SOD in Pulmonary Fibrosis- Lack of EC-SOD leads to Syndecan shedding. Am J of Resp. Crit. Care Med, 2008 April; 177: A470. Abstract
9. **Kliment, CR**, Tobolewski, J, Oury, T. Heparin/Heparan sulfate and EC-SOD Interactions in Pulmonary Fibrosis. *FRBM*, 2007 Nov.; 43(1):S111. Abstract
10. **Kliment, CR**, Tobolewski, J, Oury, T. Heparin/Heparan sulfate and EC-SOD Interactions in Pulmonary Fibrosis. MD/PhD National Conference, Keystone, CO, July 25-28, 2007. Abstract
11. **Kliment, CR**, Tobolewski, J, Oury, T. Heparin/Heparan sulfate and EC-SOD Interactions in Pulmonary Fibrosis. Annual Pathology Department Retreat – Poster and oral presentation, Pittsburgh, PA, June 1, 2007. Abstract
12. **Kliment, CR**, Tobolewski, J, Oury, T. Heparin/Heparan sulfate and EC-SOD Interactions in Pulmonary Fibrosis. Keystone International Symposium – Molecular Mechanisms of Fibrosis Meeting, Tahoe City, CA, March 11-14, 2007. Abstract
13. **Kliment, CR**, Tobolewski, J, Oury, T. Heparin/Heparan sulfate and EC-SOD Interactions in Pulmonary Fibrosis. Annual Pathology Research Day, University of Pittsburgh, November 2006 and 2007. Abstract
14. **Kliment, C.R.**, Romberger, D.J., Wyatt, T. Modulation of Airway Epithelial Cell Cytokine Release by Hog Barn Dust and Cigarette Smoke. American Thoracic Society (ATS) International Conference, Seattle, WA - May 2003, *American Journal of Respiratory and Critical Care Medicine*, Vol. 167, No. 7: p.A717. Abstract
15. **Kliment, C.R.**, Pardy, R.L. Analysis of the Biological Effects of Algal Lipopolysaccharide on Human Whole Blood. Nebraska Academy of Science Annual Meeting, April 25, 2003, *Programs and Proceedings 2003*: p.41. Abstract

16. **Kliment, C.R.,** Pardy, R.L. Analysis of the Biological Effects of Algal Lipopolysaccharide on Human Whole Blood. 17th Annual National Conference for Undergraduate Research, University of Utah, March 13-15, 2003, Abstract Book: p.249. Abstract
17. **Kliment, C.R.,** Romberger, D.J., Wyatt, T. Modulation of Airway Epithelial Cell Cytokine Release by Hog Barn Dust and Cigarette Smoke. University of Nebraska Undergraduate Creativity and Research Experience (UCARE) Poster Symposium, October 2002. Abstract
18. **Kliment, C.R.,** Romberger, D.J., Wyatt, T. Immunosuppressant Drugs Block IL-6 and IL-8 Release in Airway Epithelial Cells Exposed To Dust Extracts From Swine Confinement Facilities. American Thoracic Society (ATS) International Conference, Atlanta, GA - May 2002, *American Journal of Respiratory and Critical Care Medicine*, Vol. 165, No. 8: p.A525. Abstract
19. **Kliment, C.R.,** Pardy, R.L. The Biological Activity of Novel aLPS Assessed in Mouse and Human Macrophages. International Endotoxin Society, 7th Conference, Abstract 2002
20. **Kliment, C.R.,** Pardy, R.L. The Biological Activity of Novel aLPS Assessed in Mouse and Human Macrophages. Nebraska Academy of Science Annual Meeting, April 26, 2002, *Program and Proceedings 2002*: p.37. Abstract
21. **Kliment, C.R.,** Romberger, D.J., Wyatt, T. Immunosuppressant Drugs Block IL-6 and IL-8 Release in Airway Epithelial Cells Exposed To Dust Extracts From Swine Confinement. University of Nebraska Undergraduate Creativity and Research Experience (UCARE) Poster Symposium, October 2001.